MODELLING OF ECLIPSING BINARIES

by

PATRICIA LEIGH SKELTON

submitted in fulfilment of the requirements for the

degree of

MASTER OF SCIENCE

in the subject of

ASTRONOMY

at the

UNIVERSITY OF SOUTH AFRICA

SUPERVISOR: PROF D P SMITS

AUGUST 2009

Student Number: 3482-891-5

I declare that

MODELLING OF ECLIPSING BINARIES

is my own work and that all the sources that I have used or quoted have been indicated and acknowledged by means of complete references.

.....

Patricia Leigh Skelton

.....

Date

Acknowledgements

I would like to thank my supervisor Prof. D. P. Smits for his guidance and support throughout the course of this study.

To my family: Thank you for your love and support throughout my studies.

Figures 2.2 and 2.3 were provided by Ms A. Prozesky. Thanks for being a great friend and colleague.

Thanks are due to the following individuals:

- The anonymous referees for their comments on the paper by Skelton & Smits (2009).
- Prof. C. Koen (UWC) for his comments on the method of error analysis (private communication).
- Prof. B. Warner (UCT) for his comments on my Honours project ("Modelling of W UMa-type Variable Stars").

I would like to thank the SuperWASP team for granting access to their database.

Thanks are due to the SKA SA Postgraduate Bursary Programme project for their financial assistance.

This research has made use of the SIMBAD database, operated at CDS, Strasbourg, France and the SAO/NASA Astrophysics Data Stream.

Summary

W Ursae Majoris-type (W UMa-type) variable stars are contact eclipsing binary stars whose evolution is unknown. Modelling to determine the physical parameters of as many W UMa-type variable stars as possible might provide some insight as to how these contact binaries form and evolve. The All Sky Automated Survey (ASAS) has discovered over five thousand of these systems. Using data from the ASAS and from the Wide Angle Search for Planets (SuperWASP) project, models of selected ASAS contact binaries are being created to determine their physical parameters. Some W UMa-type variable stars are known to undergo changes in orbital period. For selected ASAS contact binaries, a period analysis has been performed using SuperWASP data to determine if the systems are undergoing changes in orbital period. Results of the modelling and period analyses of selected systems are presented.

KEYWORDS: stars: binaries: eclipsing − stars: fundamental parameters − binaries: close − stars: contact − stars: variables: other − stars: individual: RW Com; ASAS 002328−2041.8; ASAS 002449−2744.3; ASAS 002821−2904.1; ASAS 015937−0331.0; ASAS 052851−3010.2; ASAS 093818−6755.4; ASAS 120036−3915.6; ASAS 134841−4012.9; ASAS 150452−3757.7; ASAS 150934−3348.5

Contents

Abbreviations and Acronyms

ASAS	All Sky Automated Survey
BM3	Binary Maker 3.0
DC	Differential Corrections
EA	Algol-type eclipsing binary
EB	Beta Lyrae-type eclipsing binary
EC	Contact eclipsing binary
ED	Detached eclipsing binary
ESD	Semi-detached eclipsing binary
EW	W UMa-type eclipsing binary
GIRAFFE	Grating High Resolution Echelle Spectrograph
LTTE	Light Travel Time Effect
mag	Magnitude
MS	Main Sequence
PHOEBE	PHysics Of Eclipsing BinariEs
PMD	Phase-Magnitude Diagram
SAAO	South African Astronomical Observatory
SuperWASP / WASP	Wide Angle Search for Planets
TRO	Thermal Relaxation Oscillations
VSI	Variable Star Investigator

Chapter 1

Introduction

W Ursae Majoris (W UMa) was discovered to be variable by Müller & Kempf (1903). They determined a period of four hours from the two observed minima which, at the time, made it the shortest period variable star known. The light curve obtained by the authors is shown in Fig. 1.1. The fast variation in light is noticeable. The cause of the variation was not understood but the authors suggested that "... the light-variation is produced by two celestial bodies almost equal in size and luminosity whose surfaces are at a slight distance from each other, and which at times almost centrally occult each in their revolution. In this case the observed light curve can be almost exactly represented by computation." They also acknowledged the problems associated with the suggestion: were these systems physically possible and could they remain stable? Shapley & van der Bilt (1917) observed that the colour of W UMa did not change throughout its orbital cycle, suggesting that the two components had similar temperatures. Further observations of W UMa were focussed on refining the period of the star and monitoring its decreasing period (Schilt 1925, van Gent 1929). From a photo-electric study of W UMa, Huffer (1934) determined a period of 0.33 d (from primary minimum to primary minimum) and suggested that the observed light variation was due to two ellipsoidal bodies that eclipse each other during their orbit, thus supporting the idea of Müller & Kempf (1903). Huffer (1934) also suggested that both components displayed limb darkening and differed slightly in size, mass and brightness. Kwee (1956) observed that the light curve of W UMa was variable with maxima of different heights and referred to it as a "remarkable feature".

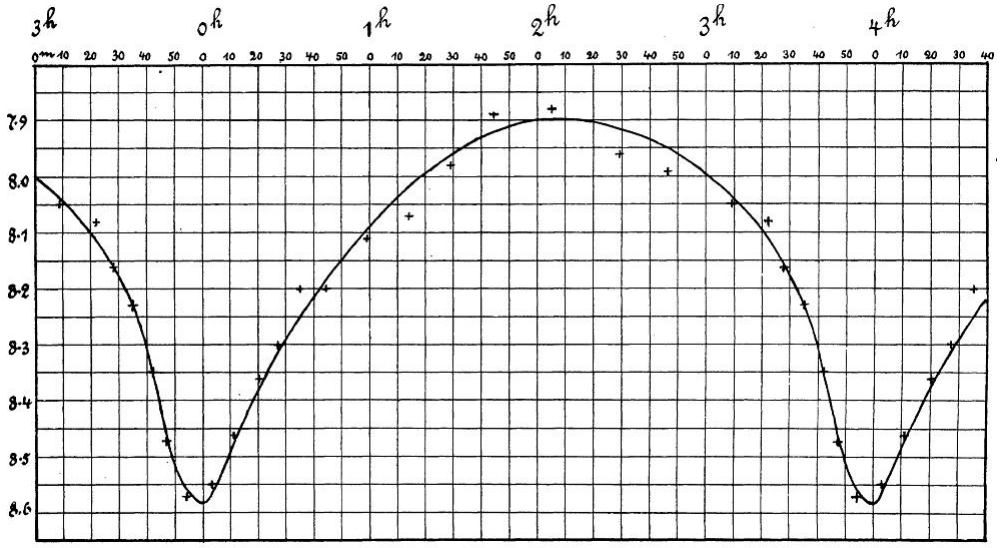

Figure 1.1: The light curve of W Ursae Majoris taken from Müller & Kempf (1903). The fast variation in light is noticeable. The period was calculated as the time between the two observed minima.

Kwee also noted a shift in the secondary minimum and suggested that it was possibly caused by the unequal maxima.

Observationally, it was found that the spectral types of W UMa-type stars are concentrated between late-A and early-K types. The lack of variation in colour observed throughout the orbital cycle of W UMa was observed in other W UMa-type stars. Popper (1948) inspected spectrographic data of seven W UMa-type stars. Of five stars observed to have unequal minima, the data indicated that for four of the stars, the brighter, more massive star was the cooler star. As the number of W UMa candidates increased, it became increasingly obvious that the primary components either obeyed the mass-luminosity relation for Main Sequence (MS) stars or were too faint for their mass, and that for most of the systems the secondary components were too bright for their masses. In a large number of W UMa-stars studied, it was observed that the brighter, massive star had a lower surface brightness while for other stars, the two components had an almost equal surface brightness (Kuiper 1948). Kuiper argued that a common envelope in which strong currents transferred matter from one star to the other could explain the observations. The observed light curves of some W UMa systems displayed maxima of different heights, suggesting that the surface brightness of the stellar hemispheres were different for the two

maxima.

Kopal (1955) suggested that W UMa-type stars belong to a group of contact[1] binaries where both components fill their Roche limits. Based on this suggestion, Lucy (1968) proposed a model for calculating the light curves of W UMa-type stars. The model assumes that the surfaces of contact binaries are equipotential surfaces as given by the Roche model. The important feature of Lucy's model is the common envelope formed by a single, connected convection zone. W UMa-type stars could finally be explained in terms of a physical model.

W UMa has become the prototype of variable stars displaying continuous variation and minima of almost equal depth. Based on observations of known W UMa-type stars and the work of Kopal (1955) and Lucy (1968), W UMa-type variable stars are defined as contact eclipsing binary stars with orbital periods between 0.2 d and 1 d (Shore 1994) and mass ratios between 0.08 and 0.8. The amplitude of the variations in the V band is around 0.75 magnitudes, and the difference between the minima in the light curve is about $0.1 - 0.2$ magnitudes. Each component is assumed to be a MS star with spectral type ranging from mid-A to late-K. By Space density, these binary stars are the most abundant of interacting binaries (Webbink 2003) yet their structure and evolution is still unknown (Moss & Whelan 1970, Lapasset & Claria 1986, Paczynski 1997).

The traditional view is that a W UMa-type star forms from a close, detached binary that loses angular momentum through magnetic stellar winds. Evolution through angular momentum losses due to mass lost in magnetized winds (Vilhu 1982, van't Veer & Maceroni 1989, Stepien 1995, Ibanoğlu et al. 2006), Thermal Relaxation Oscillations (TRO) due to mass exchange between the two components (Lucy 1976, Flannery 1976, Wang 1999, Qian 2003) or a combination of both processes, are possible ways these systems evolve over time. During the course of their evolution, the interacting components may become semi-detached. If so, TRO will take place until the system settles into a contact state. More observational data are needed to establish whether either one of the above mechanisms controls the evolution of these stars, or whether some other, as yet unidentified

[1]There is an ongoing debate as to the use of the term "overcontact" when describing W UMa-type systems. For this dissertation, W UMa-type stars are defined to be contact binaries based on the argument presented by Rucinski (1997) that the term "overcontact" should be used when there is genuine overflow of the outer critical equipotential surface.

process, is driving changes in the system. What W UMa-type stars ultimately evolve into is also a matter of debate. These stars may be the progenitors of Blue Stragglers or FK Comae-type stars (Şenavcı et al. 2008). Detecting, monitoring and modelling as many of these stars as possible may help fill in the blanks of the evolutionary paths of W Ursae Majoris-type stars.

The All Sky Automated Survey (ASAS)[2](Paczyński et al. 2006) is a project that has discovered thousands of variable stars since 1996, and continues to monitor them on a regular basis. While the survey only concentrated on a V band range of $8-12$ magnitude (mag), it has detected over 5 000 W UMa-type stars, making it a rich source for studies of these systems. The Wide Angle Search for Planets (SuperWASP)[3] project is another source of data for binary star research. SuperWASP searches for extrasolar planets via transiting events. Because this involves taking multiple images of the sky, the project has photometric data of variable stars.

Some W UMa-type stars are known to display changes in their orbital period. The period of a binary star changes with time either due to a redistribution of the matter between the stars, or when angular momentum is gained or lost by the system (Hilditch 2001). For conservative mass exchange, the period decreases if mass is transferred from the more massive star to the less massive star, and increases if the opposite occurs. By tidal dissipation, orbital angular momentum may be transferred to, or drawn from, the spin motion of a star, causing the period to either increase or decrease until a spin equilibrium is reached in which the tidal torque vanishes (Pilecki et al. 2007). The period of a W UMa-type star can also be reduced by magnetic braking through a magnetized stellar wind. Period changes observed in binary stars do not have to be intrinsic phenomena. Light travel time effects (propagation delays), also known as LTTE, are produced when a binary system is a member of a triple or mulitple stellar system. Luminosity changes on parts of the binaries' photosphere can also lead to shifts in the time of minima or maxima, thus mimicking period changes.

Analysing systems that appear to be undergoing changes in their orbital period may shed some light on the important physical processes that occur in close binary systems. Pilecki

[2]http://www.astrouw.edu.pl/asas/
[3]http://www.superwasp.org

et al. (2007) searched the ASAS data for eclipsing binaries with high period change rates. From a sample of 1711 systems that fulfilled all their criteria of data quality, they present 31 interacting binaries whose periods either increased (10) or decreased (21) in a five year interval of observations. The authors also noted that seven of the stars that were selected for period analysis presented significant trends in their average brightness. One particular star had a linear trend of approximately $+0.025$ mag yr^{-1}. An increase or decrease in brightness may correspond to magnetic activity due to the appearance or disappearance of stellar spots on the surfaces of the stars. According to a mechanism proposed by Applegate (1992), changes in orbital period can lead to changes in the observed luminosity, the requirement being that variations in brightness have the same period as the orbital period modulation. Observations of systems that appear to be displaying increases or decreases in flux and are known to be undergoing changes in orbital period can be used to test the validity of this mechanism.

For this dissertation, W UMa-type stars were selected from the ASAS database for modelling. The light curves of the stars were inspected to find systems that may be undergoing changes in orbital period, and to look for features in the light curves that are suggestive of possible magnetic activity. Stars suspected of being magnetically active are potential candidates for future radio observations. Because SuperWASP South is located at the South African Astronomical Observatory (SAAO) in Sutherland, South African astronomers are allowed access to the SuperWASP data. Consequently, SuperWASP data were used to obtain complete light curves of selected ASAS stars. The stars were modelled using software packages Binary Maker 3.0 (BM3) and the PHysics Of Eclipsing BinariEs (PHOEBE). For the stars suspected of undergoing changes in orbital period, SuperWASP data were used to perform a period analysis of selected stars.

The lay out of this dissertation is as follows:

Chapter 2 describes the Roche Model and its applicability to contact binaries. The morphological classification of eclipsing binaries is discussed.

Observed features and the formation and evolution scenarios of W UMa-type stars are discussed in more detail in Chapter 3.

Chapter 4 provides details of the ASAS and SuperWASP. The applicability of these

projects to binary stars is discussed.

In Chapter 5, the selection process and methods used to model selected ASAS stars are discussed. Models of six ASAS stars are presented and the results of the modelling are discussed.

The use of O−C diagrams for period analysis is discussed in Chapter 6. The selection process and methods used for the period analysis of selected stars are discussed. The period analyses of eight stars are presented and the results are discussed.

A summary of the results of the modelling and period analyses is presented in Chapter 7. Unexpected discoveries and future research are discussed.

Chapter 2

The Roche Model

> "If a certain star should be situated at any, perhaps immense, distance behind another, and but very little deviating from the line in which we see the first, we should then have the appearance of a double star. But these stars, being totally unconnected, would not form a binary system. If, on the contrary, two stars should really be situated very near each other, and at the same time, so far insulated as not to be materially affected by the attractions of the neighbouring stars, they will then compose a separate system, and remain united by the bond of their own mutual gravitation towards each other. This should be called a real double star; and any two stars that are thus mutually connected, form the binary sidereal system which we are now to consider....."
>
> Herschel (1802)[1]

In the words of Herschel, eclipsing binaries are "binary sidereal systems". The Roche model is the basis of the morphological classification of eclipsing binaries and is discussed in this chapter.

[1] Taken from Hilditch (2001).

2.1 Morphological Classification of Eclipsing Binaries

Initially, eclipsing binaries were classified according to the shape and features of their light curves (Kallrath & Milone 1999). Three classical light curves were identified that are designated EA, EB and EW after their protostars Algol, β Lyrae and W UMa, respectively. The prototypical light curves are shown in Fig. 2.1. The features of EA light curves include obvious start and end times of the eclipses, while outside the eclipses the light variations are almost negligible. Observationally it has been found that the orbital periods for these stars are greater than one day. EB light curves display primary and secondary minima with noticeably different depths and the light curve shows continuous variation outside of the eclipses. In general, the orbital period is greater than one day. Continuous variation is seen in the light curves of EW systems but the defining feature is the small difference between primary and secondary minima, no more than 0.1 to 0.2 magnitudes. The orbital periods of EW systems are less than one day. This initial classification scheme lacked any physical basis (Kopal 1955).

An alternative classification scheme describes binary star systems in terms of the Roche model. Consider a system of two point masses, m_1 and m_2, with $m_1 > m_2$, in circular orbit about C, the common centre-of-mass. Choose a reference frame with its origin at m_1 that is corotating with the system at an angular velocity ω. Let m_2 be at the point $(a, 0, 0)$ with the z-axis perpendicular to the orbital plane, as illustrated in Fig. 2.2. The gravitational potential experienced by a third body with infinitesimal mass at any point $\mathrm{P}(x, y, z)$ will be the sum of the gravitational potential of the two point masses and the centrifugal potential due to the rotation of the system.

The potential, Φ, is described by

$$\Phi(x, y, z) = -\frac{Gm_1}{r_1} - \frac{Gm_2}{r_2} - \frac{\omega^2}{2}\left[\left(x - \frac{m_2}{m_1 + m_2}\right)^2 + y^2\right] \tag{2.1}$$

with

$$r_1 = \sqrt{x^2 + y^2 + z^2} \quad \text{and} \quad r_2 = \sqrt{(x-a)^2 + y^2 + z^2}$$

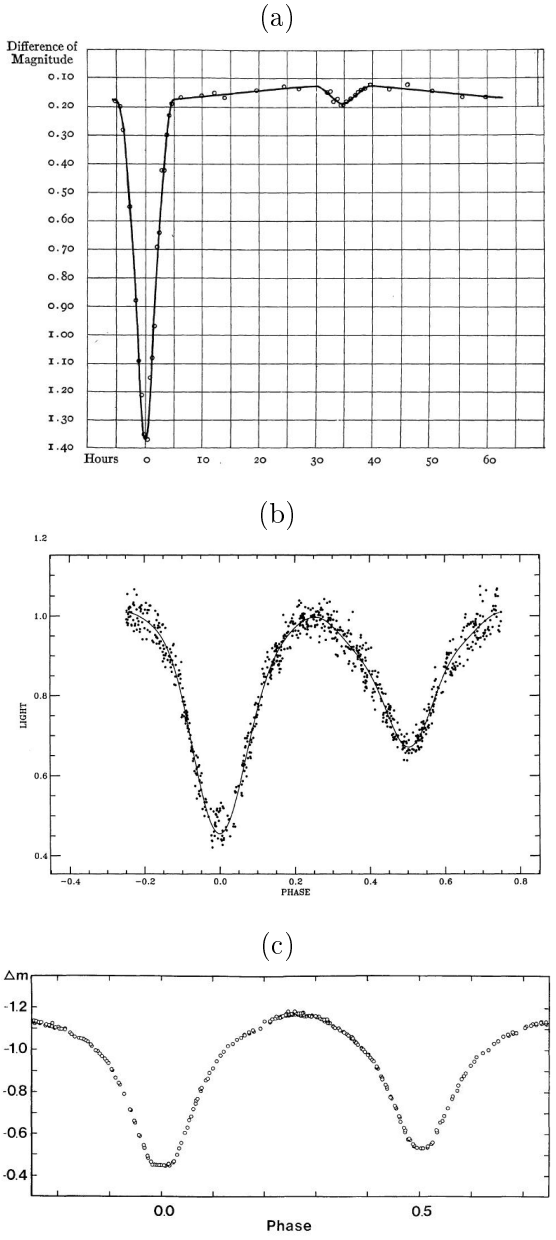

Figure 2.1: Light curves of the prototype eclipsing binary stars. (a) Algol, taken from Stebbins (1910). There is little variation between the eclipses which have well-defined start and end times. (b) β Lyrae, taken from van Hamme et al. (1995). There is continuous variation between the eclipses but the minima have different depths. (c) W UMa, taken from Breinhorst (1971). As with the EB light curve, there is continuous variation. An important feature is the nearly equal depth of the minima.

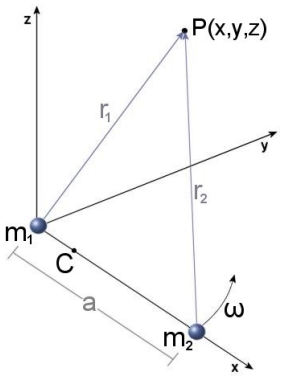

Figure 2.2: Frame of reference for a system consisting of two point masses m_1 and m_2, which are orbiting their centre-of-mass C with angular speed ω in the x-y plane. An arbitrary point P is a distance r_1 and r_2 away from m_1 and m_2 respectively.

Assumptions made in the Roche model are that there is a spherically symmetric distribution of mass for each star, that the stars are rotating synchronously, and that the orbit is circular (Meyer-Hofmeister & Ritter 1993). The shape of the potential in 3D space is defined by the separation between the two stars, a, and the mass ratio, q, which is given by

$$q = \frac{m_2}{m_1}$$

An alternative form of the Roche potential is the dimensionless Roche potential given by

$$\Phi = \frac{1}{r_1} + \frac{q}{r_2} + \frac{1+q}{2}\left[\left(x - \left(\frac{q}{1+q}\right)^2 + y^2\right)\right] - \frac{q^2}{2\,(1+q)}$$

where Φ is the potential at a point P, r_1 (r_2) is the distance between P and the centre of gravity of star 1 (star 2) in units of orbital separation of the binary, and x and y are the Cartesian coordinates of P, in units of the orbital separation (Li et al. 2004).

The applicability of the Roche model becomes apparent when one considers that the physical interpretation of the equipotential surfaces is that they coincide with the surfaces of constant pressure of the two stars, which are motionless in the orbit frame. The normals of the equipotential surfaces give the direction of the local effective gravity. The density and pressure are uniform on the equipotential surfaces and, with the assumption that

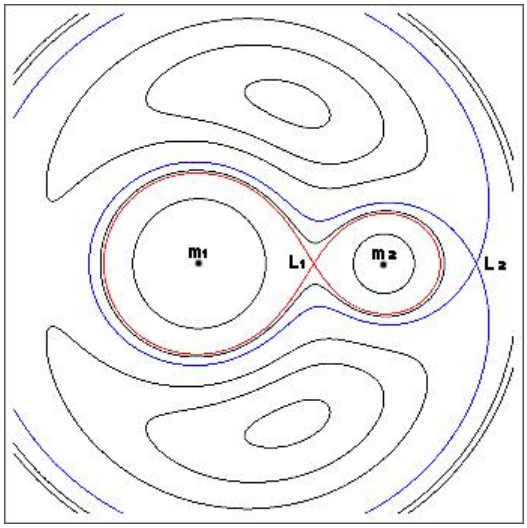

Figure 2.3: A contour map of equipotentials in the orbital plane of a binary star with mass ratio $q = 0.3$. The centres of mass of the larger and smaller star are indicated by m_1 and m_2 respectively. The inner Lagrangian surface that specifies the Roche lobes is indicated in red while the outer Lagrangian surface is in blue. The inner and outer Lagrangian points are labelled L_1 and L_2 respectively.

the gas is in hydrostatic equilibrium, it follows that the temperature is also uniform along the equipotential surfaces. The photosphere of a star can be considered to be approximately the surface at which the density falls to zero. Therefore, the photosphere of a synchronously rotating star lies on one of the equipotential surfaces generated by the Roche model.

The shapes of the equipotential surfaces near the centres of the stars are spherical, whereas far away from the centres the equipotential surfaces of the two masses intersect and jointly enclose both stars. The equipotential surfaces for a binary system with $q = 0.3$ is shown in Fig. 2.3.

The change from two separate spheres to a single shape occurs via a figure-of-eight shape which is known as the inner critical potential. There are five points where the gravitational and centripetal acceleration vanishes. These points are known as the Lagrangian points. The equipotential surface that passes through the inner Lagrangian point L_1 is the inner critical potential. The 3D lobes that form this equipotential surface are called the Roche lobes. A second critical surface, the outer critical surface, corresponds to the surface

passing through L_2, the second Lagrangian point. The Roche lobes define the upper limit for the volume of each star for which all its matter is under its own gravitational control. At L_1, matter can flow from one star to the other while at L_2 matter can escape from the system. Matter that lies between these two critical surfaces forms a common envelope around the stars. L_3 lies beyond the larger component of the binary system and is another point, at a higher potential than L_2, at which matter can leave the system. The points $L_1 - L_3$ lie on a line that joins the mass centres of both stars. The points L_4 and L_5 form equilateral triangles with the two masses.

Using the Roche model, eclipsing binaries can be separated into morphological classes. If the stars are far apart from each other, the mass of each star is contained within equipotential surfaces that are essentially spheres around the centre of each star. As the ratio of their separation to their radii decreases, the shape of the star becomes distorted by the gravitational influence of its neighbour. In a detached system, the photospheres of both stars lie well within their Roche lobes. The lack of variation between eclipses suggests that the effects due to their proximity are negligible. EA light curves are typical for detached systems although the prototype of the class, Algol, is actually a semi-detached binary.

If the photosphere of one star lies within its Roche lobe while the photosphere of the other star coincides with its Roche lobe, the system is classified as a semi-detached system. Mass transfer from the lobe-filling star to its companion takes place through L_1. As the stars fill their Roche lobes, the distortion from a circular to a tear-drop shape is a result of the shape of the inner critical surface. Because the shape of the Roche lobe-filling star is non-spherical, the surface area seen by an observer changes throughout the orbital cycle. Due to the change in surface area, the flux outside of the eclipses continuously varies producing EB light curves. Detached, semi-detached and, in some cases, marginally contact systems can produce EB light curves.

If the photospheres of both stars equal or exceed their Roche lobes, a contact system is formed. In these systems, both stars overfill their Roche lobes with a narrow neck of material occurring around L_1. Because they effectively share a common stellar atmosphere, these stars are referred to as common envelope binaries. This common envelope will tend to equalise the surface temperatures of the stars. The EW light curves are produced by

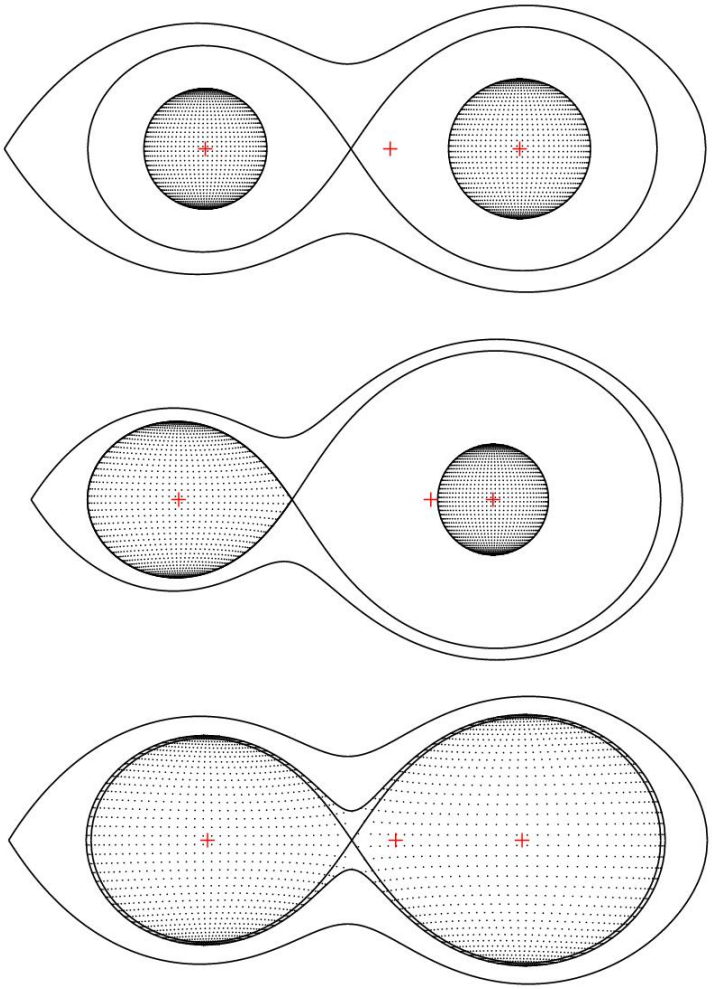

Figure 2.4: Inner and outer Lagrangian surfaces of detached (top), semi-detached (middle), and contact (bottom) systems.

these systems. Fig. 2.4 shows the critical surfaces for detached, semi-detached and contact systems.

The classification of eclipsing binaries into EA, EB and EW systems is not used by the ASAS team. They use ED, ESD and EC to classify eclipsing binaries. This classification scheme is discussed in more detail in Chapter 4.

Chapter 3

W UMa-type Variable Stars

W UMa-type variable stars, or EW systems, are identified by the continuous variation in their light curves, nearly equal depth minima, short orbital periods and a mass ratio less than one. The colour of an EW system varies by a small amount suggesting that the temperature difference between the components is only a few hundred degrees. This in turn implies that the common envelope is optically thick with an almost uniform temperature. Most EW systems are observed to be of spectral types indicative of convective stars, which suggests that the common envelope is convective (Webbink 2003). Spectral features for these stars include rotationally broadened and blended absorption lines. There are also emission lines in the UV which is an indication that these stars can be chromospherically active. EW systems are known to be sources of X-rays (Chen et al. 2006). However, from observations made in the X-ray, visual, UV and radio regimes (Rucinski & Seaquist 1988), EW systems were found to have magnetic activity levels lower than those measured for single, rapidly rotating stars. This suggests that the common envelope may be suppressing dynamo action to some extent.

The formation and evolution of W UMa-type variable stars is poorly understood. TRO models and evolution through angular momentum losses are possible ways in which these systems form and evolve. According to Mochnacki (1981), the formation and evolution of EW systems relies heavily on magnetic braking. An alternative formation mechanism is based on observations which suggest that many EW systems are members of triple or

multiple star systems. Hendry & Mochnacki (1998) suggest that a tertiary component (or multiple components) may play a vital part in the formation of an EW system by removing angular momentum from the system. This suggestion is supported by Pribulla & Rucinski (2006) who argue that the most distant component of the triple or multiple system takes most of the angular momentum so that the close binary system is left with low angular momentum. van Hamme & Cohen (2008) argue that formation through the interactions between members of triple or multiple systems may be the way in which EW stars form. If more EW stars are found to be members of multiple systems, it will support the arguments of Hendry & Mochnacki (1998) and Pribulla & Rucinski (2006).

Binnendijk (1970) divided EW systems into two subclasses which he called A-type and W-type. The classification depends on which component of the binary system has the higher temperature. In the A-type systems, the larger component has a higher temperature than its companion, whereas in the W-type systems the smaller component has a higher temperature than its companion. Observationally it has been found (Csizmadia & Klagyivik 2004) that the A-type systems tend to have low mass ratios ($q < 0.3$) and spectral type from A to F. W-type systems usually have mass ratios $q > 0.3$ and spectral types of G or K. The necks of W-type systems are thinner than those for A-type systems. In most cases, the orbital periods of W-type systems are smaller than those of the A-types (Wadhwa 2005). There are arguments as to whether the A-type and W-type systems arise as a result of evolution in a similar manner but under different circumstances (van Hamme 1982, Li et al. 2008). Li et al. (2008) collected the determined physical parameters of 69 W-type and 61 A-type systems. The results of their analysis suggests that the secondary components of all the systems studied are more evolved than the primary components, which they argue is a result of the transfer of energy from the primary to the secondary. They suggest that the only difference between the subtypes is that they are in different stages of TRO with the A-type sytems moving from a contact configuration to a semi-detached configuration or from semi-detached to contact. Gazeas & Stępień (2008) argue that A-types and W-types form as a result of close detached binaries forming contact binaries. Due to different mass/energy transfer rates, different evolutionary paths are followed resulting in the two different subtypes being formed. Wilson (1978) argues that the A-type systems are in equilibrium and the W-type systems are not in equilibrium. Consequently, the W-types would undergo TRO. Hilditch et al. (1988) sug-

gest two types of evolution of contact binaries with the result that, depending on which path is followed, different subtypes are produced. Both evolutionary processes begin with a close, detached binary. If the system moves directly from a detached configuration to a marginal-contact system, a shallow contact W-type system is formed. If the short period detached binary becomes a semi-detached binary (as a result of case-A mass transfer i.e. mass transfer that occurs during core hydrogen burning), the binary system moves to a marginal-contact state and finally becomes a deep-contact A-type system.

Another subtype, the B-type system, has been suggested by Lucy & Wilson (1979). These systems are in geometrical but not thermal contact, resulting in large temperature differences between the component stars. The observed light curves resemble that of an EB system, hence the B in the subtype name. Csizmadia and Klagyivik (2004) introduced a new subtype, the high mass ratio or H-type system. These systems are characterized by $q > 0.72$. The issue regarding the formation and evolution of the different subtypes can only be answered by studying and determining the physical parameters of as many EW systems as possible.

Because both components are assumed to be MS dwarf stars, EW systems are expected to follow the MS mass-luminosity relation (Csizmadia 2005) given by

$$\frac{L_2}{L_1} = \left(\frac{M_2}{M_1}\right)^4 \tag{3.1}$$

Lucy (1968, 1973) determined the following mass ratio-luminosity ratio of EW systems:

$$\frac{L_2}{L_1} = \left(\frac{M_2}{M_1}\right)^{0.92} \tag{3.2}$$

Clearly, EW systems do not obey the same mass-luminosity relation as MS stars. According to van Hamme & Cohen (2008), the luminosity ratio determined by Lucy (1968, 1973) indicates that energy is transferred from the larger component to the smaller component. The convective common envelope is believed to play a role in the transfer of energy. The transfer of energy supports the suggestion of Kuiper (1948) in explaining the observed lower surface brightness of the primary components. Although Lucy determined a mass-luminosity relation for EW systems, Csizmadia & Klagyivik (2004) argue that, based on the results of their work, there is no definite relation for contact binaries.

The rapid rotation of EW systems suggests that they should be more magnetically active than stars with longer rotational periods. Light curves of some EW systems display maxima with different heights which is interpreted as magnetic activity and is referred to as the O'Connell effect (Hilditch 2001). The difference in heights of the maxima is attributed to the presence of stellar spots on the surfaces of the stars, which is an indication that the star is magnetically active. If the maximum following the primary minimum is brighter than the secondary maximum, the O'Connell effect is said to be positive; if the first maximum is fainter than the secondary maximum, the effect is said to be negative (Liu & Yang 2003). The O'Connell effect is more prevalent in the light curves of W-type systems, suggesting that they are more magnetically active than the A-type systems. It has been noted for many EW systems that their light curves display a variety of features that tend to be variable (Maceroni & van't Veer 1993). These features include the O'Connell effect, phase shifts of the maxima and changes in minima depths. Generally, the variability of these features is of the order of months or years. If any of these features are detected, it is an indication that there is some activity occurring in these systems. Studies of these systems may improve our understanding of the evolution and structure of EW systems.

Some EW systems are known to display complex period patterns where intervals of constant period are interrupted with intervals where the period increases or decreases. From a statistical study by van't Veer (1991), it was found that positive and negative jumps in period are randomly distributed. For some systems, the period may either only increase or decrease. Changes in period can arise due to a number of reasons. If there is a periodic oscillation in the period, this may be evidence of the LTTE (Zavala 2005). The presence of a third body, or more, can be inferred from periodic variations in the O−C diagrams. Mass transfer between the two components that conserves angular momentum and mass can also lead to changes in the period of the system. The orbital period of the system will either increase or decrease (Kwee 1958). Applegate (1992) proposed a mechanism that related changes in orbital period to changes in the distribution of angular momentum in the active star, which in turn varies the oblateness of the star producing variations in the luminosity. The variation must have the same period as the orbital period modulation, and extrema in brightness should coincide with extrema in the corresponding O−C diagram of the system. EW systems displaying increases or decreases in flux are good tests

of this mechanism.

The structure and evolution of EW systems is poorly understood. The existence of different subclasses coupled with the lack of models for the formation and evolution of EW systems only strengthens the importance of studying as many EW systems as possible and identifying those that display the O'Connell effect or period changes. This is where mass sky surveys such as the ASAS and SuperWASP are beneficial to binary star research. These surveys are described in the next chapter.

Chapter 4

Automated Sky Surveys

Most of the variable stars listed in astronomical catalogues were discovered by large scale monitoring programmes (Paczynski 1997). Large scale sky surveys can be set up to detect different types of objects, including eclipsing binaries, and then, through followup observations, monitor them. These sky surveys can be performed by small telescopes. In the words of Paczynski, "One may envision beginning the all sky variability survey with very low cost equipment: a telephoto lens attached to a CCD camera, with the cost at the level of a personal computer." This idea is the basis of two large scale surveys namely the ASAS and SuperWASP. This chapter discusses the features of the two surveys.

4.1 The All Sky Automated Survey

The ASAS is a project that was set up in 1996 to detect and monitor the variability of stars between 8^{th} and 12^{th} mag south of declination $+28°$. Observations are carried out at the Las Campanas Observatory in Chile using two wide-field telecopes, one narrow field telescope and one very-wide-field telescope. Each of the two wide-field telescopes is equipped with a 200 mm $f/2.8$ Minolta telephoto lens and a 2K $\times$ 2K CCD camera. One telescope is equipped with a standard V-band filter and the other with a standard I-band filter (Paczynski et al. 2006). Images of an $8.8° \times 8.8°$ field of view are captured on

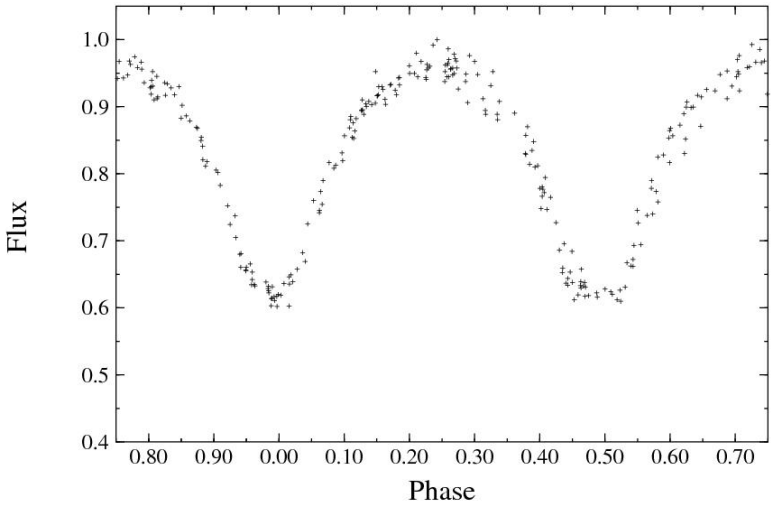

Figure 4.1: Light curve of ASAS 120036−3915.6 obtained from approximately 8 years of observations.

the CCD cameras, with 60% of the sky visible from the observatory. The ASAS V-band data comes from the wide-field telescope; the default exposure time for the wide-field V system is three minutes. All stars are observed once every one to three nights, creating a raw data stream of 1.5 GB to 2 GB per instrument per night.

Simultaneous photometry is performed through different apertures ranging from two to six pixels in diameter. All the data are processed separately; for faint stars data from the smallest apertures are used, while for bright stars data from the largest aperture are used. The data are flux calibrated into standard Johnson V-magnitudes with each measurement graded according to the quality of the data. Each star that is observed is given an ASAS identification that is coded from the coordinates of the star e.g. ASAS 120036−3915.6. Cross references are made to stars listed in other astronomical catalogues. The ASAS team calculate a period P and a reference time of minimum T_0. By folding the data on the ASAS period, a phase-magnitude diagram (PMD) is obtained. An example of an ASAS PMD is shown in Fig. 4.1. This particular light curve consists of 278 points obtained from approximately eight years worth of observations. The ASAS database is available to the public.

Eclipsing binaries in the ASAS database are subdivided using a Fourier analysis method developed by Ruciński (1973). Expressing the time-dependent V magnitudes $V(t)$ as a

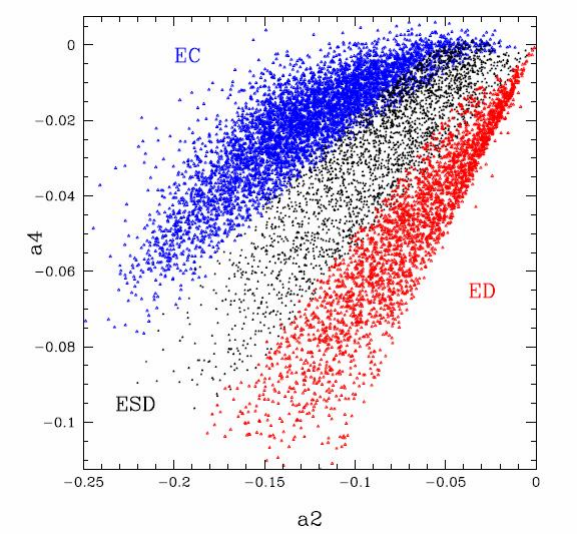

Figure 4.2: Plot of the a_4 vs a_2 Fourier coefficients for eclipsing binaries in the ASAS database taken from Paczynski et al. 2006. While there are areas of overlap, the three groups can be clearly identified.

Fourier series

$$V(t) = \sum_{i=0}^{\infty} (a_i \cos i\omega t + b_i \sin i\omega t) \tag{4.1}$$

it has been found that in a plot of a_4 against a_2 for all stars, the eclipsing sytems divide into three regions. ASAS label detached systems as ED, semi-detached as ESD and contact as EC. As shown in Fig. 4.2, the different systems can be distinguished in the $a_2 - a_4$ plane but there are areas of overlap resulting in a multiple classification of certain stars. According to Paczynski et al. (2006), "Our classification into EC, ESD and ED types should be considered preliminary....", therefore the applicability of the above method as a classification scheme can only be verified once more data or complete light curves for the stars have been obtained.

This project has already discovered over 50,000 variable stars, a large portion of which have not been classified previously as variable stars. Of the 50,000 variable stars, over 5 000 have been classified as EC systems using the method described above. An interesting result from the survey is the very small number of detached systems with periods less than one day. These systems have been proposed as possible progenitors of EW systems but the small number detected by ASAS does not support this formation scenario.

Clearly, long-term sky surveys are beneficial to determining how EW systems form and evolve as they may not only discover new systems, but may also help to fill in the gaps between the progenitor and the final state.

4.2 The Wide Angle Search for Planets

SuperWASP is a programme designed for detecting exoplanets via transit events. The programme is a joint effort between eight academic institutions in the United Kingdom. SuperWASP is designed to operate throughout the year and covers both celestial hemispheres. SuperWASP-North is situated on the island of La Palma, while SuperWASP-South is situated at the SAAO, just outside Sutherland, South Africa. These robotic observatories each consist of eight wide-angle cameras. Each camera has an aperture of 11.1 cm consisting of a Canon 200mm $f/1.8$ lens and a 2K $\times$ 2K CCD camera (Pollacco et al. 2006). The field of view for each observatory is approximately 482 deg^2. The magnitude range covered by SuperWASP is $V \sim 7.0 - 11.5$ which is similar to that of the ASAS. The cameras continuously image the night sky (exposure times of 30 seconds) producing a raw data stream of about 50GB per night per observatory. All stars are given a SuperWASP identification that is coded from the star's coordinates e.g. 1SWASP J150452.17−375739.0.

To detect extrasolar planets requires continuous monitoring of stars in order to detect the small dips in magnitude caused by a planet transiting its host star. Thus, mulitple images of a patch of the sky are obtained every night. Due to the short orbital period of EW systems, a complete light curve is often obtained in just one night of observing. According to Willems et al. (2006), surveys like SuperWASP will not only detect eclipsing binaries but also provide photometric data for newly detected and existing eclipsing binaries. An example of a SuperWASP light curve is shown in Fig. 4.3. Due to the similar magnitude response of SuperWASP and the ASAS, SuperWASP data are available for many ASAS stars.

The ASAS collect one data point every three days whereas SuperWASP obtain two data points of the same field every ten minutes. This set of data often covers the minima

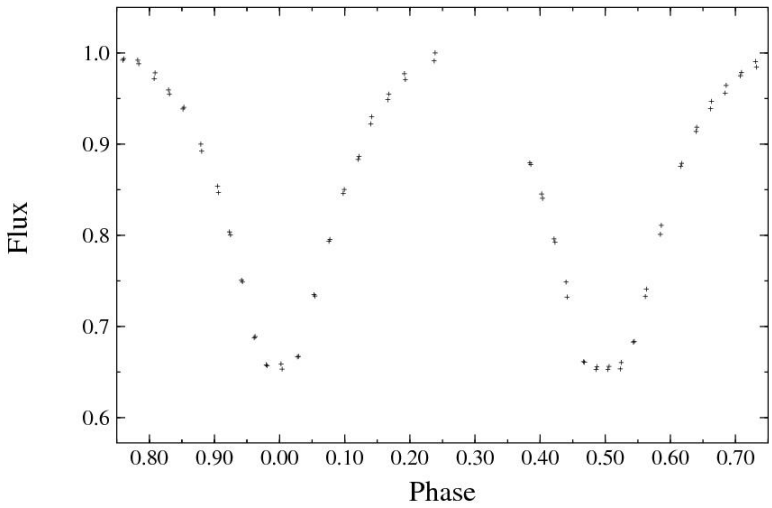

Figure 4.3: WASP light curve of ASAS120036−3915.6. This light curve was obtained from a single night's observing.

in the light curves, from which it is possible to determine accurate times of minimum brightness. Therefore, the SuperWASP data are extremely useful for period analysis of W UMa systems.

The Variable Star Investigator (VSI) is a web based tool designed to allow easy access to the SuperWASP database. When an object's coordinates, SuperWASP identification or name is entered, the VSI queries online data sources, including the ASAS database. The VSI returns SuperWASP data (if available), information from other astronomical databases, a SuperWASP determined V magnitude and an image thumbnail of the object.

The ASAS has discovered thousands of W UMa-type variable stars and while ASAS and SuperWASP are designed for different purposes, the SuperWASP data complements the ASAS data. The SuperWASP data can be used to model EW systems since complete light curves are often observed.

Chapter 5

Modelling of Selected ASAS Contact Binaries

The large number of EC systems discovered by the ASAS can greatly improve our understanding of how W UMa-type variable stars form and evolve. While ASAS provides the orbital periods of the systems, the physical parameters (such as the mass ratio) of many of these systems has yet to be determined. By modelling the systems using photometric and/or spectroscopic data and modelling software such as BM3 and PHOEBE, the physical parameters can be determined. EC systems were selected from the ASAS database and modelled using BM3 and PHOEBE. This chapter describes the methods used to model the selected systems. The results of the photometric modelling of six ASAS EC systems are presented.

5.1 Selection Process & Modelling Procedure

EC systems brighter than 11^{th} V mag and with orbital periods of 0.4 d or less were selected from the ASAS EC database. These selection criteria were imposed so that complete light curves of the systems could be observed in one night and, for future work, radial velocity measurements can be obtained using the SAAO's Grating High Resolution Echelle

Spectrograph (GIRAFFE) which can be attached to the 1.9 m telescope at Sutherland. Two systems were exempted from the above criteria namely ASAS 015937−0331.0 and ASAS 134841−4012.9. These systems had previously been identified as total eclipsing systems (from their ASAS data) in earlier work. Using the period and epoch of minimum as provided by ASAS, the data for each system were folded to obtain their PMD. The purpose of this was two-fold: to identify total eclipsing systems and systems where the period appears to be changing. Total eclipsing systems are easier to model when only photometric data are available as the shape and duration of the total eclipse constrains the mass ratio, inclination angle and omega potentials of the system. According to Terrell & Wilson (2005), for a total eclipsing contact system, in most cases the photometrically determined mass ratio is close, if not equal to the spectroscopic mass ratio. Four total eclipsing systems met the selection criteria listed above and, including the other two ASAS systems, were selected for modelling. The six systems for which models have been made are ASAS 015937−0331.0, ASAS 093818−6755.4, ASAS 120036−3915.6, ASAS 134841−4012.9, ASAS 150452−3757.7 and ASAS 150934−3348.5.

The coordinates of the objects were entered into the SuperWASP VSI tool and data were obtained for five of the systems; no SuperWASP data are available for ASAS 093818−6755.4. Effective temperatures were obtained from the $J-H$ and $V-K$ colour indices listed by SuperWASP. For ASAS 093818−6755.4 $B-V$, $V-K$ and $J-H$ colour indices were calculated from the SIMBAD database. SuperWASP data were used in the modelling, except for ASAS 093818−6755.4 for which ASAS data were used. The data were folded using the ASAS period and epoch of minimum. With regards to the SuperWASP data, as observations are performed through different cameras, it was checked that data used for modelling all came from the same camera. This was done to avoid having a double light curve, i.e. having two light curves at slightly different magnitudes caused by using data from the different cameras. To determine the subtypes of the systems, the PMD was used. The definition of the primary minimum of an EW system often leads to confusion. For the purposes of this dissertation, the primary minimum is defined as the deeper minimum corresponding to the eclipse of the hotter component (primary component). The shallower minimum is the secondary minimum. This definition depends largely on whether the difference in depths is clearly discernible. If the primary minimum occurs at phase zero, the system is an A-type system ($T_1 > T_2$) while if the primary

minimum occurs at phase 0.5, the system is a W-type system ($T_2 > T_1$).

The programme used to model the selected contact binary systems is PHOEBE, version 0.31a[1](Prša & Zwitter 2005), a software package based on the Wilson-Devinney code (Wilson & Devinney 1971). Light curves are computed from the solution of the inverse problem (determining the elements of the binary system from the observed light curve). The Wilson-Devinney programme works as follows. Using a selected model (e.g. over-contact mode) and parameters entered by the user, a synthetic light curve is generated in the Light Curve (LC) routine (Milone & Kallrath 2008). The Differential Corrections (DC) routine yields a set of parameters determined through a least squares analysis. The parameters are refined and returned to the user for inspection along with the corresponding residuals value. PHOEBE is released under the GNU General Public License. BM3[2][3] (Bradstreet 2005) is a commercially available software package that calculates light and radial velocity curves. BM3 was used to generate the light curves and graphical representations of the selected systems.

PHOEBE was set to "Overcontact not in thermal contact" mode to model the systems. Because all the temperatures returned by the SuperWASP VSI tool are less than 7200 K, the stars are considered to be convective and the reflection coefficient was set to 0.5 (Ruciński 1969). Gravity brightening coefficients were set to 0.32 (Lucy 1967). Using the temperatures returned by the VSI, an average effective temperature was calculated and T_1 and T_2 were both set to this temperature. PHOEBE interpolates limb darkening coefficients using the tables of van Hamme (1993) and the particular limb darkening law selected. To be compatible with BM3, a linear cosine limb darkening law was used.

For a total eclipsing system, restrictions are placed on the range of values for the mass ratio q and inclination angle i. According to Mochnacki & Doughty (1972), for total eclipsing systems, the times of the contacts of the inner eclipses are determined by the mass ratio and the orbital angle. It is possible to restrict the range of values for the mass ratio by using an iterative procedure in which certain parameters are adjusted for each given value of q (Wadhwa & Zealey 2005).

[1]http://phoebe.fiz.uni-lj.si/
[2]http://www.binarymaker.com/
[3]License No 2NGGK-VHKK5-A26X9-BWLXU-PNMJY

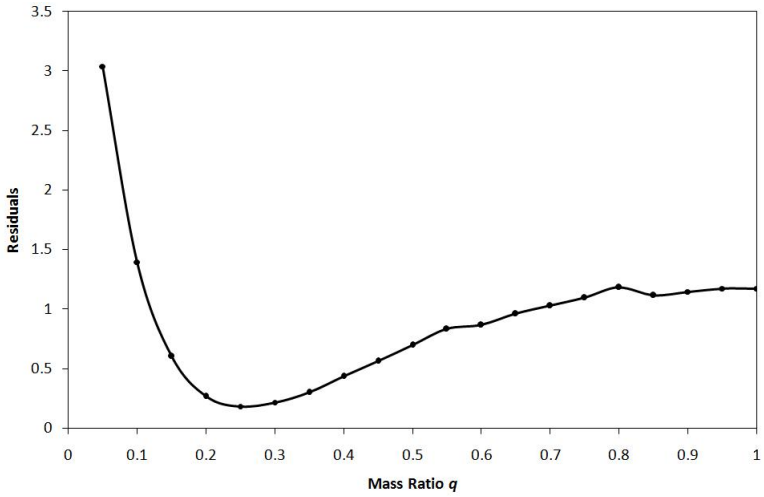

Figure 5.1: By using an iterative procedure to find the mass ratio, it is clear that the minimum of the residuals occurs for q in the range of 0.2−0.3. This particular example is for ASAS 120036−3915.6 with steps in q of 0.05.

For each system, a starting value of 0.1 for q was used. With q set, the potentials Ω_1 and Ω_2, temperature of the secondary T_2, luminosity of the primary component L_1 and i (set to a starting value of 75°) were adjusted. This process was repeated for q values from $0.1 - 1.0$ in steps of 0.1. By plotting the residual values against the mass ratios, the mass ratios that give the lowest residual values can be identified. An example of how the range of values for q can be restricted is shown in Fig. 5.1. By using a finer grid search, the range for the mass ratio can be restricted significantly, particularly for total eclipsing systems. The parameters associated with the lowest residual value, obtained from the finer grid search, are used as the starting point for the DC component of PHOEBE. During the differential corrections q, i, T_2, Ω_1 and L_1 were selected for adjustment. The value of q for which the lowest DC residual value occurred was then set as a free parameter and the DC method was employed to refine the parameters. Although total eclipsing systems provide constraints on the parameters, because no radial velocity observations are available for the systems, absolute parameters can not be determined and the photometrically determined mass ratios can not be confirmed.

For contact systems, the degree of contact is determined by the fillout of the system. The

fillout parameter f of a contact system is defined as

$$f = \frac{\Omega_{\text{inner}} - \Omega}{\Omega_{\text{inner}} - \Omega_{\text{outer}}} \tag{5.1}$$

where Ω_{inner}, Ω_{outer} and Ω are the inner critical, outer critical and surface potential of the binary star respectively. When the photospheres of the component stars are in contact with the inner critical surface $f = 0$ (fillout of 0%), while if the contact is with the outer critical surface $f = 1$ (fillout of 100%). The thickness of the neck of an EW system depends on the fillout parameter. Based on the fillout values of contact binaries studied by van Hamme (1982), an average fillout value of 0.30 (30%) is calculated for the A-type systems and an average value of 0.10 (10%) is found for the W-type systems. From the results of papers I−VI of "Physical parameters of components in close binary systems" (Kreiner et al. 2003, Baran et al. 2004, Zola et al. 2004, Gazeas et al. 2005, Zola et al. 2005, Gazeas et al. 2006), an average fillout value of the contact binaries studied is calculated to be 0.35 (35%).

If the light curve of an EC system displayed the O'Connell effect, BM3 was used to determine the radius, temperature factor and coordinates of the spot that improved the residuals value the most. All the light curves, residuals and models of the systems presented in the following section were created in BM3 using the data used for modelling and the parameters determined with PHOEBE. The best fit in PHOEBE also occurs in BM3. Due to the large number of SuperWASP data points available for each contact binary, only a small number of data points were used to model the systems. Information regarding the data used for a system is mentioned in the relevant subsection.

5.2 Results

5.2.1 ASAS 015937−0331.0 ≡ 1SWASP J015936.82−033056.3

This system has $P_{\text{ASAS}} = 0.63152$ d and $V_{\text{max}} = 9.35$ mag. The WASP light curve is shown in Fig. 5.2. The light curve is composed of 300 points taken from the following HJDs: 2454685, 2454686, 2454687, 2454688, 2454689, 2454689, 2454713 and 2454770.

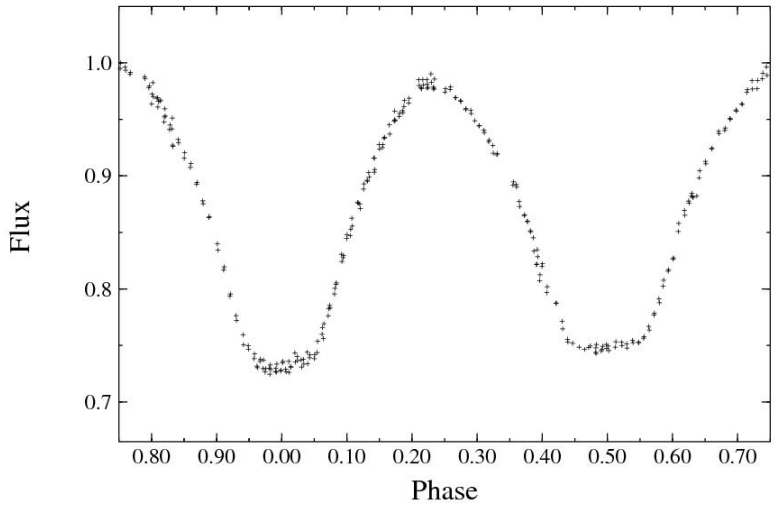

Figure 5.2: Light curve for ASAS 015937−0331.0. The O'Connell effect is present in the light curve: the maximum at phase 0.25 is lower than the maximum at phase 0.75.

Because the SuperWASP light curves suggested that the period of the sysem had changed, the period was changed to 0.6315178 d. A starting temperature of T = 6624 K, corresponding to an F-type star, was adopted. The lowest residual value occurred for the following parameters:

q	$\Omega_{1,2}$	T_1 (K)	T_2 (K)	i (°)
0.094203	1.881519	6624	6824	77.98

The generated light curve, light curve residuals and rendering of the system are shown in Fig. 5.3. The mass ratio, spectral type, orbital period and deeper primary minimum suggest it is an A-type system. The temperature of the secondary component is modelled as being higher than that of the primary component, suggesting a W-type system, which may be a result of the combined effects of limb darkening and gravity brightening reducing the flux of the smaller star. Compared to the calculated average fillout values of contact binaries, the fillout value of $f = 0.97$ (97 %) is exceptionally large.

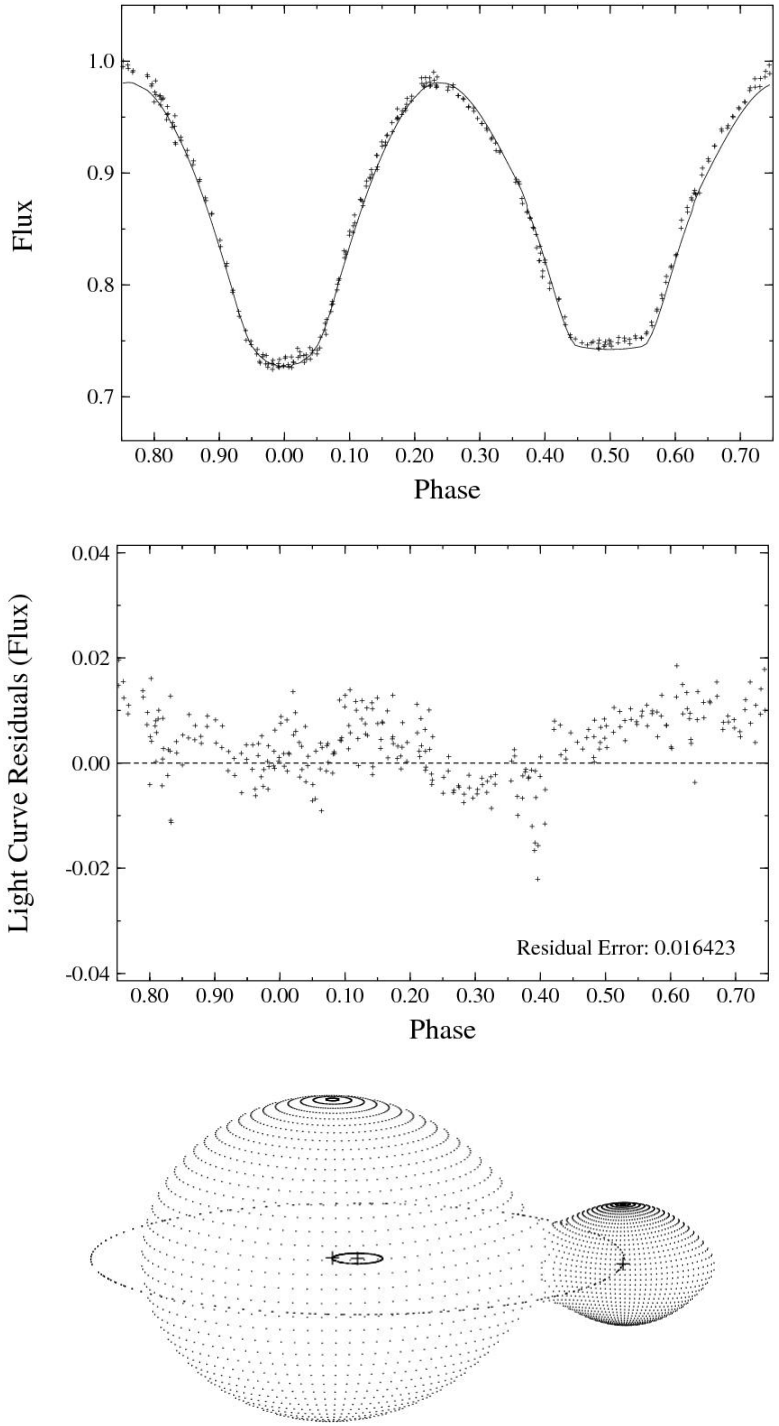

Figure 5.3: Light curve, residuals and rendering of the system ASAS 015937−0331.0. The synthetic light curve does not fit the observed data well at the secondary minimum.

From phase 0.1 to 0.25 and from 0.5 to 0.75, the residual values are quite large. The O'Connell effect is evident in the light curve of the system. Modelling spots on systems when only photometric data are available is unreliable because different combinations of spots (i.e. different sizes, temperatures, locations on the component stars) produce similar effects on the synthetic light curve. Experimenting with different spots on the primary and secondary component, the residuals improved the most with the placement of a spot on the larger component. The spot parameters are: radius of 15°, temperature factor of 1.05, colatitude of 45° and longitude of 90°. Fig. 5.4 shows the resulting light curve, light curve residuals and model of the system with the spot indicated in red. Although the overall fit has improved from a residual of 0.016423 to 0.010556, the fit between phase 0.1 and 0.25 has not been improved by the spot.

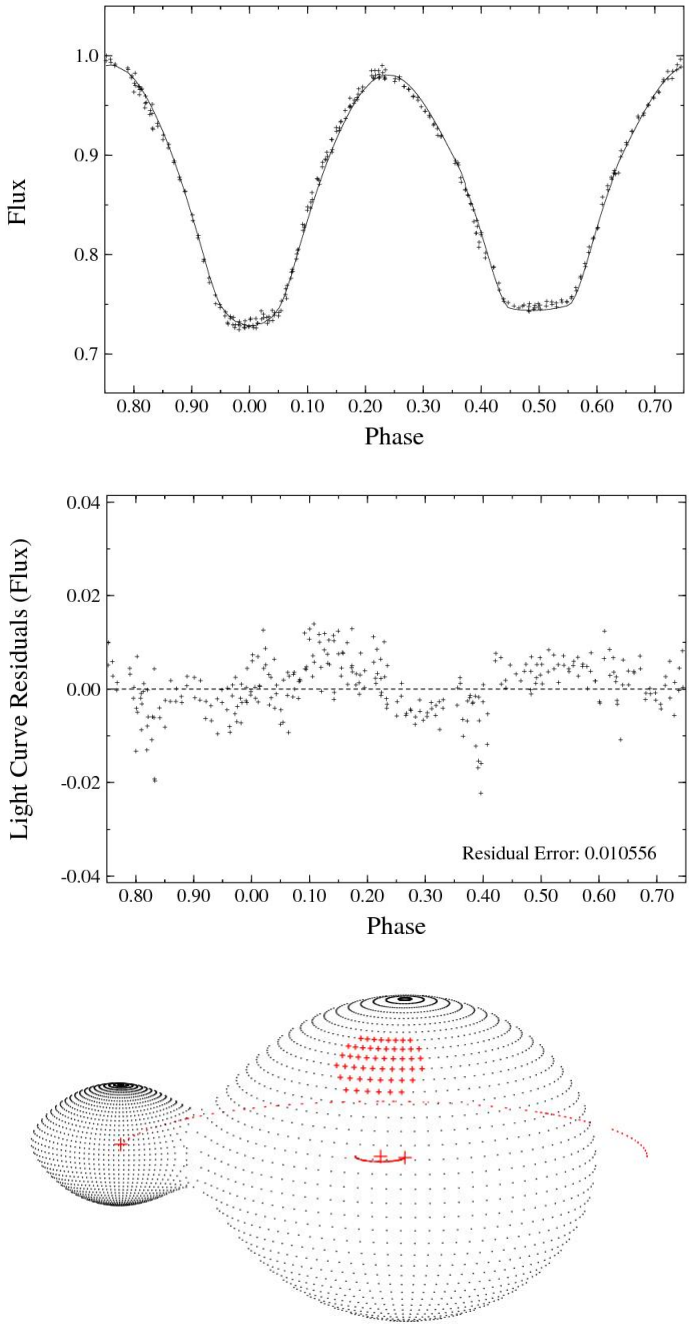

Figure 5.4: Light curve, residuals and rendering of ASAS 015937−0331.0 after modelling with a spot on the primary component. The red area on the primary component is the spot.

5.2.2 ASAS 093818−6755.4

This system has $P_{\mathrm{ASAS}} = 0.389902$ d and a maximum V mag of 10.26. The secondary minimum indicates a total eclipsing system. SuperWASP data are not available for this system thus ASAS data were used for modelling. The light curve of the system, consisting of 710 ASAS data points, is shown in Fig. 5.5. A temperature of T = 5750 K, corresponding to a G-type star, was adopted as the starting temperature for both components.

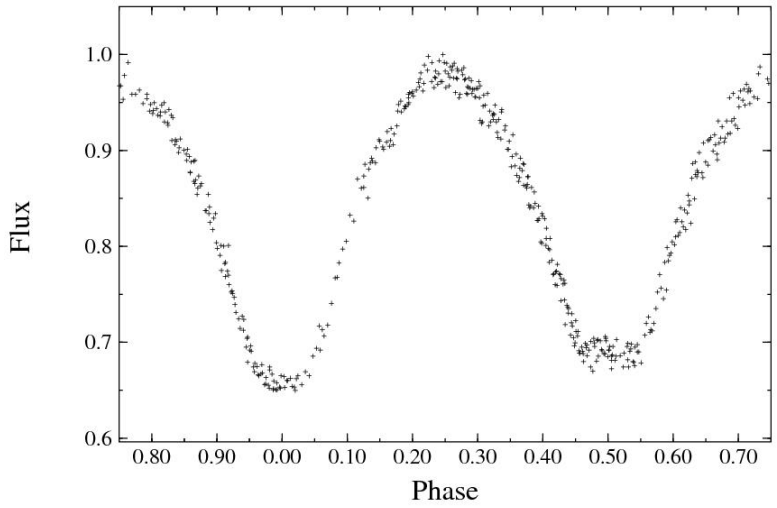

Figure 5.5: Light curve of ASAS 093818−6755.4. The secondary minimum is flat while the scatter around the maxima may be due to changing magnitude or magnetic activity..

Fig. 5.6 shows the synthetic light curve, light curve residuals and rendering of the system. The lowest residual value occurred for the following parameters:

q	$\Omega_{1,2}$	T_1 (K)	T_2 (K)	i (°)
0.169858	2.083254	5750	5760	81.18

The orbital period, $q = 0.169858$ and primary minimum indicate an A-type system while the spectral type is consistent with a W-type system. T_1 and T_2 are similar, making it difficult to assign a subtype classification based on the temperatures. The scatter around the maxima and minima is large. This scatter could be due to time variable magnitude due to magnetic activity (appearance of spots). A spot model was not attempted.

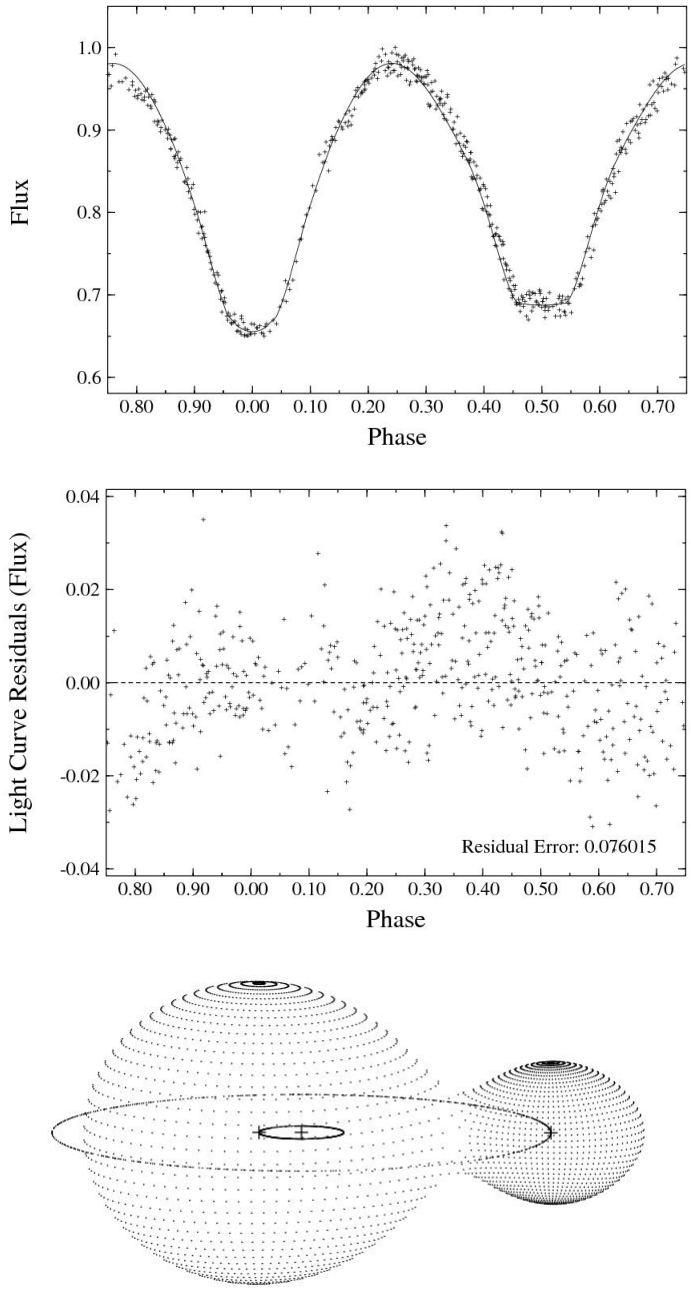

Figure 5.6: Synthetic light curve, residuals and model of ASAS 093818−6755.4. The large residuals value is due to the scatter in data around the maxima and minima.

5.2.3 ASAS 120036−3915.6 ≡ 1SWASP J120036.31−391535.0

The eclipsing contact system ASAS 120036−3915.6 has $P_{\rm ASAS}$ = 0.29267 d and $V_{\rm max}$ = 10.45 mag. An initial model for this system was obtained from BM3 as part of an Honours project. The parameters as determined for the system from BM3 are $q = 0.255$, $\Omega_{1,2} = 2.353273$, $T_1 = 5200$K, $T_2 = 5315$K and $i = 81.2°$. The WASP light curve of the star is shown in Fig. 5.7. The light curve consists of 328 points taken from the following HJDs: 2453860, 2453862, 2453863 and 2453864.

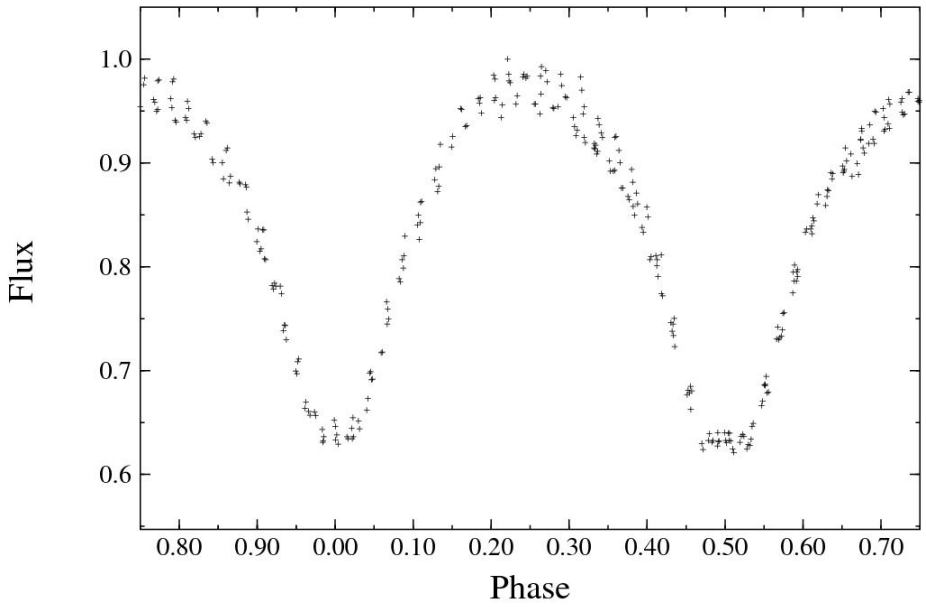

Figure 5.7: WASP light curve of ASAS 120036−3915.6.

The DC mode of PHOEBE was used to refine the BM3 parameters. The lowest residual value occurred for the following parameters:

q	$\Omega_{1,2}$	T_1 (K)	T_2 (K)	i (°)
0.256483	2.363142	5200	5314	79.31

The generated light curve, light curve residuals and rendering of the system are shown in Fig. 5.8. The minimum at phase 0.5 appears to be deeper than the minimum at phase zero

suggesting a W-type system. This subtype is confirmed by the orbital period, spectral type and $T_2 > T_1$. However, the mass ratio of the system is consistent with an A-type system. There is scatter around the maxima and minima which may be due to time varying magnetic activity. A spot model was tested but did not improve the residuals.

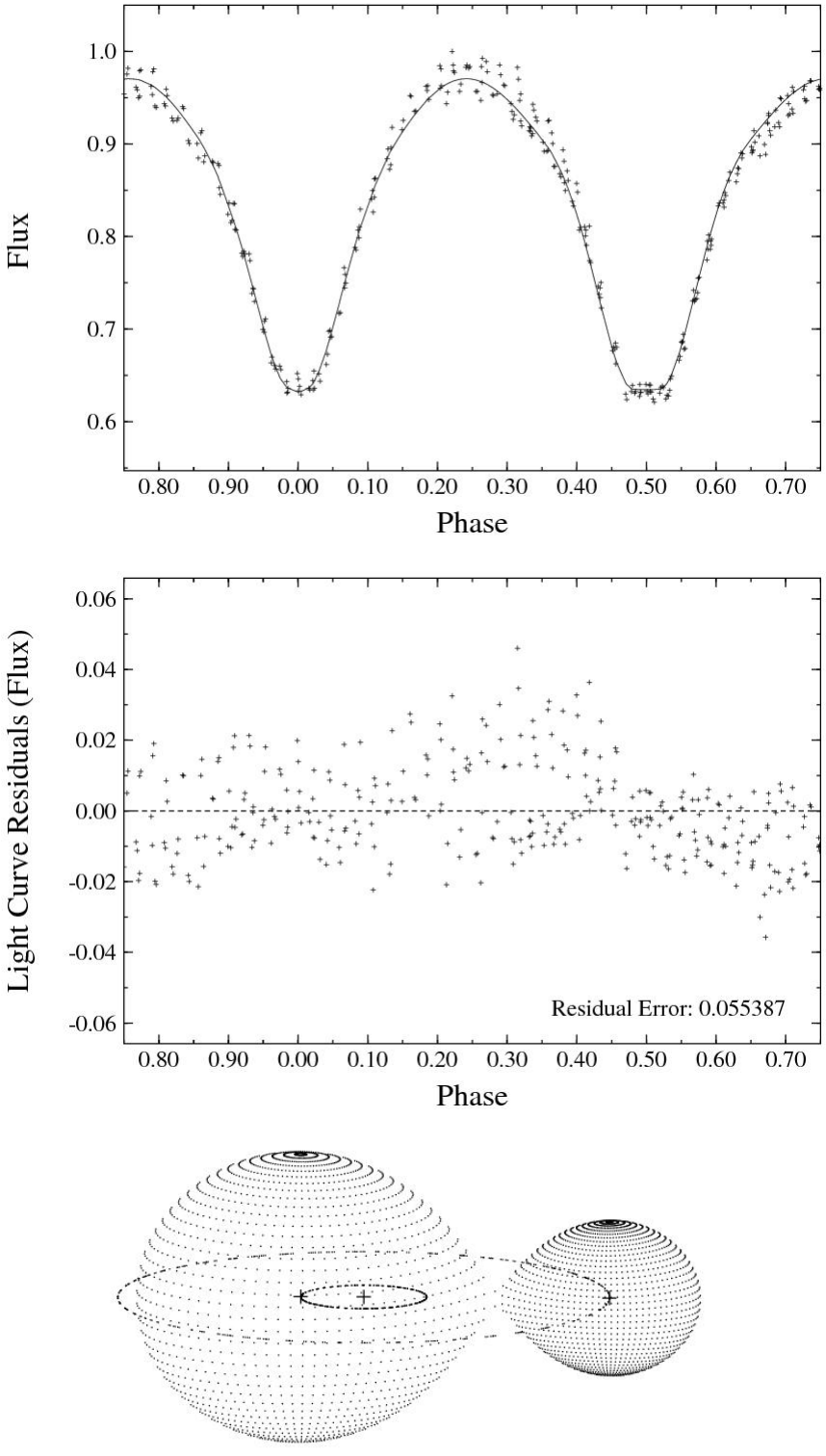

Figure 5.8: Light curve, residuals and model for ASAS 120036−3915.6

5.2.4 ASAS 134841−4012.9 ≡ 1SWASP J134840.90−401251.1

This system has $P_{\rm ASAS} = 0.351299$ d and $V_{\rm max} = 11.44$ mag. The PMD obtained using the ASAS period was smeared, suggesting a changing period for the system. The WASP light curve shown in Fig. 5.9 was obtained using $P = 0.3513195$ d. It consists of 587 points taken from the following HJDs: 2453880, 2453904, 2453905 and 2453906.

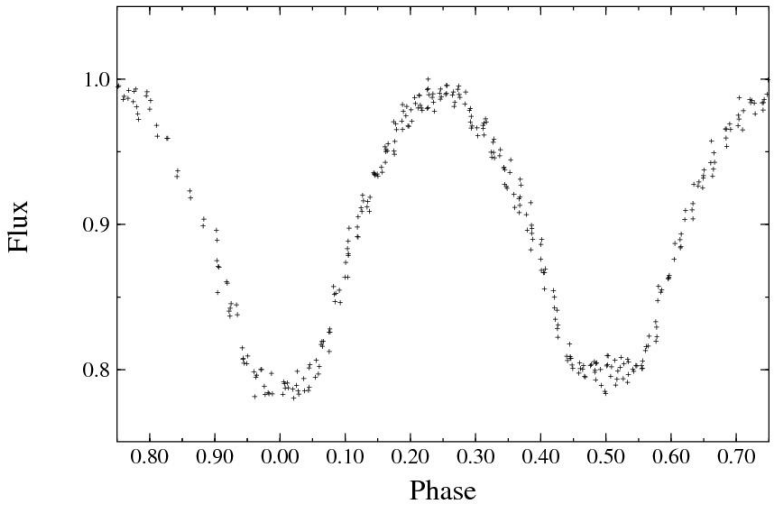

Figure 5.9: Light curve of ASAS 134841−4012.9. It is difficult to determine which minimum is the primary minimum.

A temperature of T = 5941 K (G-type star) was adopted as the starting temperatures for both components. The lowest residual value occurred for the following parameters:

q	$\Omega_{1,2}$	T_1 (K)	T_2 (K)	i (°)
0.086801	1.888422	5941	5974	73.50

Fig. 5.10 shows the synthetic light curve, light curve residuals and model of the system.

The scatter around both minima makes it difficult to determine which minimum is the primary. The spectral type, orbital period and $T_2 > T_1$ indicates a W-type system while the low mass ratio is more consistent with an A-type system.

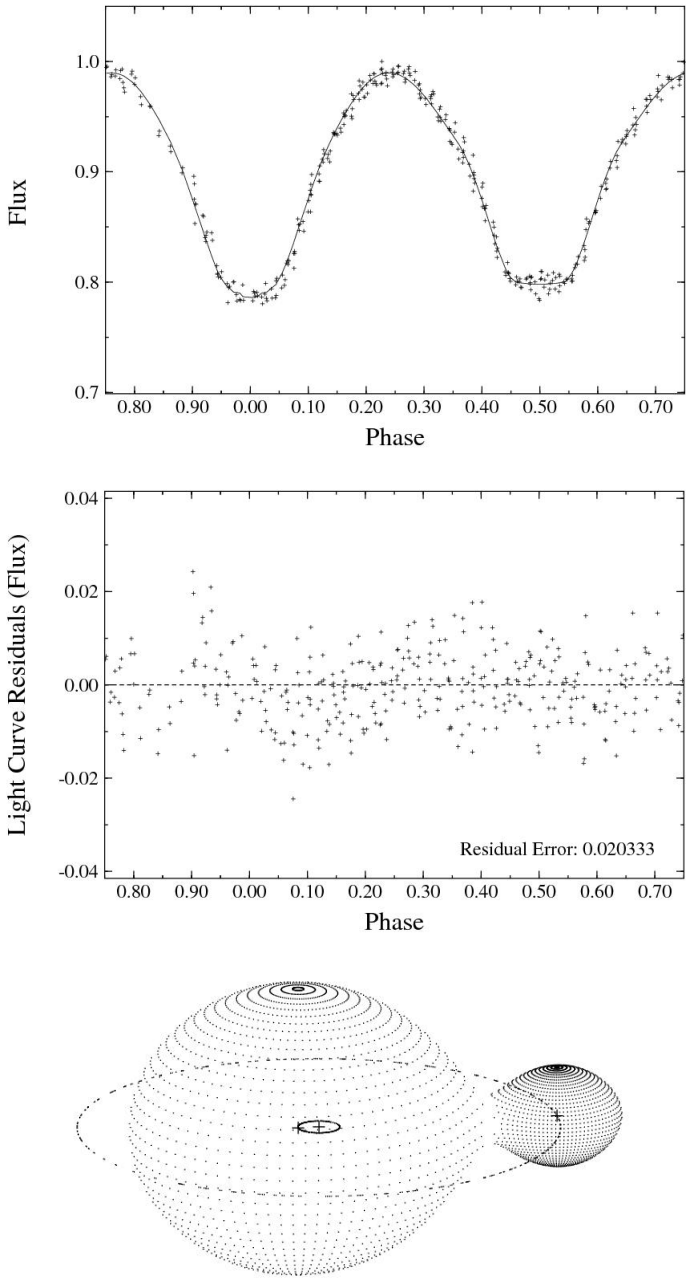

Figure 5.10: Synthetic light curve, residuals and model of ASAS 134841−4012.9.

5.2.5 ASAS 150452−3757.7 ≡ 1SWASP J150452.17−375739.0

This system has $P_{\mathrm{ASAS}} = 0.374131$ d and a maximum V mag of 10.36. This star has been identified as NSV06917. The minimum at phase zero indicates a total eclipsing system. Because the primary minimum is the flat minimum, a phase shift of 0.5 had to be used in PHOEBE so that the total eclipse would occur at the correct phase. The SuperWASP data of the system suggests that the period changed. A new period of $P = 0.3741334$ d was used to create the light curve used for modelling the system. Both components were set to T = 6000 K. The O'Connell effect is seen in some of the light curves obtained from the SuperWASP data, thus two models for the system were obtained: a model for the standard system and a model for when the O'Connell effect was evident.

5.2.5.1 No Spot

The light curve used to model the system is shown in Fig. 5.11. It consists of 248 points taken from the following HJDs: 2454553 and 2454557.

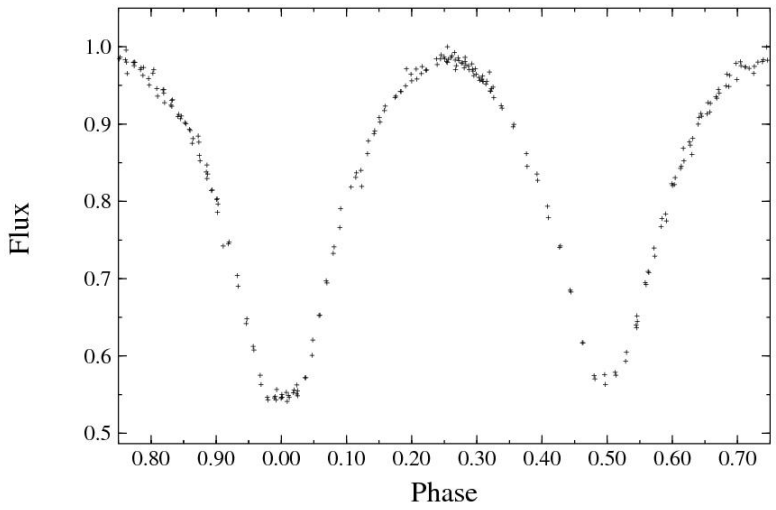

Figure 5.11: Light curve of ASAS 150452−3757.7. The maxima have equal heights.

Fig. 5.12 shows the generated light curve, light curve residuals and model of the system obtained using the parameters corresponding to the lowest residual value.

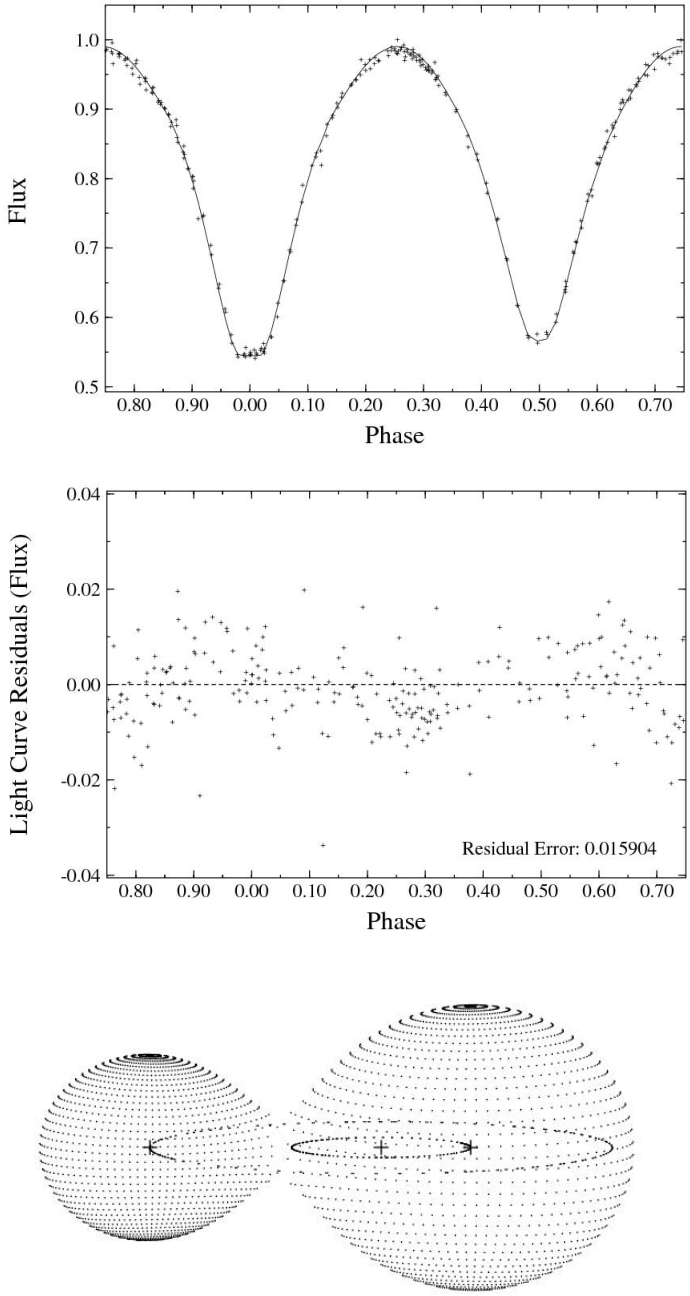

Figure 5.12: Generated light curve, residuals and rendering of ASAS 150452−3757.7.

The best fit parameters are:

q	$\Omega_{1,2}$	T_1 (K)	T_2 (K)	i (°)
0.387213	2.602863	6000	6265	83.55

The orbital period, and parameters obtained from the modelling are typical of a W-type system but the primary minimum suggests an A-type system. The spectral type for the system (late F- early G) suggests either an A- or W-type system.

5.2.5.2 Model with spot

The O'Connell effect is seen in the light curve shown in Fig. 5.13. The light curve consists of 160 points taken from HJDs 2453906 and 2453907. Using the parameters obtained from the modelling, the synthetic light curve does not fit the observed data. This is shown in Fig. 5.14.

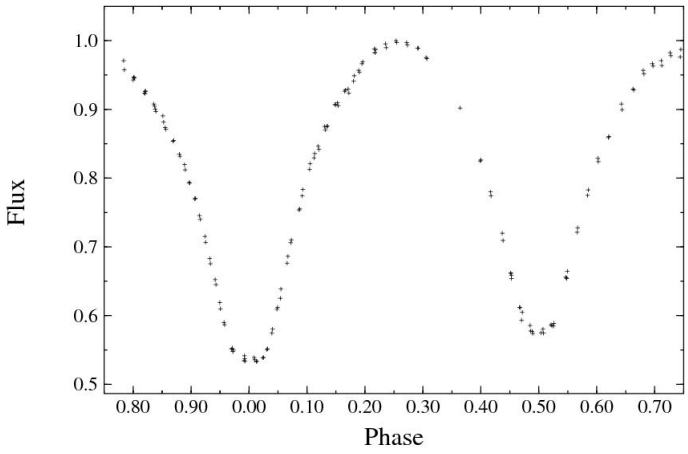

Figure 5.13: Light curve for ASAS 150452−3757.7 displaying the O'Connell effect. The maximum at phase 0.75 lies below a flux of 1.

Using BM3, various spots were tested to try and improve the fit and the residual value. The lowest residual value occurred for a spot of radius 15° and a temperature factor of 1.07 placed on the larger component at a colatitude of 60° and longitude of 30°. The

corresponding light curve, light curve residuals and rendering of the system is shown in Fig. 5.15. While the spot has improved the residuals, the residual value from phase 0.8 − 0.85 is large.

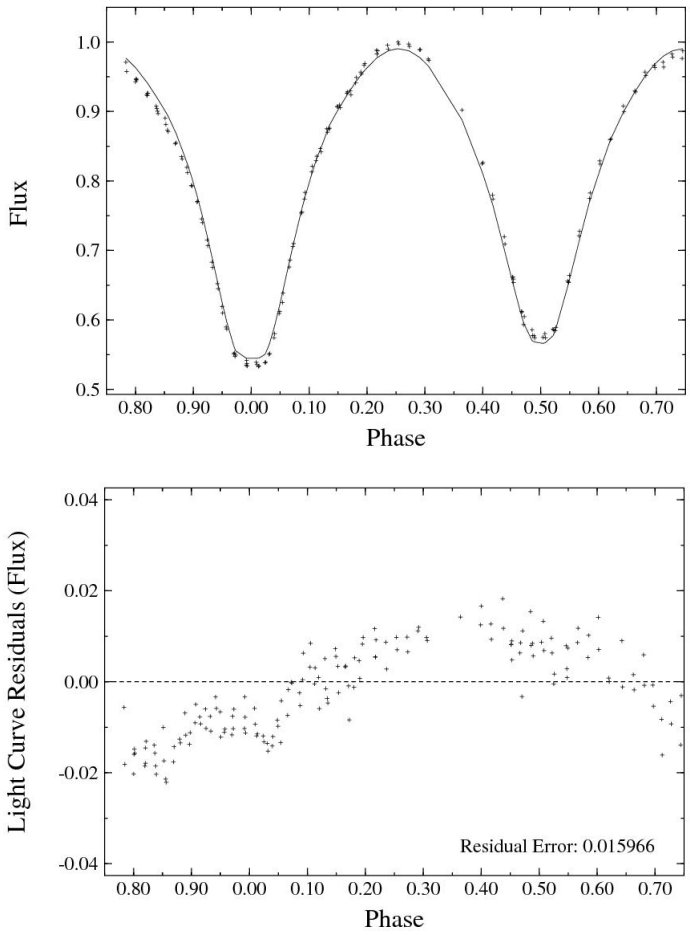

Figure 5.14: Calculated light curve and residuals for ASAS 150452−3757.7 when O'Connell effect is present and the "no spot" parameters are used. The generated light curve does not fit the observed data.

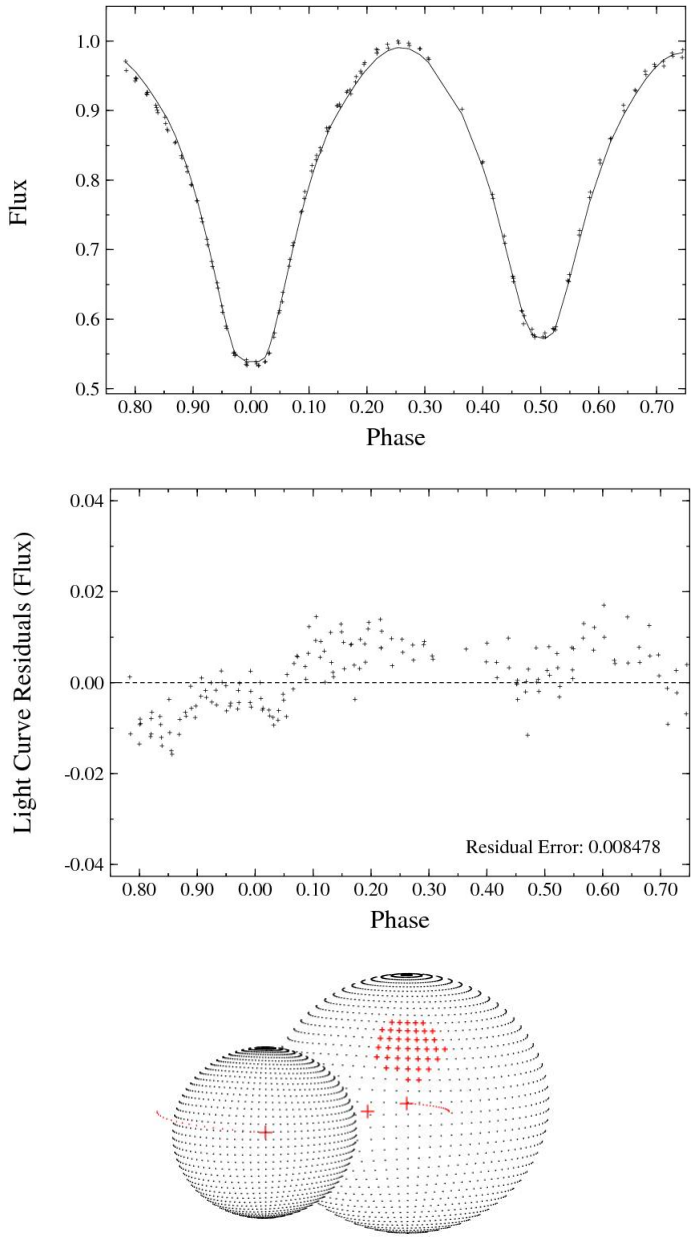

Figure 5.15: Calculated light curve, residuals and model of ASAS 150452−3757.7 obtained when a spot (red area) is placed on the larger component.

5.2.6 ASAS 150934−3348.5 ≡ 1SWASP J150933.60−334830.4

This eclipsing system has $P_{\rm ASAS} = 0.360320$ d and $V_{\rm max} = 10.10$ mag. This system has been identified as NSV06959. The SuperWASP data suggest that the period of the system changed. The light curve used to model the system was obtained using $P = 0.360317$ d. The light curve is shown in Fig. 5.16. It consists of 295 points taken from HJDs 2453880, 2453881 and 2453890. A temperature of T = 5850 K (G-type star) was adopted as the starting temperature of both components.

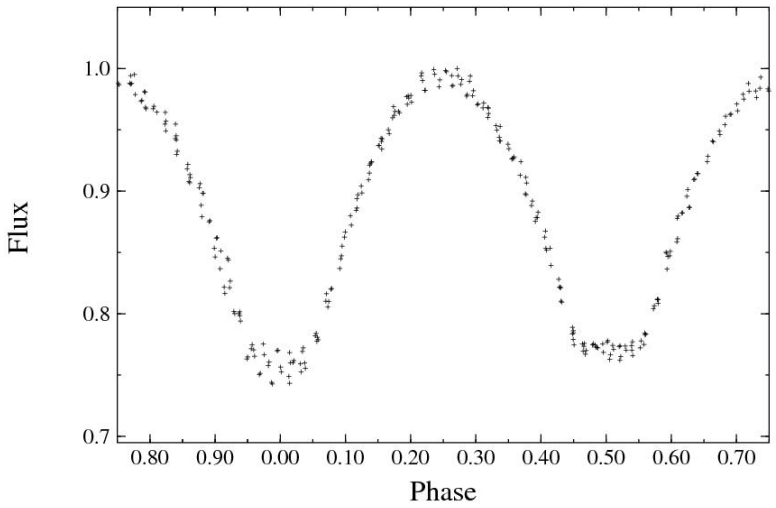

Figure 5.16: Light curve of ASAS 150934−3348.5. The primary minimum appears to be the minimum at phase zero but the scatter around the minimum makes it difficult to decide which minimum is the primary minimum.

The best fit occurred for the following parameters:

q	$\Omega_{1,2}$	T_1 (K)	T_2 (K)	i (°)
0.118772	1.987656	5850	5832	83.55

Fig. 5.17 shows the synthetic light curve, corresponding residuals and model of the system. The fit from phase 0.3 to 0.5 is not good. Some of the light curves obtained from the SuperWASP data show the minimum at phase zero varying in depth. This could explain the scatter at that phase seen in Fig. 5.16. The scatter makes it difficult to determine

which minimum is the primary minimum. With $T_1 > T_2$ and $q < 0.3$, the system would be classified as an A-type while the spectral type and period indicate a W-type.

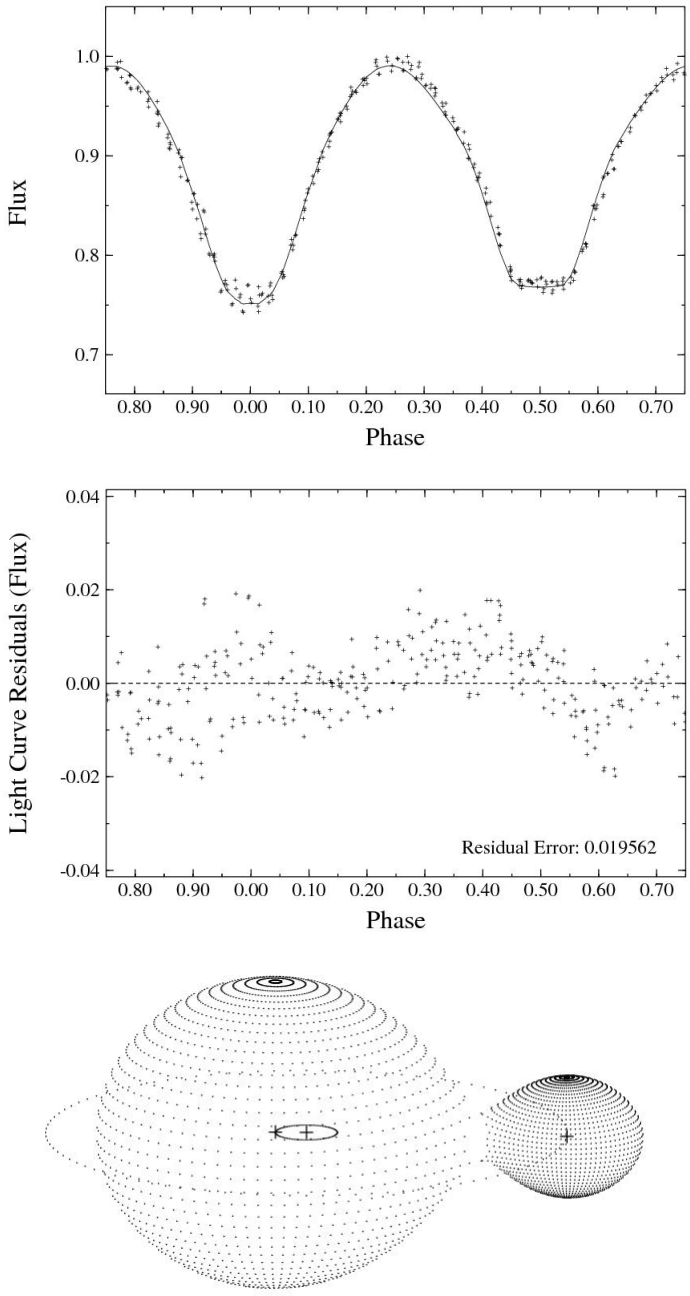

Figure 5.17: Generated light curve, residuals and rendering of ASAS 150934−3348.5.

5.3 Discussion

The models of six total eclipsing ASAS contact binaries are presented. The parameters of the binary stars are listed in Table 5.1.

Three systems, namely ASAS 015937−0331.0, ASAS 093818−6755.4 and ASAS 150452−3757.7, are classified as A-type systems based on the observed primary minimum for each star. For the other three EC systems, subtype classifications based on the observed primary minimum is difficult due to scatter in the data around the minimum. Three systems are modelled with q less than 0.25 and f values larger than 50%: ASAS 015937 − 0331.0, ASAS 093818−6755.4 and ASAS 134841−4012.9. Based on the work by Shengbang et al. (2006), these systems would be classified as low-mass ratio, deep contact binaries. The authors argue that these types of binaries may evolve into Blue Straggler or FK Com-type stars and that the period changes that occur in these systems may be important in understanding how contact binaries merge. They obtained photometric observations of 12 deep, low-mass ratio contact binary stars. Of the stars they studied, GSC 619-232 has the largest fillout value (93.4%). The photometric model of ASAS 015937 − 0331.0 has q less than 0.1 and $f = 97\%$ which would make it a very deep contact binary. Compared to this, the photometric model for ASAS 120036−3915.6 has $f = 3\%$ which is very low. This system may be a shallow contact system and could be a relatively young contact binary. Both of these systems are very interesting and will continue to be monitored using the SuperWASP data.

The residual values of two EC systems, ASAS 015937−0331.0 and ASAS 150452−3757.7, were improved with the inclusion of a spot. Modelling with spots is unreliable as different combinations of spots can produce the same light curves. Therefore, the spot models of these two systems should be considered as possible spot models.

The lowest residual values, and thus the best fits, are those of the photometric models for ASAS 015937 − 0331.0 and ASAS 150452-3757.7. Although the light curve for ASAS 015937−0331.0 displays the O'Connell effect, the light curve of the star appears to remain fairly constant as there is little scatter around the minima and maxima. The spot model for ASAS 150452-3757.7 has a low residual value, but this is also due to the small number of data points used to create the PMD. The light curves of the other EC systems display

	ASAS ID					
	015937−0331.0	093818−6755.4	120036−3915.6	134841−4012.9	150452−3757.7	150934−3348.5
q	0.094203	0.169858	0.256483	0.086801	0.387213	0.118772
f	97%	67%	03%	51%	21%	36%
$\Omega_{1,2}$	1.881519	2.083254	2.363142	1.888422	2.602863	1.987656
T_1(K)	6624	5750	5200	5941	6000	5850
T_2 (K)	6824	5760	5314	5974	6265	5832
i (°)	77.98	81.18	79.31	73.50	83.55	83.55
Spot: Temp Factor	1.05	–	–	–	1.07	–
Radius (°)	15	–	–	–	15	–
Longitude (°)	90	–	–	–	30	–
Colatitude (°)	45	–	–	–	60	–
LC Residual	0.010556	0.076015	0.055387	0.020333	0.008478	0.019562

Table 5.1: Table of parameters for the modelled systems. q is the mass ratio, f the fillout value (in percent), $\Omega_{1,2}$ are the omega potentials of the two components, T_1 and T_2 the temperatures of the two components, and i the inclination angle of the system. Spot parameters are also listed (where applicable). The light curve residual value for each star is listed.

scatter around the minima and/or maxima. Although the light curve residual values for the modelled EC systems depends on the number of points used, the variations in the light curves affects the residual values. Some of the light curves are smeared suggesting changes in orbital period. This smearing will also affect the calculated residual values.

The photometric models of the selected ASAS EC systems presented here should be considered as possible models of the systems. Radial velocity measurements are needed to determine the mass ratios of the systems. A combination of spectroscopic and SuperWASP photometric data can be used to construct more reliable/accurate models of the systems.

Chapter 6

Period Analysis

Some W UMa-type variable stars are known to undergo changes in orbital period. The changes may be a result of conservative mass exchange or due to the LTTE. By monitoring the orbital period, it is possible to determine if the period is changing and the rate at which the period changes. Changes in orbital period can be inferred from an Observed minus Calculated (O−C) diagram. This chapter describes how O−C diagrams provide information regarding changes in orbital period. Eight contact binaries were selected for period analysis. The selection process, method of analysis and the results of the analyses are presented.

6.1 Theory

For a periodically variable star, the expected time of minimum T_{Exp} is defined by

$$T_{Exp} = T_0 + \epsilon P \tag{6.1}$$

where T_0 is a reference time of a flux minimum,ϵ is the number of cycles since T_0 and P is the period.

The cycle number ϵ can be calculated using P, T_0 and an observed time of minimum T_{Obs}:

$$\epsilon = \frac{T_{Obs} - T_0}{P} \tag{6.2}$$

where T_{Obs} is an observed time of minimum brightness determined experimentally from the light curve of the star.

By comparing the observed times of minima with the expected or calculated times, an observed minus calculated (O−C) diagram is obtained. That is

$$(O - C) = T_{Obs} - T_{Exp} = T_{Obs} - T_0 - \epsilon P \tag{6.3}$$

Because of timing measurement errors, the O−C values for a star with constant P scatter about a straight line on a graph of O−C versus time. Scatter in the O−C values can also be caused by changes in the system such as star spots, a third companion or changes in angular momentum. If the period P of the system and the time of reference T_0 are correct, the slope of the line is zero and all points will be scattered about O−C equal to zero. If the slope is positive, the real period of the system is longer than the period used to calculate T_{Exp} while if the slope is negative, the real period is shorter (Sterken 2005). If the shape of the O−C diagram is parabolic, the change in period is linear with time. When the time of reference is incorrect and the period is correct, the values of O−C will be scattered about a straight line that is shifted either above or below the x-axis. If both the reference time of minimum and period are incorrect, the O−C values will be scattered around a line offset from zero with the data following a negative or positive slope. Examples are shown in Fig. 6.1. The plots presented in the diagram represent the following conditions:

- Circles: Correct P, Correct T_0
- Squares: Shorter assumed P, Correct T_0
- Triangles: Longer assumed P, Correct T_0
- Plus signs: Correct P, Incorrect T_0
- Dashes: Incorrect P, Incorrect T_0

The diagram has been exaggerated to show the effects of the different situations. If a third body is present, the O−C diagram will display an oscillation as shown in Fig. 6.2. The oscillation must be strictly periodic and additional bodies in the system add additional oscillations.

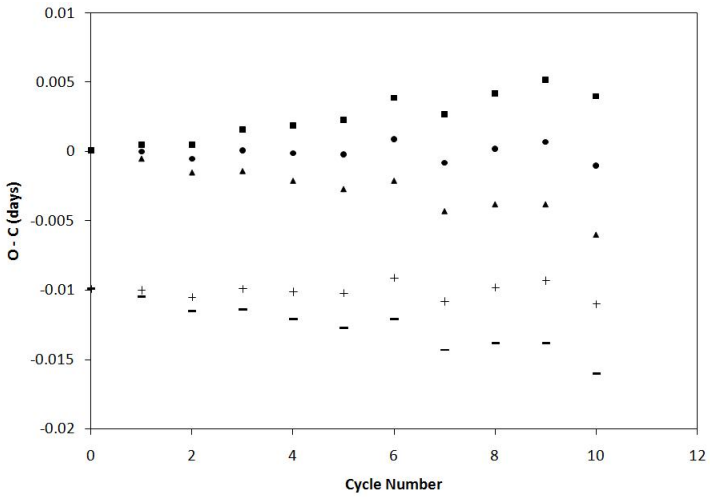

Figure 6.1: O−C diagram showing the different effects that the period and reference time of minimum have if the assumed values are correct or incorrect.

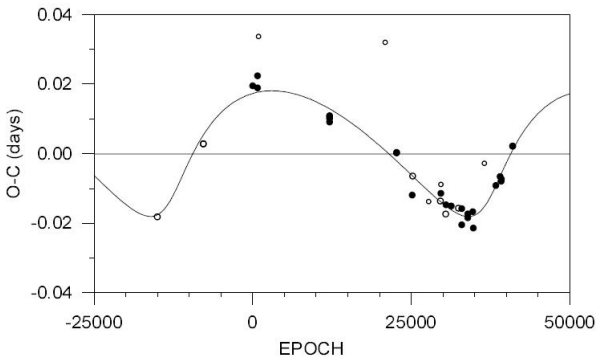

Figure 6.2: O−C diagram of Y Sextantis, taken from Wolf et al. (2000). The authors argue that the variation is consistent with a third body orbit.

If data covering months or years are available, it is possible to determine if the period is changing.

6.2 Method of Analysis

6.2.1 Selection Process & Observed Times of Minimum

Systems that were selected for period analysis included the following:

1. Systems selected for modelling in Chapter 5 that have SuperWASP data.
2. ASAS EC systems identified by Pilecki et al. (2007) as having high period change rates and for which SuperWASP data are available.
3. RW Com: An EW system that has SuperWASP data and an established dP/dt value. RW Com was selected to be used as a check on the SuperWASP data and method of analysis.

One exception to the first two criteria is ASAS 002328 − 2041.8. The brightness of the system is seen to decrease and then return to its normal level (see section 6.3) and was selected for analysis to see if there is any correlation between changes in brightness and orbital period. For each system selected, the light curves were inspected to identify if they were total eclipsing systems. This was particularly important as the non-total eclipsing minimum was used for the period analysis. Techniques needed to determine the time of minimum, T_{min}, for a flat minimum were not developed for this dissertation. The following systems were selected for period analysis: RW Com, ASAS 002328 − 2041.8, ASAS 002449 − 2744.3, ASAS 002821 − 2904.1, ASAS 052851 − 3010.2, ASAS 120036 − 3915.6, ASAS 150452 − 3757.7 and ASAS 150934 − 3348.5.

Due to the geometry of EW systems, the minima should be symmetrical in shape. In the case of a minimum that is not flat, for a small phase-interval about the minimum, the minimum can be considered to be parabolic in shape. Therefore, to determine the time of minimum, a second order polynomial can be used to fit the data. It is known that for some EW systems, the minima display asymmetry due to the presence of a spot on either the primary or secondary component. In these cases, a third order polynomial can be used to find the time of minimum. Rovithis-Livaniou et al. (2003) examined the

effects of cool spots in close eclipsing binaries. They showed that spots not only affect the light curve of an eclipsing binary outside of the eclipses but, depending on the size and location of the spot, can produce asymmetrical minima which are notably shifted away from their respective phases. They modelled a spot on the primary and secondary components and looked at the effect the spot had on the minima of the generated light curves. To demonstrate the effects they found, a binary star was modelled using BM3. A spot with an angular diameter of 20° and a temperature factor of 0.9 (based on typical spot values for W UMa-type systems) was first placed on the larger component then on the smaller component. Synthetic light curves were generated and are shown in Fig. 6.3. The shift in the observed time of minimum is quite noticeable for a spot on the larger component while a spot on the smaller component does not affect the shape of the minimum. Note that the direction of the shift indicates an approximate location of the spot. For the systems selected for period analysis, T_{min} for asymmetric minima were not used. Such systems were noted for further spot analysis.

For this project, the data on separate HJDs were looked at for each system. Minima that were selected had to fulfill the following criteria:

1. The minimum is not flat.
2. There are enough data around the minimum, at least a coverage of 0.05 to 0.07 phase around either side of T_{min}.

To obtain the time of minimum for a flat minimum would require complete coverage of ingress and egress of the total eclipse portion of the light curve. This in turn requires a large number of data points. For the total eclipsing systems, there was not enough coverage of the flat minima and since no method to determine T_{min} was developed, it was decided not to use these minima for the period analysis. The motive for the second criterion stems from the method that was used to obtain the times of minimum. The method that is widely used to obtain the time of minimum of an EW star is the method of Kwee & van Woerden (1956).

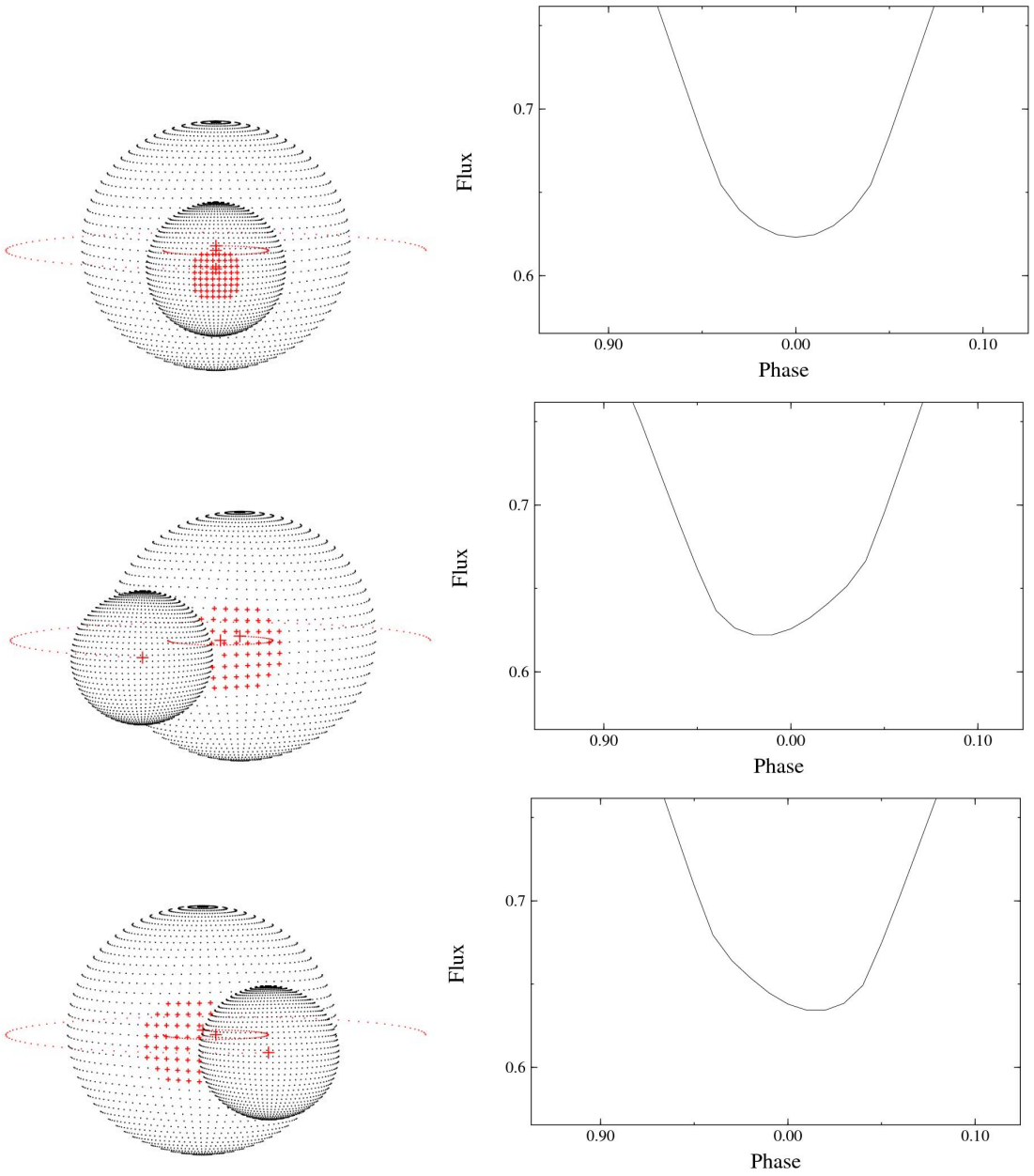

Figure 6.3: Light curves displaying the effect a spot has on the shape of the minimum at phase zero. The effect is most noticeable for a spot on the primary component.

Times of minima are obtained by fitting a second order polynomial to data within a certain phase interval around the minimum, thus assuming a symmetric light curve. For asymmetric minima, the method described can be adjusted so that the asymmetry is

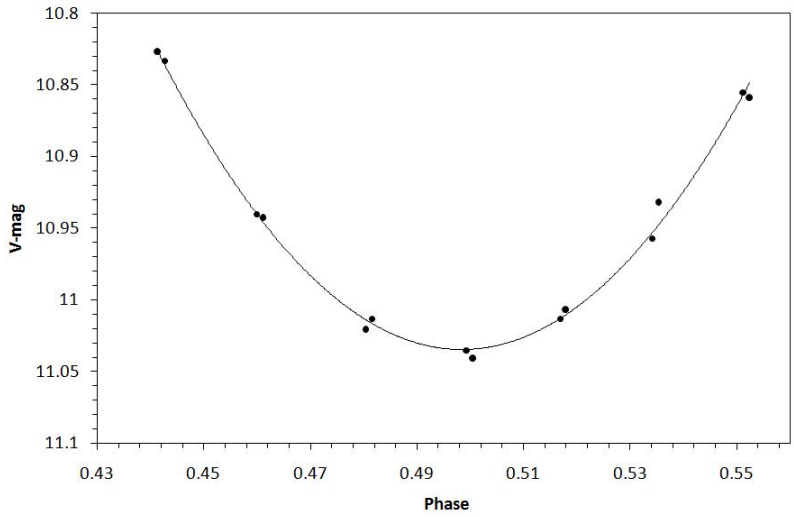

Figure 6.4: Example of a parabolic fit to a minimum of an eclipsing binary.

included when T_{min} is determined. According to Kwee & van Woerden (1956), all phases of the eclipse should be used in order to determine T_{min}. When fitting a second order polynomial, it is important to select a phase interval around the minimum that is parabolic in shape.

In order to determine the range in phase that could be used, a test was conducted. An EW system with well sampled minima was selected. Second order polynomials were fitted to phase intervals of 0.05 to 0.1 around T_{min}. The results of the fits, the regression and the values of R^2 (the correlation coefficient) indicated that a phase interval of 0.05 to 0.07 around T_{min} corresponded to the parabolic part of the minimum. An example of the parabolic fit used is shown in Fig. 6.4.

Primary minima (Min. I) were used for the period analysis with the exception of ASAS 150452−3757.7 for which the secondary minimum (Min. II) was used. For each system, once minima were identified and data corresponding to a specific phase interval were selected, the data were imported into Mathematica[1]. The data were fit with a parabola and the time of minimum was obtained by using the built-in function "FindMinimum". The data were regressed so that the coefficients of the best fit parameters and the covariance matrix could be obtained.

[1]License No L2707-7388, registered to the Department of Mathematical Sciences, UNISA

The equation of the best fit parabola is $Flux = at^2 + bt + c$, thus the time of minimum of the parabola is given by $T_{min} = \frac{-b}{2a}$. The error on the minimum was calculated using

$$\mathrm{Var}\left(T_{min}\right) = \frac{b^2}{4a^4}\mathrm{Var}(a) + \frac{1}{4a^2}\mathrm{Var}(b) - \frac{b}{2a^3}\mathrm{Cov}(a,b) \tag{6.4}$$

where a and b are the parameters of the best fit parabola. The variance of a variable x is defined as

$$\mathrm{Var}(x) = \sigma_x^2 = \frac{1}{n}\sum_{i=1}^{n}(x_i - \overline{x})^2 \tag{6.5}$$

and the covariance of two variables x and y is defined as

$$\mathrm{Cov}(x,y) = \sigma_{xy} = \frac{1}{n}\sum_{i=1}^{n}(x_i - \overline{x})(y_i - \overline{y}) \tag{6.6}$$

$\mathrm{Var}(a)$ and $\mathrm{Var}(b)$ are diagonal entries of the covariance matrix obtained from Mathematica, while $\mathrm{Cov}(a,b)$ is an off-diagonal entry.

For each system, the cycle numbers were obtained using eqn. (6.2) and T_0 is an observed minimum from the SuperWASP data. Using the cycle numbers, T_0 and the ASAS period of the system, an O−C diagram was created. If there was evidence of a period change in the O−C diagram, a least squares analysis was performed to determine a new period for the system. The errors on the determined times of minimum brightness were used as weights in the analysis.

Because there are seasons when SuperWASP collects data towards a particular position, the data of the different seasons were analysed separately. For each season or subset of data, the T_0 used to calculate the cycle number ϵ is a time of minimum belonging to the subset. For each system, a new period and ephemeris were determined. If data for a system were analysed in separate subsets, a value for $\frac{\Delta P}{\Delta t}$ was calculated, where ΔP is the period difference, in days, between the subsets and Δt is the difference in years between T_{Mid} of each subset. T_{Mid} is given by

$$T_{mid} = T_{Start} + \left(\frac{T_{End} - T_{Start}}{2}\right)$$

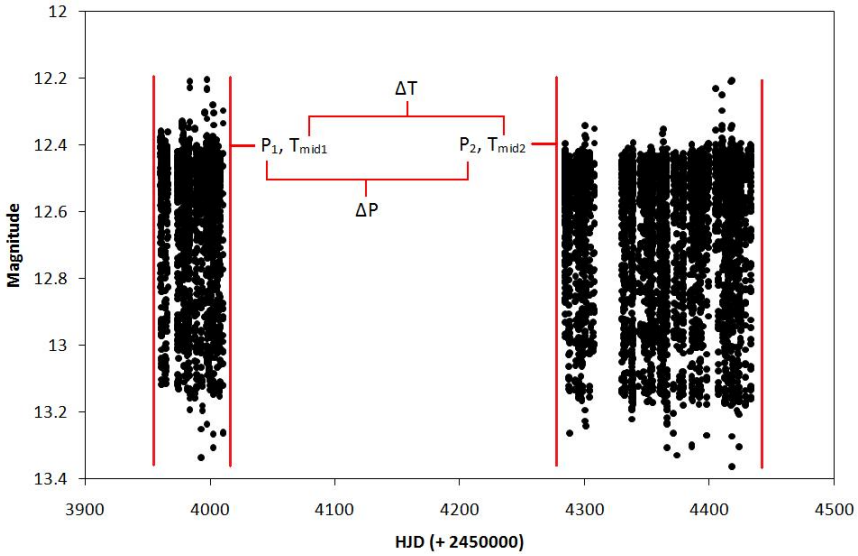

Figure 6.5: Example of how $\frac{\Delta P}{\Delta t}$ is calculated using the subsets of SuperWASP data.

where T_{Start} and T_{End} are the first and last observation times (in HJD) of the subset. $\frac{\Delta P}{\Delta t}$ is a measure of how much the period has changed over an interval of time and is not necessarily the instantaneous rate of change of the period $\left(\frac{dP}{dt}\right)$. An example of how $\frac{\Delta P}{\Delta t}$ is calculated is shown in Fig. 6.5.

The results of the O−C analysis for the selected systems are presented in the following section.

6.3 Results of Analysis

6.3.1 RW Com

RW Com is known to undergo changes in orbital period. Qian (2002) and Liu & Yang (2003) determined dP/dt values of -6.06×10^{-8} d yr^{-1} and -0.43×10^{-7} d yr^{-1} for RW Com respectively. Qian noted weak evidence of a small-amplitude oscillation (P about 13.3 years) superimposed on the secular decrease, while Liu & Yang noted the presence of an oscillation with an amplitude $\Delta P = 5.4 \times 10^{-7}$ d and a period of $P = 13.7$ years. For

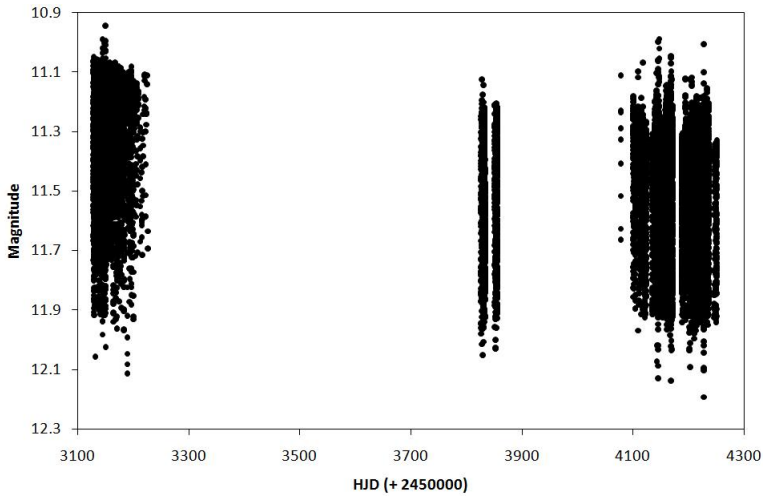

Figure 6.6: Plot of the SuperWASP data of RW Com.

this paper, this additonal oscillation was ignored considering that the star was observed over a short time period. The system has $P_{\rm ASAS} = 0.237348$ d. The SuperWASP data are shown in Fig. 6.6.

The following ephemeris was determined from the analysis of the first subset of data covering HJD 2453129.5826 to HJD 2453193.4296

$$\text{Min. I} = \text{HJD } 2453179.4264(07) + 0.2373499(06)\epsilon \tag{6.7}$$

with the uncertainty of the last figures listed in brackets. The period returned by the analysis is consistent with the period determined by Qian. The plot of the O−C residuals for the first subset of data, obtained using equation (6.7), is shown in Fig. 6.7. A quadratic ephemeris does not improve the residuals. The observed times of minimum for the first subset are listed in Table 6.1. Only 5 usable minima were obtained from the interval covering HJD 2453827 − 2453856 so a period analysis was not performed.

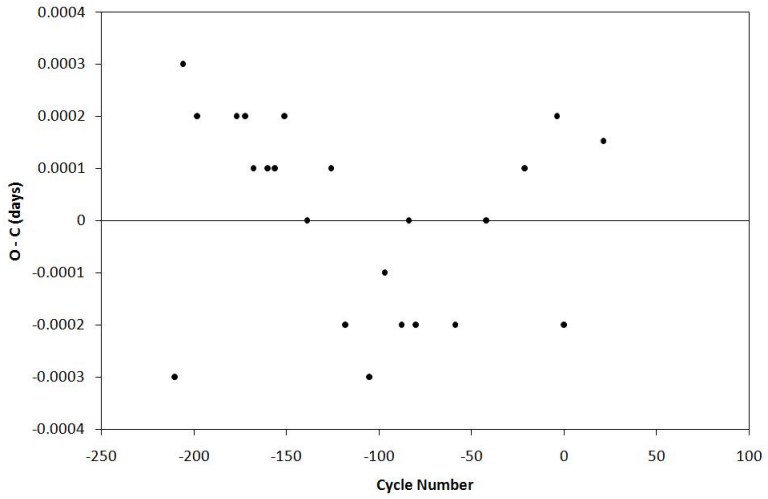

Figure 6.7: O−C residuals for the first subset of data of RW Com.

For the second subset of data, HJD 2454120.7443 to HJD 2454251.522, the following ephemeris was determined:

$$\text{Min. I} = \text{HJD } 2454195.5081(05) + 0.2373447(03)\epsilon \tag{6.8}$$

The period determined from the analysis is consistent with the period determined by Liu & Yang. Fig. 6.8 shows the plot of the O−C residuals obtained using the above ephemeris. A quadratic ephemeris does not improve the residuals. The observed times of minimum for the second subset are listed in Table 6.2.

From subset 1 to subset 2, $\frac{\Delta P}{\Delta t} = -0.19 \times 10^{-5}$ d yr^{-1}. This is larger than the values determined by Qian and Liu & Yang; however they used a quadratic ephemeris from which they obtained their respective values of dP/dt.

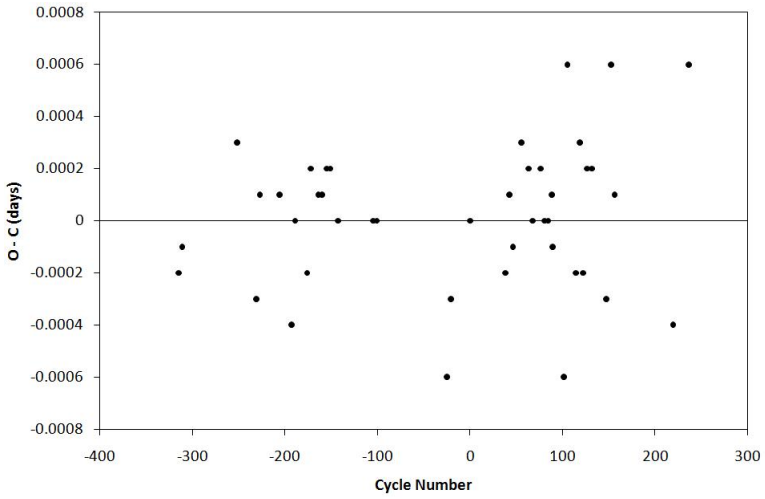

Figure 6.8: O−C residuals for the second subset of data of RW Com.

Cycle Number ϵ	Observed +2450000 (HJD)	Calculated +2450000 (HJD)	O − C (d)
−210	3129.5826(29)	3129.5829	−0.0003
−206	3130.5326(16)	3130.5323	0.0003
−198	3132.4313(04)	3132.4311	0.0002
−177	3137.4157(04)	3137.4155	0.0002
−172	3138.6024(03)	3138.6022	0.0002
−168	3139.5517(07)	3139.5516	0.0001
−160	3141.4505(02)	3141.4504	0.0001
−156	3142.3999(02)	3142.3998	0.0001
−151	3143.5868(30)	3143.5866	0.0002
−139	3146.4348(05)	3146.4348	0.0000
−126	3149.5204(02)	3149.5203	0.0001
−118	3151.4189(06)	3151.4191	−0.0002
−109	3153.5548(09)	3153.5553	−0.0005
−105	3154.5044(10)	3154.5047	−0.0003
−97	3156.4034(15)	3156.4035	−0.0001
−88	3158.5394(09)	3158.5396	−0.0002
−84	3159.4890(18)	3159.4890	0.0000
−80	3160.4382(03)	3160.4384	−0.0002
−59	3165.4226(03)	3165.4228	−0.0002
−42	3169.4577(16)	3169.4577	0.0000
−21	3174.4422(02)	3174.4421	0.0001
−4	3178.4772(48)	3178.4770	0.0002
0	3179.4262(03)	3179.4264	−0.0002
21	3184.4109(16)	3184.4107	0.0001
59	3193.4296(14)	3193.4300	−0.0005

Table 6.1: List of cycle numbers, observed times of minimum, calculated times of minimum (obtained using the ephemeris returned from the analysis) and O−C values for the first subset of data of RW Com.

Cycle Number ϵ	Observed +2450000 (HJD)	Calculated +2450000 (HJD)	O − C (d)
−315	4120.7443(05)	4120.7445	−0.0002
−311	4121.6937(02)	4121.6938	−0.0001
−252	4135.6975(16)	4135.6972	0.0003
−231	4140.6811(06)	4140.6814	−0.0003
−227	4141.6309(35)	4141.6308	0.0002
−206	4146.6151(04)	4146.6150	0.0001
−193	4149.7001(08)	4149.7005	−0.0004
−189	4150.6499(06)	4150.6499	0.0000
−176	4153.7352(01)	4153.7354	−0.0002
−172	4154.6850(02)	4154.6848	0.0002
−164	4156.5836(01)	4156.5835	0.0001
−160	4157.5330(11)	4157.5329	0.0001
−155	4158.7198(02)	4158.7196	0.0002
−151	4159.6692(04)	4159.6690	0.0002
−143	4161.5678(05)	4161.5678	0.0000
−105	4170.5869(06)	4170.5869	0.0000
−101	4171.5362(06)	4171.5362	0.0000
−25	4189.5738(12)	4189.5744	−0.0006
−21	4190.5235(05)	4190.5238	−0.0003
0	4195.5081(05)	4195.5081	0.0000
38	4204.5269(03)	4204.5271	−0.0002
42	4205.4766(02)	4205.4765	0.0001
46	4206.4258(02)	4206.4259	−0.0001
55	4208.5623(24)	4208.5620	0.0003
63	4210.4610(08)	4210.4608	0.0002
67	4211.4101(01)	4211.4101	0.0000
76	4213.5464(08)	4213.5462	0.0002
80	4214.4956(05)	4214.4956	0.0000
84	4215.4450(03)	4215.4450	0.0000
88	4216.3945(02)	4216.3944	0.0001
89	4216.6316(11)	4216.6317	−0.0001
101	4219.4793(29)	4219.4799	−0.0006
105	4220.4298(05)	4220.4292	0.0006
114	4222.5651(05)	4222.5653	−0.0002
118	4223.5150(10)	4223.5147	0.0003
122	4224.4639(01)	4224.4641	−0.0002
126	4225.4137(02)	4225.4135	0.0002
131	4226.6004(04)	4226.6002	0.0002
147	4230.3974(02)	4230.3977	−0.0003
152	4231.5850(09)	4231.5844	0.0006
156	4232.5339(07)	4232.5338	0.0001
219	4247.4861(27)	4247.4865	−0.0004
236	4251.5220(22)	4251.5214	0.0006

Table 6.2: Observed times of minimum for the second subset of data of RW Com.

6.3.2 ASAS 002449−2744.3 ≡ 1SWASP J002449.36−274418.9

Presented by Pilecki et al. (2007) as a high period change rate system with $P = 0.313661$ d and $\mathrm{dP/dt} = -0.23(5) \times 10^{-5}$ d yr^{-1}, this system is listed with an ASAS period of $P = 0.31367$ d. Fig. 6.9 shows a plot of the SuperWASP data.

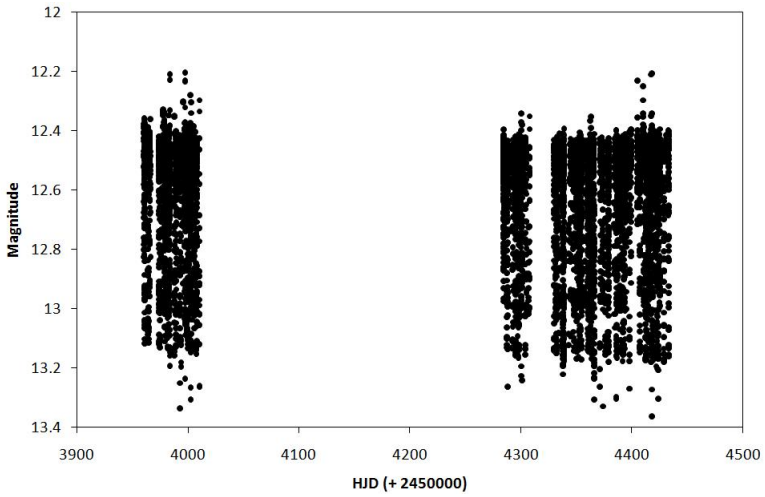

Figure 6.9: Plot of the SuperWASP data of ASAS 002449−2744.3.

For the first subset of data, from HJD 2453960.5484 to HJD 2454008.5378, the following ephemeris was determined:

$$\text{Min. I} = \text{HJD } 2453961.4891(01) + 0.313659(03)\epsilon \tag{6.9}$$

The plot of the O−C residuals for the first subset of data is shown in Fig. 6.10 and the observed times of minimum brightness are listed in Table 6.3.

Fig. 6.11 shows the O−C diagram for the second subset of data (HJD 2454294.5952 to HJD 2454416.2962), obtained using the ASAS period. The diagram appears to have a parabolic shape.

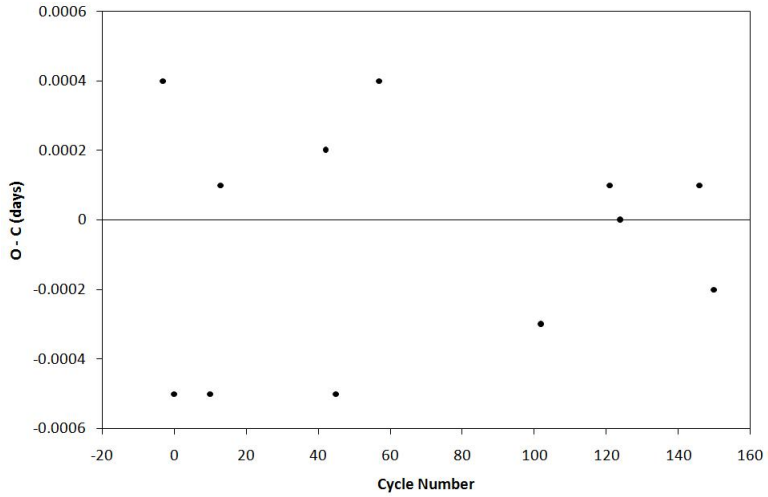

Figure 6.10: O−C residuals for first subset of data of ASAS 002449−2744.3.

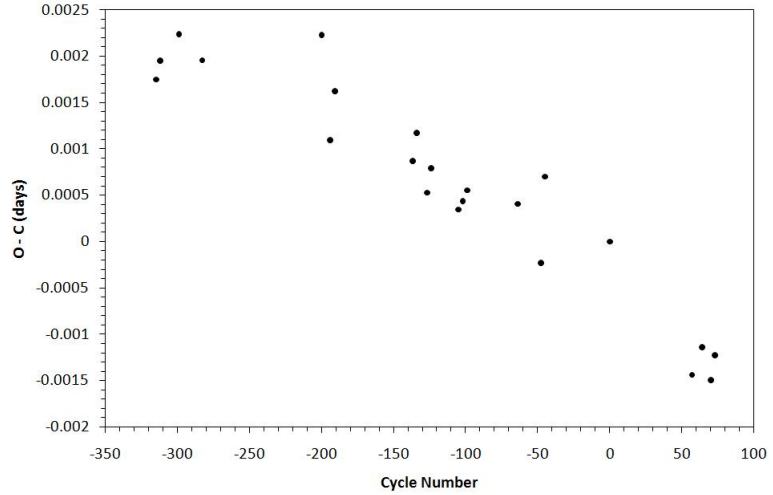

Figure 6.11: O−C diagram for the second subset of data for ASAS 002449−2744.3.

Using equal weights for the data, both a linear ephemeris and quadratic ephemeris were determined. The linear ephemeris returned from the analysis is

$$\text{Min. I} = \text{HJD2454299.6144(01)} + 0.3136612(05)\epsilon \tag{6.10}$$

and the quadratic ephemeris is

$$\text{Min. I} = \text{HJD2454299.6142(01)} + 0.313665(01)\epsilon - 1.1 \times 10^{-8}(0.3 \times 10^{-8})\epsilon^2 \qquad (6.11)$$

Fig. 6.12 shows the O−C residuals obtained for both a linear and a quadratic ephemeris. The overall residuals value using the linear ephemeris is −0.0018 while −0.0009 is obtained for the quadratic ephemeris. The quadratic ephemeris improves the residuals value and the O−C diagram. The observed times of minimum for the second subset are listed in Table 6.4 along with the O−C residuals. The following values of $\frac{\Delta P}{\Delta t}$ were calculated:

- Using the period of the linear ephemeris for the second subset:

$$\frac{\Delta P}{\Delta t} = 0.20 \times 10^{-5}\,\mathrm{d\,yr^{-1}}$$

- Using the period of the quadratic ephemeris for the second subset:

$$\frac{\Delta P}{\Delta t} = 0.59 \times 10^{-5}\,\mathrm{d\,yr^{-1}}$$

Both of the values suggest that the period of the system is increasing. The value determined by Pilecki et al. (2007) indicated that the period of the system was decreasing. It is possible that the period of the system was decreasing when the ASAS data were obtained and increased while the SuperWASP data were obtained.

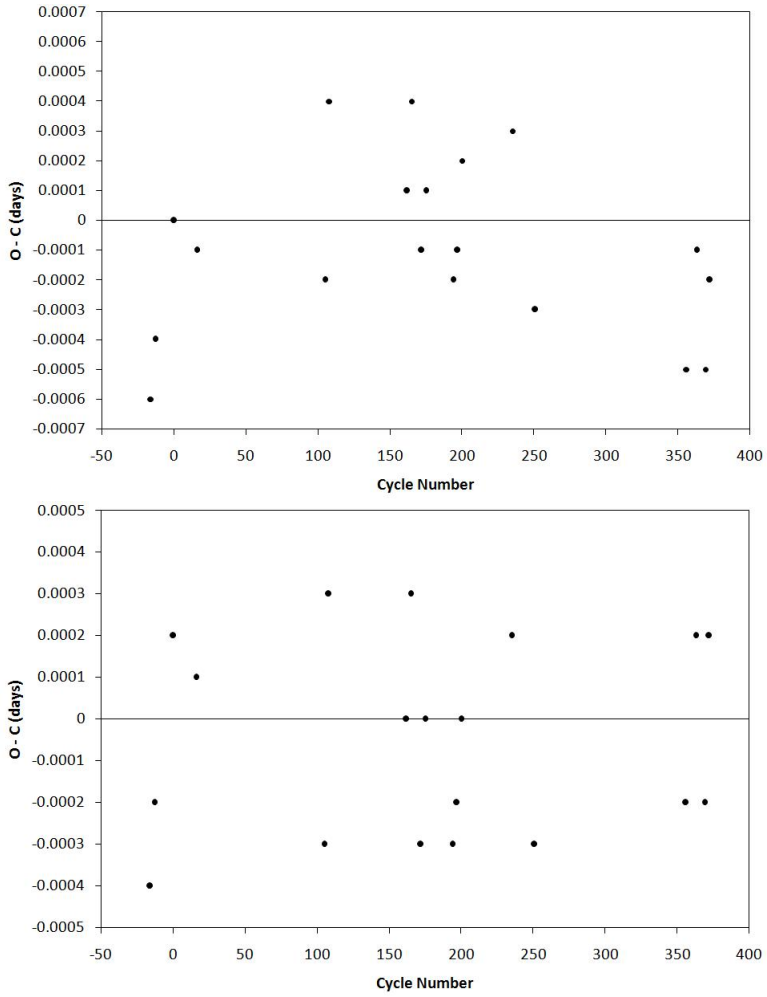

Figure 6.12: O−C residuals for the second subset of data of ASAS 002449−2744.3 obtained using a linear ephemeris, top, and quadratic ephemeris, bottom.

Cycle Number ϵ	Observed +2450000 (HJD)	Calculated +2450000 (HJD)	O − C (d)
−3	3960.5484(20)	3960.5481	0.0003
0	3961.4886(12)	3961.4891	−0.0005
10	3964.6251(22)	3964.6257	−0.0006
13	3965.5668(06)	3965.5667	0.0001
42	3974.6629(27)	3974.6628	0.0001
45	3975.6032(05)	3975.6038	−0.0006
57	3979.3680(04)	3979.3677	0.0003
102	3993.4820(07)	3993.4823	−0.0003
121	3999.4419(03)	3999.4418	0.0001
124	4000.3828(05)	4000.3828	0.0000
146	4007.2834(02)	4007.2833	0.0001
150	4008.5378(04)	4008.5380	−0.0002

Table 6.3: Observed times of minimum for the first subset of data of ASAS 002449−2744.3.

Cycle Number ϵ	Observed +2450000 (HJD)	Calculated (L) +2450000 (HJD)	Calculated (Q) +2450000 (HJD)	O − C (L) (d)	O − C (Q) (d)
−16	4294.5952(04)	4294.5958	4294.5956	−0.0006	−0.0004
−13	4295.5364(07)	4295.5368	4295.5366	−0.0004	−0.0002
0	4299.6144(04)	4299.6144	4299.6142	0.0000	0.0002
16	4304.6329(07)	4304.6330	4304.6328	−0.0001	−0.0002
105	4332.5486(02)	4332.5488	4332.5489	−0.0002	−0.0003
108	4333.4901(02)	4333.4898	4333.4899	0.0003	0.0002
162	4350.4276(03)	4350.4275	4350.4276	0.0001	0.0000
165	4351.3689(04)	4351.3685	4351.3686	0.0004	0.0003
172	4353.5639(03)	4353.5641	4353.5643	−0.0002	−0.0004
175	4354.5052(06)	4354.5051	4354.5052	0.0001	0.0000
194	4360.4645(02)	4360.4647	4360.4648	−0.0002	−0.0003
197	4361.4056(07)	4361.4057	4361.4058	−0.0001	−0.0002
200	4362.3467(03)	4362.3466	4362.3468	0.0001	−0.0001
235	4373.3250(03)	4373.3248	4373.3249	0.0002	0.0001
251	4378.3431(04)	4378.3434	4378.3434	−0.0003	−0.0003
356	4411.2772(11)	4411.2778	4411.2775	−0.0006	−0.0003
363	4413.4732(02)	4413.4734	4413.4731	−0.0002	0.0001
369	4415.3549(03)	4415.3554	4415.3551	−0.0005	−0.0002
372	4416.2962(02)	4416.2964	4416.2960	−0.0002	0.0002

Table 6.4: List of observed times of minimum brightness for the second subset of data of ASAS 002449−2744.3.

6.3.3 ASAS 002821−2904.1 ≡ 1SWASP J002821.32−290404.7

This system is presented by Pilecki et al. (2007) as a high period change rate system with $dP/dt = -0.23(5) \times 10^{-5}$ d yr^{-1}. The authors determined a period of $P = 0.269892$ d which is shorter than the listed ASAS period of $P = 0.269896$ d. Fig. 6.13 shows a plot of the SuperWASP data.

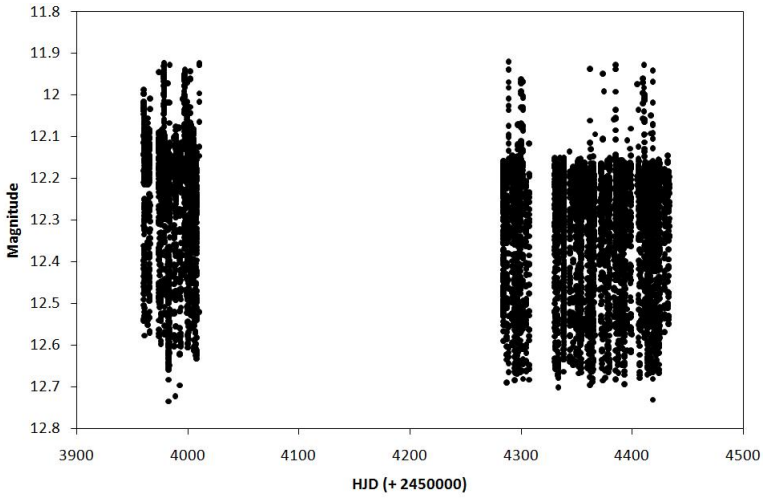

Figure 6.13: Plot of the SuperWASP data of ASAS 002821−2904.1. The magnitude of the system appears to have decreased.

The O−C diagram for the first subset of data (HJD 2453960.6695 to 2454008.4420) is shown in Fig. 6.14. The weighted least squares analysis of the first subset of data returned the ASAS period and the following ephemeris was determined:

$$\text{Min. I} = \text{HJD } 2454006.2824(02) + 0.269896(01)\epsilon \tag{6.12}$$

The observed times of minimum are listed in Table 6.5.

For the second subset of data (HJD 2454268.6160 to 2454422.4528), the O−C diagram obtained using the ASAS period, as shown in Fig. 6.15, appears to be parabolic. For the analysis, equal weights were used. The following linear ephemeris was determined:

$$\text{Min. I} = \text{HJD } 2454294.5263(01) + 0.2698905(05)\epsilon \tag{6.13}$$

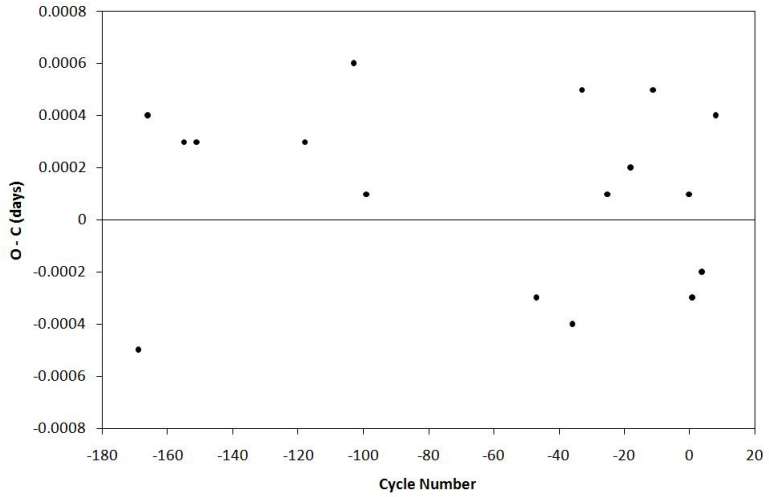

Figure 6.14: O−C residuals for the first subset of data for ASAS 002821−2904.1.

The overall O−C residuals value is 0.0017.

A quadratic ephemeris was also determined:

$$\text{Min. I} = \text{HJD } 2454294.5263(01) + 0.269894(01)\epsilon - 1 \times 10^{-8}(0.2 \times 10^{-8})\epsilon^2 \qquad (6.14)$$

The overall residuals value obtained using the quadratic ephemeris is −0.0004. Fig. 6.16 shows the O−C diagrams obtained for both a linear and quadratic ephemeris. The plot of the residuals obtained using the linear ephemeris has a peak around $\epsilon = 150$ which produces the large residuals value. For the quadratic ephemeris, the O−C residuals suggest that the period obtained is the correct period for the second subset.

While the residuals were improved, it is difficult to discern if the observed change in period seen in the original O−C diagram is abrupt or continuous. The observed times of minimum for the second subset of data are listed in Table 6.6.

Using median times and the periods determined for the two subsets, the following values for $\frac{\Delta P}{\Delta t}$ were calculated:

- Linear ephemeris for second subset: $\frac{\Delta P}{\Delta t} = -0.51 \times 10^{-5}\,\mathrm{d\,yr^{-1}}$

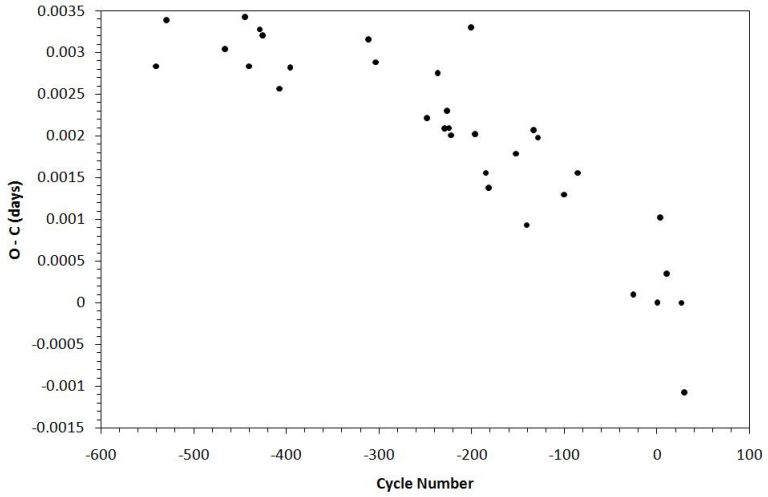

Figure 6.15: O−C diagram for second subset of data for ASAS 002821−2904.1. Note the decrease in the values.

- Quadratic ephemeris for second subset: $\frac{\Delta P}{\Delta t} = -0.20 \times 10^{-5}\,\mathrm{d\,yr^{-1}}$

The value for $\frac{\Delta P}{\Delta t}$ calculated using the period of the quadratic ephemeris is closest to the value for dP/dt determined by Pilecki et al. (2007).

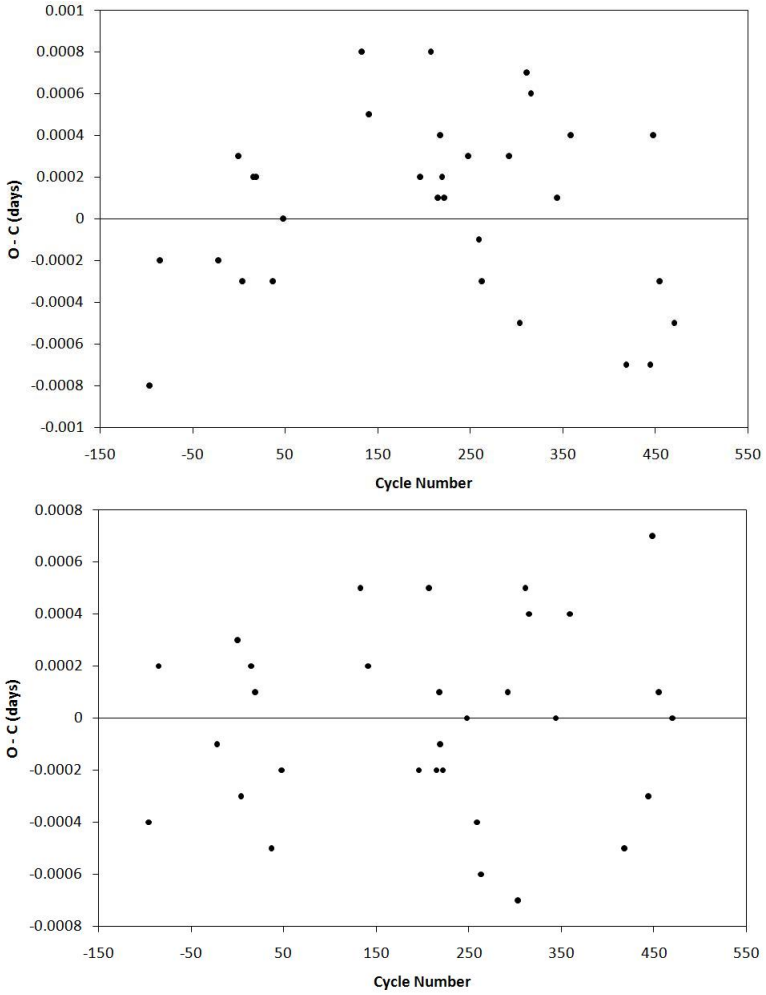

Figure 6.16: O−C diagram for the second subset of data for ASAS 002821−2904.1 obtained from using a linear ephemeris, top, and a quadratic ephemeris, bottom.

Cycle Number ϵ	Observed +2450000 (HJD)	Calculated +2450000 (HJD)	O − C (d)
−169	3960.6695(62)	3960.6700	−0.0005
−166	3961.4801(28)	3961.4797	−0.0004
−155	3964.4488(07)	3964.4485	0.0003
−151	3965.5284(23)	3965.5281	0.0003
−118	3974.4350(21)	3974.4347	0.0003
−103	3978.4837(03)	3978.4831	0.0006
−99	3979.5628(16)	3979.5627	0.0001
−47	3993.5970(12)	3993.5973	−0.0003
−36	3996.5657(07)	3996.5661	−0.0004
−33	3997.3763(05)	3997.3758	0.0005
−25	3999.5351(10)	3999.5350	0.0001
−18	4001.4245(05)	4001.4243	0.0002
−11	4003.3140(07)	4003.3135	0.0005
0	4006.2825(13)	4006.2824	0.0001
1	4006.5520(28)	4006.5523	−0.0003
4	4007.3618(09)	4007.3620	−0.0002
8	4008.4420(06)	4008.4416	0.0004

Table 6.5: List of observed times of minimum for the first subset of data of ASAS 002821−2904.1.

Cycle Number ϵ	Observed +2450000 (HJD)	Calculated (L) +2450000 (HJD)	Calculated (Q) +2450000 (HJD)	O − C (L) (d)	O − C (Q) (d)
−96	4268.6160(16)	4268.6168	4268.6164	−0.0008	−0.0004
−85	4271.5854(30)	4271.5856	4271.5852	−0.0002	0.0002
−22	4288.5885(06)	4288.5887	4288.5886	−0.0002	−0.0001
0	4294.5266(13)	4294.5263	4294.5263	0.0003	0.0003
4	4295.6056(08)	4295.6059	4295.6059	−0.0003	−0.0003
15	4298.5749(08)	4298.5747	4298.5747	0.0002	0.0002
19	4299.6544(02)	4299.6542	4299.6543	0.0002	0.0001
37	4304.5119(18)	4304.5122	4304.5124	−0.0003	−0.0005
48	4307.4810(19)	4307.4810	4307.4812	0.0000	−0.0002
133	4330.4225(11)	4330.4217	4330.4220	0.0008	0.0005
141	4332.5814(03)	4332.5809	4332.5812	0.0005	0.0002
196	4347.4250(06)	4347.4248	4347.4252	0.0002	−0.0002
207	4350.3944(25)	4350.3936	4350.3939	0.0008	0.0005
215	4352.5529(22)	4352.5528	4352.5531	0.0001	−0.0002
218	4353.3628(05)	4353.3624	4353.3627	0.0004	0.0001
219	4353.6325(22)	4353.6323	4353.6326	0.0002	−0.0001
222	4354.4421(20)	4354.4420	4354.4423	0.0001	−0.0002
248	4361.4594(09)	4361.4591	4361.4594	0.0003	0.0000
259	4364.4278(11)	4364.4279	4364.4282	−0.0001	−0.0004
263	4365.5072(19)	4365.5075	4365.5078	−0.0003	−0.0006
292	4373.3346(13)	4373.3343	4373.3345	0.0003	0.0001
303	4376.3026(04)	4376.3031	4376.3033	−0.0005	−0.0007
311	4378.4629(08)	4378.4622	4378.4624	0.0007	0.0005
315	4379.5424(14)	4379.5418	4379.5420	0.0006	0.0004
344	4387.3687(25)	4387.3686	4387.3687	0.0001	0.0000
359	4391.4174(05)	4391.4170	4391.4170	0.0004	0.0004
418	4407.3398(04)	4407.3405	4407.3403	−0.0007	−0.0005
444	4414.3570(01)	4414.3577	4414.3573	−0.0007	−0.0003
448	4415.4376(05)	4415.4378	4415.4369	−0.0002	0.0007
455	4417.3262(09)	4417.3265	4417.3261	−0.0003	0.0001
470	4421.3743(17)	4421.3748	4421.3743	−0.0005	0.0000

Table 6.6: Observed times of minimum for the second subset of data of ASAS 002821−2904.1. L and Q denote Linear and Quadratic respectively.

6.3.4 ASAS 052851−3010.2 ≡ 1SWASP J052850.62−301012.8

This system was presented by Pilecki et al. (2007) as a high period change rate system with $P = 0.302101$ d (equal to the ASAS period) and $\mathrm{dP/dt} = -0.17(4) \times 10^{-5}$ d yr^{-1}. A plot of the SuperWASP data is shown in Fig. 6.17. The magnitude of the system appears to have decreased from the start of the observations. For the interval covering HJD 2453993 to HJD 2454008, two usable minima were obtained while for the interval covering HJD 2454105 to HJD 2454145, only five minima were obtained. These minima were not used in the analysis.

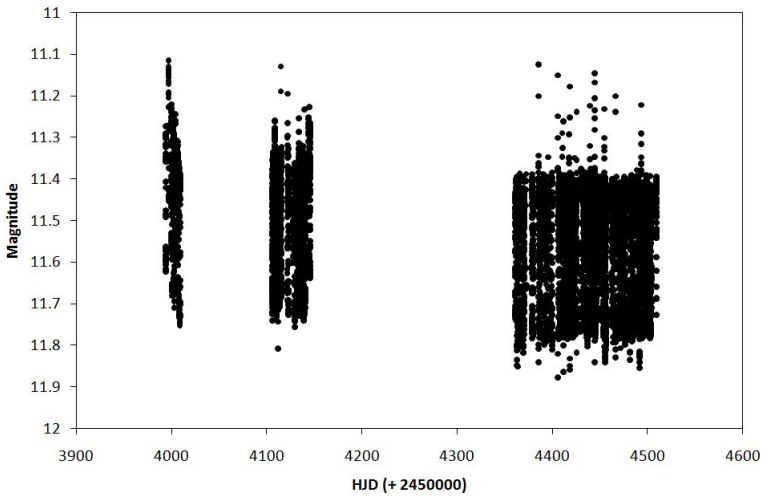

Figure 6.17: Plot of the SuperWASP data of ASAS 052851−3010.2.

From the analysis of the interval covering HJD 2454360.4987 to HJD 2454509.3881, the following ephemeris was determined:

$$\text{Min. I} = \text{HJD } 2454497.3209(04) + 0.302101(02)\epsilon \tag{6.15}$$

The plot of the O−C residuals obtained from using this ephemeris is shown in Fig. 6.18. The period of the system does not appear to have changed.

As no other usable minima were extracted from the SuperWASP data, a value for $\frac{\Delta P}{\Delta t}$ could not be determined. The observed times of minimum are listed in Table 6.7.

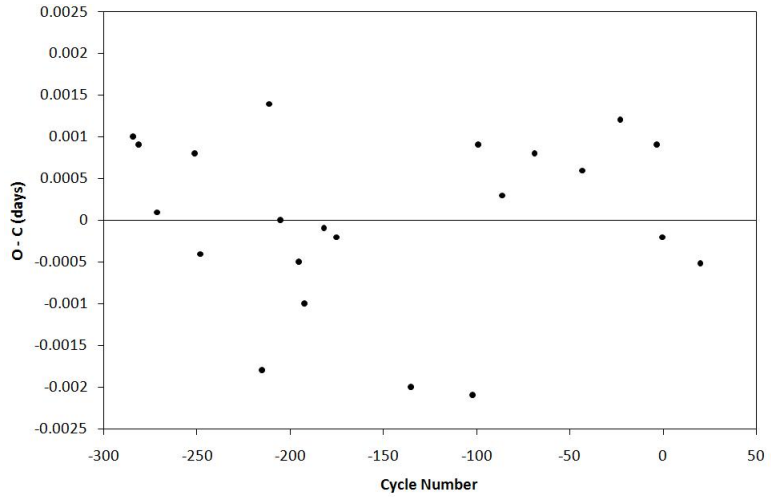

Figure 6.18: O−C diagram for ASAS 052851−3010.2.

Cycle Number ϵ	Observed +2450000 (HJD)	Calculated +2450000 (HJD)	O − C (d)
−284	4411.5252(17)	4411.5242	−0.0010
−281	4412.4314(08)	4412.4305	0.0009
−271	4415.4516(30)	4415.4515	0.0001
−251	4421.4943(20)	4421.4935	0.0008
−248	4422.3995(25)	4422.3999	−0.0004
−215	4432.3674(08)	4432.3692	−0.0018
−211	4433.5790(13)	4433.5776	0.0014
−205	4435.3902(09)	4435.3902	0.0000
−195	4438.4107(06)	4438.4112	−0.0005
−192	4439.3165(07)	4439.3175	−0.0010
−182	4442.3384(07)	4442.3385	−0.0001
−175	4444.4530(07)	4444.4532	−0.0002
−135	4456.5353(10)	4456.5373	−0.0020
−102	4466.5045(20)	4466.5066	−0.0021
−99	4467.4138(06)	4467.4129	0.0009
−86	4471.3405(06)	4471.3402	0.0003
−69	4476.4767(07)	4476.4759	0.0008
−43	4484.3312(22)	4484.3306	0.0006
−23	4490.3738(13)	4490.3726	0.0012
−3	4496.4155(17)	4496.4146	0.0009
0	4497.3207(08)	4497.3209	−0.0002
20	4503.3624(11)	4503.3629	−0.0005

Table 6.7: Observed times of minimum of ASAS 052851−3010.2.

6.3.5 ASAS 120036−3915.6 ≡ 1SWASP J120036.31−391535.0

From the analysis of the ASAS data, the light curve of the system is smeared out thus it was suspected that this system was undergoing changes in its orbital period (Skelton & Smits 2009). As there are less than 300 good quality data points, this system was not selected by Pilecki et al. (2007). The period of the system as determined by ASAS is $P = 0.292670$ d. A plot of the SuperWASP data is shown in Fig. 6.19.

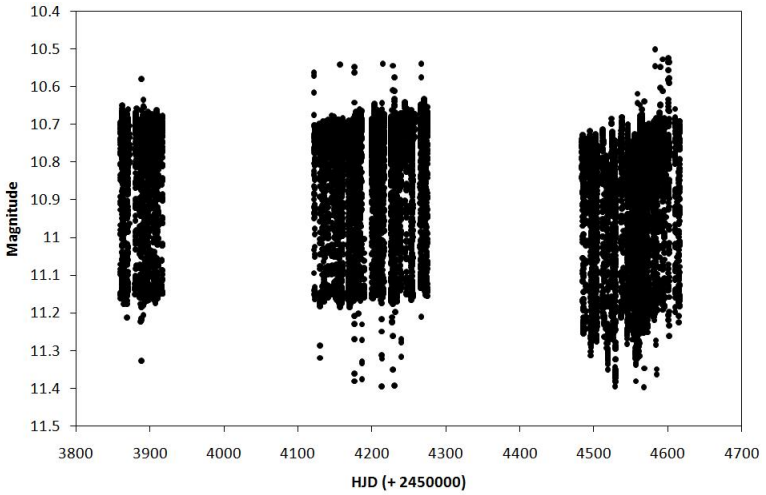

Figure 6.19: Plot of the SuperWASP data of ASAS 120036−3915.6.

For the first subset of data, covering HJD 2453862.36057 to HJD 2453911.23736, the following ephemeris was determined:

$$\text{Min. I} = \text{HJD } 2453906.26162(15) + 0.2926741(13)\epsilon \tag{6.16}$$

The O−C diagram for the first subset of data is shown in Fig. 6.20. The observed times of minimum are listed in Table 6.8.

For the second subset of data, HJD 2454132.49781 to HJD 2454273.27348, the following ephemeris was determined:

$$\text{Min. I} = \text{HJD } 2454266.24906(11) + 0.2926726(04)\epsilon \tag{6.17}$$

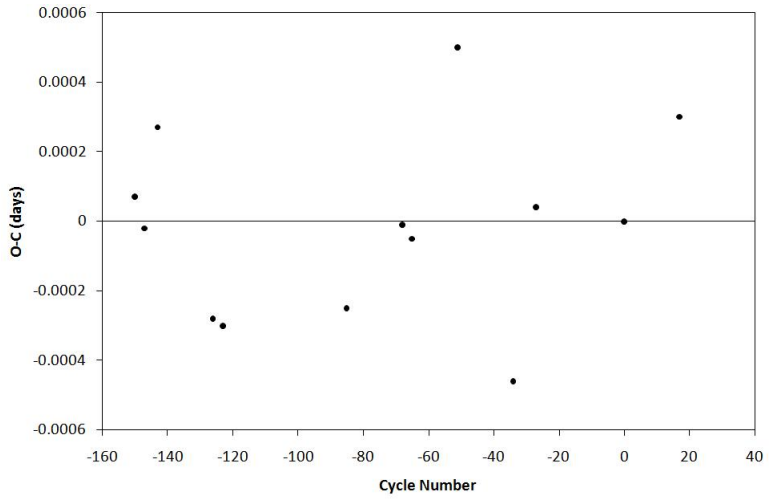

Figure 6.20: O−C diagram for the first subset of data of ASAS 120036−3915.6.

The plot of the O−C residuals is shown in Fig. 6.21. The observed times of minimum are listed in Table 6.9. Due to the uncertainties in the periods, the period of the system does not appear to have changed between the first and second subsets.

For the third subset of data, covering HJD 2454524.38695 to HJD 2454581.45718, the ephemeris determined from the analysis is

$$\text{Min. I} = \text{HJD } 2454560.38461(08) + 0.2926648(11)\epsilon \tag{6.18}$$

Fig. 6.22 shows the plot of the O−C residuals for the third subset of data. The observed times of minimum are listed in Table 6.10. Between the second and third subsets, the period decreased with $\frac{\Delta P}{\Delta t} = -0.82 \times 10^{-5}$ d yr^{-1}. In comparison to the values listed by Pilecki et al. (2007) for the system they present as high period change rate systems, this system could be classified as one. More observations are needed to determine if the period and $\frac{\Delta P}{\Delta t}$ continue to change. Comparing the periods determined here to the listed ASAS period for the system, the period of the first two subsets are longer while the period for the third subset is shorter. It is possible that the period of the system increased from 0.292670 d to 0.292674 d and is now decreasing.

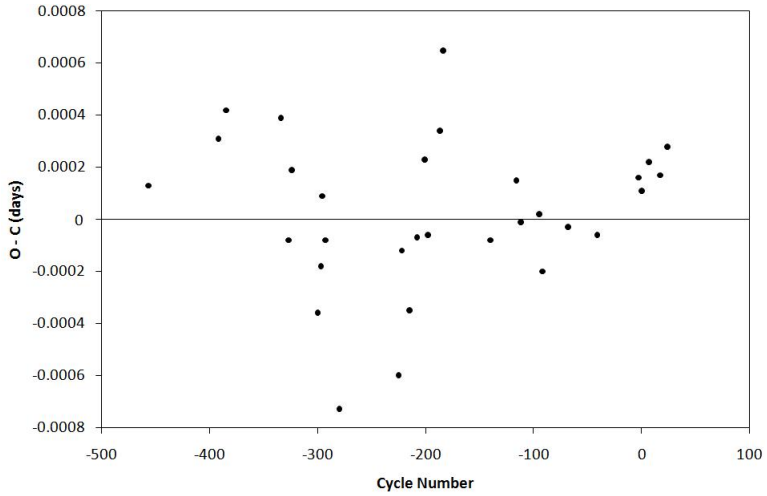

Figure 6.21: O−C diagram for the second subset of data for ASAS 120036−3915.6.

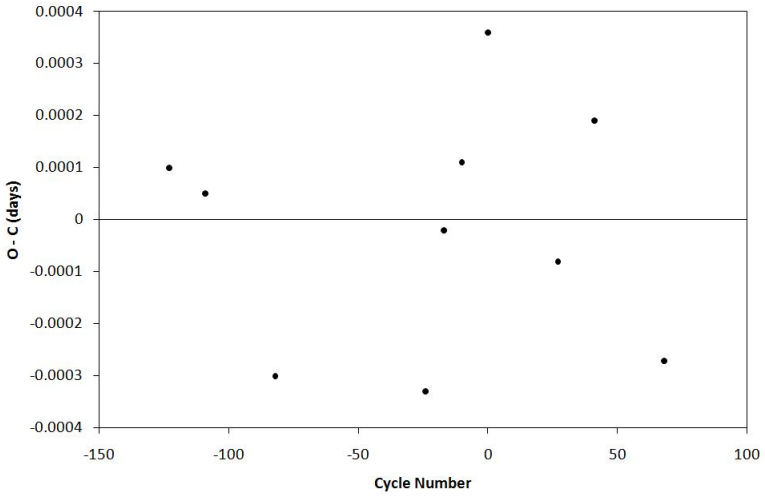

Figure 6.22: O−C diagram for third subset of data for ASAS 120036−3915.6.

Cycle Number ϵ	Observed +2450000 (HJD)	Calculated +2450000 (HJD)	O − C (d)
−150	3862.36057(59)	3862.36050	0.00007
−147	3863.23850(16)	3863.23852	−0.00002
−143	3864.40949(87)	3864.40922	0.00027
−126	3869.38440(84)	3869.38468	−0.00028
−123	3870.26240(05)	3870.26270	−0.00030
−85	3881.38406(17)	3881.38431	−0.00025
−68	3886.35976(12)	3886.35977	−0.00001
−65	3887.23774(14)	3887.23779	−0.00005
−51	3891.33573(15)	3891.33523	0.00050
−34	3896.31022(20)	3896.31068	−0.00046
−27	3898.35944(30)	3898.35940	0.00004
0	3906.26160(28)	3906.26160	0.00000
17	3911.23736(28)	3911.23706	0.00030

Table 6.8: Observed times of minimum for the first subset of data of ASAS 120036−3915.6.

Cycle Number ϵ	Observed +2450000 (HJD)	Calculated +2450000 (HJD)	O − C (d)
−457	4132.49781(62)	4132.49768	0.00013
−392	4151.52171(40)	4151.52140	0.00031
−385	4153.57053(22)	4153.57011	0.00042
−334	4168.49680(18)	4168.49641	0.00039
−327	4170.54504(86)	4170.54512	−0.00008
−324	4171.42333(37)	4171.42314	0.00019
−300	4178.44692(34)	4178.44728	−0.00036
−297	4179.32512(32)	4179.32530	−0.00018
−296	4179.61806(57)	4179.61797	0.00009
−293	4180.49591(16)	4180.49599	−0.00008
−280	4184.30000(41)	4184.30073	−0.00073
−225	4200.39713(36)	4200.39773	−0.00060
−222	4201.27562(22)	4201.27574	−0.00012
−215	4203.32410(48)	4203.32445	−0.00035
−208	4205.37309(16)	4205.37316	−0.00007
−201	4207.42210(65)	4207.42187	0.00023
−198	4208.29983(37)	4208.29989	−0.00006
−187	4211.51962(68)	4211.51928	0.00034
−184	4212.39795(26)	4212.39730	0.00065
−140	4225.27482(34)	4225.27490	−0.00008
−116	4232.29919(17)	4232.29904	0.00015
−112	4233.46972(33)	4233.46973	−0.00001
−95	4238.44518(99)	4238.44516	0.00002
−92	4239.32298(50)	4239.32318	−0.00020
−68	4246.34729(16)	4246.34732	−0.00003
−41	4254.24942(16)	4254.24948	−0.00006
−3	4265.37120(13)	4265.37104	0.00016
0	4266.24917(21)	4266.24906	0.00011
7	4268.29799(12)	4268.29777	0.00022
17	4271.22466(08)	4271.22449	0.00017
24	4273.27348(15)	4273.27320	0.00028

Table 6.9: List of observed times of minimum for the second subset of data of ASAS 120036−3915.6.

Cycle Number ϵ	Observed +2450000 (HJD)	Calculated +2450000 (HJD)	O − C (d)
−123	4524.38695(61)	4524.38682	0.00013
−109	4528.48421(19)	4528.48413	0.00008
−82	4536.38581(34)	4536.38608	−0.00027
−24	4553.36035(41)	4553.36065	−0.00030
−17	4555.40932(14)	4555.40931	0.00001
−10	4557.45810(26)	4557.45796	0.00014
0	4560.38500(29)	4560.38461	0.00039
27	4568.28652(27)	4568.28657	−0.00005
41	4572.38410(40)	4572.38388	0.00022
68	4580.28559(32)	4580.28583	−0.00024

Table 6.10: Observed times of minimum for the third subset of data of ASAS 120036−3915.6.

6.3.6 ASAS 150452−3757.7 ≡ 1SWASP J150452.17−375739.0

For the period analysis, data for the secondary minimum were used as the primary minimum is a flat minimum. The ASAS listed period of the system is 0.374131 d. Fig. 6.23 shows a plot of the SuperWASP data.

For the first subset of data, covering HJD 2453880.28785 to HJD 2453920.32083, the following ephemeris was determined:

$$\text{Min. II} = \text{HJD } 2453887.39664(06) + 0.374138(02)\epsilon \tag{6.19}$$

The corresponding plot of the O−C residuals is shown in Fig. 6.24. Compared to the original ASAS period, the period of the system has increased. Observed times of minimum for the first subset of data are listed in Table 6.11.

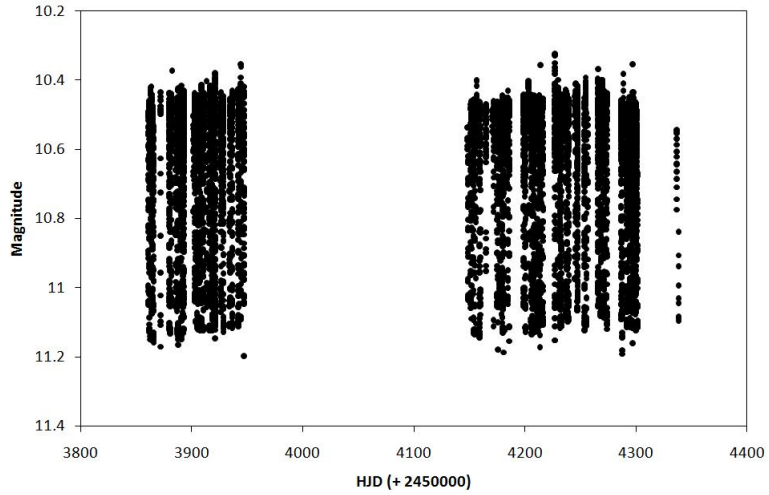

Figure 6.23: Plot of the SuperWASP data of ASAS 150452−3757.7.

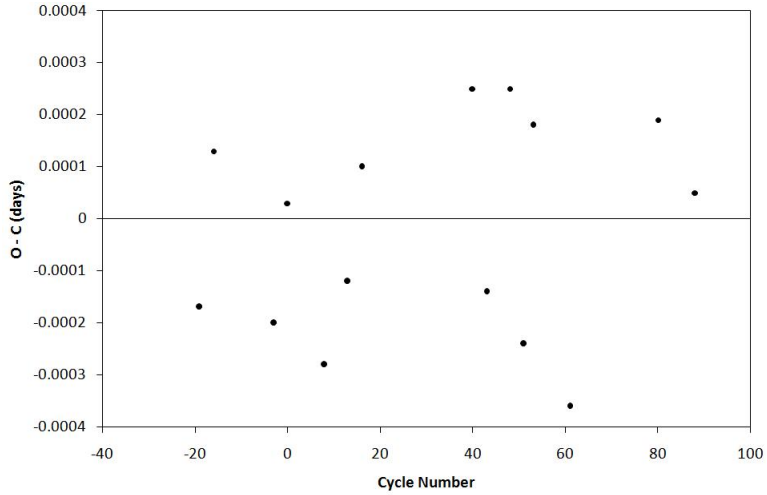

Figure 6.24: O−C diagram of the first subset of data for ASAS 150452−3757.7.

Using the ASAS period, the O−C diagram of the second subset, covering the interval from HJD 2454148.54246 to HJD 2454214.38958, has a low residuals value (−0.00024) indicating the assumed period is correct. This is confirmed by the analysis which returns the following ephemeris:

$$\text{Min. II} = \text{HJD } 2454211.39625(12) + 0.374131(01)\epsilon \tag{6.20}$$

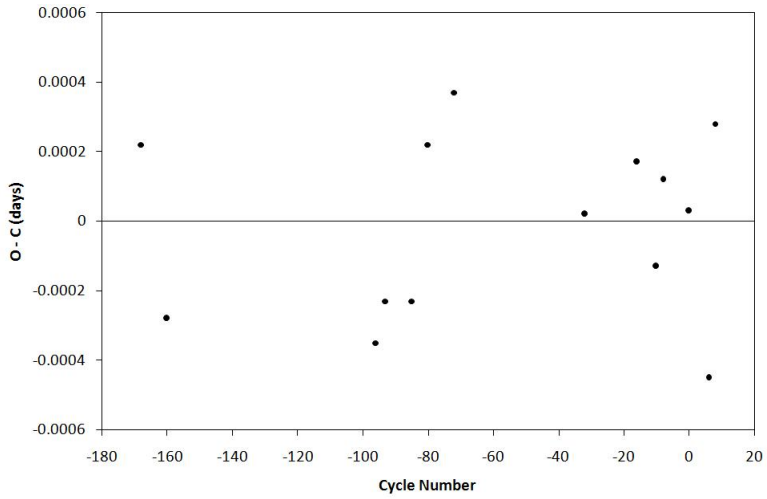

Figure 6.25: O−C diagram for the second subset of data of ASAS 150452−3757.7.

The corresponding O−C residuals are shown in Fig. 6.25 and the observed times of minimum are listed in Table 6.12. Between the two subsets, the period decreased with $\frac{\Delta P}{\Delta t} = -0.91 \times 10^{-5}$ d yr^{-1}. This value would classify the system as a high period change rate system.

Cycle Number ϵ	Observed +2450000 (HJD)	Calculated +2450000 (HJD)	O − C (d)
−19	3880.28785(11)	3880.28802	−0.00017
−16	3881.41056(24)	3881.41043	0.00013
−3	3886.27403(07)	3886.27423	−0.00020
0	3887.39667(10)	3887.39664	0.00003
8	3890.38946(04)	3890.38974	−0.00028
13	3892.26031(10)	3892.26043	−0.00012
16	3893.38295(11)	3893.38285	0.00010
40	3902.36241(17)	3902.36216	0.00025
43	3903.48443(12)	3903.48457	−0.00014
48	3905.35551(16)	3905.35526	0.00025
51	3906.47744(11)	3906.47768	−0.00024
53	3907.22613(07)	3907.22595	0.00018
61	3910.21870(08)	3910.21906	−0.00036
80	3917.32787(06)	3917.32768	0.00019
88	3920.32083(04)	3920.32078	0.00005

Table 6.11: Observed times of minimum for the first subset of data of ASAS 150452−3757.7.

Cycle Number ϵ	Observed +2450000 (HJD)	Calculated +2450000 (HJD)	O − C (d)
−168	4148.54246(14)	4148.54224	0.00022
−160	4151.53501(11)	4151.53529	−0.00028
−96	4175.47932(15)	4175.47967	−0.00035
−93	4176.60184(19)	4176.60207	−0.00023
−85	4179.59489(27)	4179.59512	−0.00023
−80	4181.46599(26)	4181.46577	0.00022
−72	4184.45919(20)	4184.45882	0.00037
−32	4199.42408(24)	4199.42406	−0.00002
−16	4205.41032(30)	4205.41015	0.00017
−10	4207.65481(03)	4207.65494	−0.00013
−8	4208.40332(06)	4208.40320	0.00012
0	4211.39628(13)	4211.39625	0.00003
6	4213.64059(25)	4213.64104	−0.00045
8	4214.38958(17)	4214.38930	0.00028

Table 6.12: Observed times of minimum for the second subset of data of ASAS 150452−3757.7.

6.3.7 ASAS 150934−3348.5 ≡ 1SWASP J150933.60−334830.4

The ASAS determined period of this system is $P = 0.360320$ d. Fig. 6.26 shows the SuperWASP data of the system.

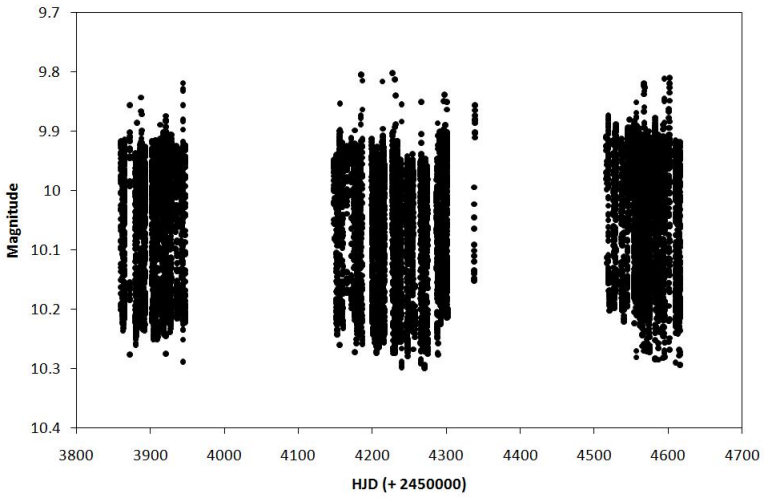

Figure 6.26: Plot of the SuperWASP data of ASAS 150934−3348.5.

For the first subset of data, covering HJD 2453865.4309 to HJD 2453943.2569, the following ephemeris was determined:

$$\text{Min. I} = \text{HJD } 2453890.2912(03) + 0.360306(08)\epsilon \tag{6.21}$$

Fig. 6.27 shows the O−C residuals for the first subset of data obtained using the ephemeris determined. Most of the points lie above O−C equal to zero with the sum of the residuals equal to 0.0043. Selecting different T_0 values for the analysis did not improve the residuals. The observed times of minimum are listed in Table 6.13.

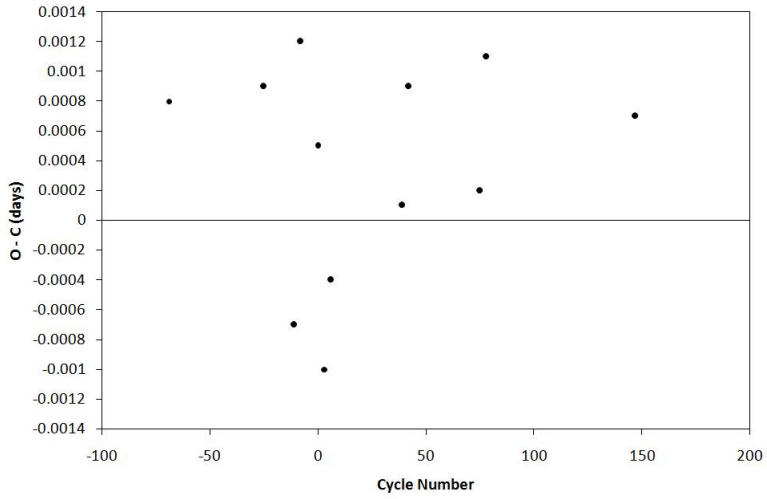

Figure 6.27: O−C diagram for the first subset of data for ASAS 150934−3348.5.

For the second subset of data, covering HJD 2454179.6228 to HJD 2454300.3254, the following ephemeris was determined:

$$\text{Min. I} = \text{HJD } 2454232.5880(02) + 0.360312(02)\epsilon \tag{6.22}$$

The plot of the O−C residuals is shown in Fig. 6.28 and the observed times of minimum are listed in Table 6.14.

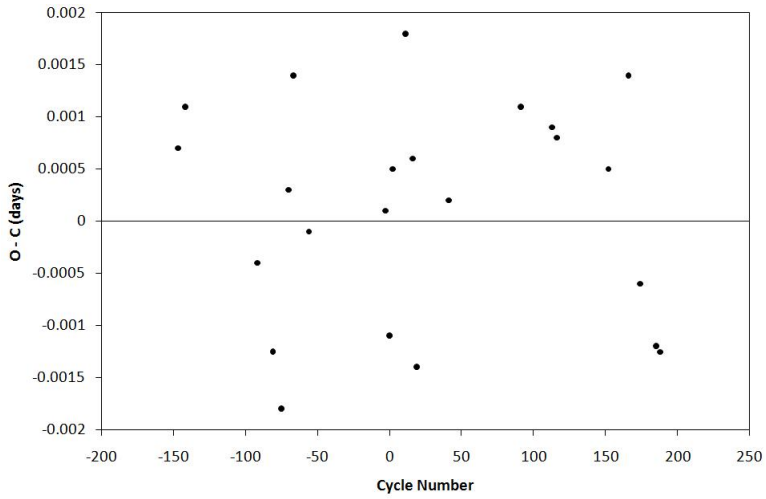

Figure 6.28: O−C diagram of the second subset of data for ASAS 150934−3348.5.

Cycle Number ϵ	Observed +2450000 (HJD)	Calculated +2450000 (HJD)	O − C (d)
−69	3865.4309(13)	3865.4301	0.0008
−25	3881.2845(07)	3881.2836	0.0009
−11	3886.3271(18)	3886.3278	−0.0007
−8	3887.4100(22)	3887.4088	0.0012
0	3890.2917(14)	3890.2912	0.0005
3	3891.3711(60)	3891.3721	-0.0010
6	3892.4526(10)	3892.4530	−0.0004
39	3904.3432(08)	3904.3431	0.0001
42	3905.4250(15)	3905.4241	0.0009
75	3917.3144(02)	3917.3142	0.0002
78	3918.3962(02)	3918.3951	0.0011
147	3943.2569(03)	3943.2562	0.0007

Table 6.13: Observed times of minimum for the first subset of data of ASAS 150934−3348.5.

From the first to the second subset the period increased with $\frac{\Delta P}{\Delta t} = 0.65 \times 10^{-5}$ d yr^{-1}.

Cycle Number ϵ	Observed +2450000 (HJD)	Calculated +2450000 (HJD)	O − C (d)
−147	4179.6228(11)	4179.6221	0.0007
−142	4181.4248(10)	4181.4237	0.0011
−92	4199.4389(09)	4199.4393	−0.0004
−81	4203.4015(35)	4203.4027	−0.0012
−75	4205.5628(06)	4205.5646	−0.0018
−70	4207.3665(09)	4207.3662	0.0003
−67	4208.4485(12)	4208.4471	0.0014
−56	4212.4104(12)	4212.4105	−0.0001
−3	4231.5072(17)	4231.5071	0.0001
0	4232.5869(18)	4232.5880	−0.0011
2	4233.3091(19)	4233.3086	0.0005
11	4236.5532(11)	4236.5514	0.0018
16	4238.3536(02)	4238.3530	0.0006
19	4239.4325(04)	4239.4339	−0.0014
41	4247.3610(05)	4247.3608	0.0002
91	4265.3775(04)	4265.3764	0.0011
113	4273.3042(05)	4273.3033	0.0009
116	4274.3850(05)	4274.3842	0.0008
152	4287.3559(10)	4287.3554	0.0005
166	4292.4012(02)	4292.3998	0.0014
174	4295.2817(07)	4295.2823	−0.0006
185	4299.2445(04)	4299.2457	−0.0012
188	4300.3254(05)	4300.3267	−0.0013

Table 6.14: Observed times of minimum for the second subset of data of ASAS 150934−3348.5.

6.3.8 ASAS 002328−2041.8 ≡ 1SWASP J002328.00−204150.0

In a plot of the ASAS observations, as shown in Fig. 6.29, the magnitude of the system decreases and then returns to the original magnitude.

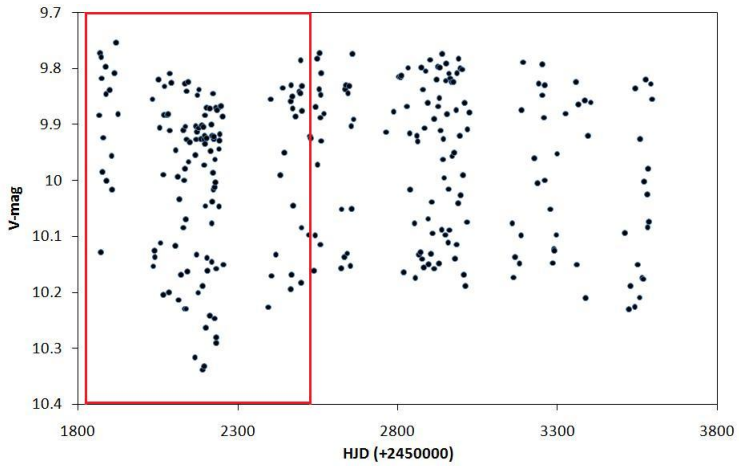

Figure 6.29: Plot of the ASAS data for ASAS 002328−2041.8. The dip in magnitude, highlighted by the red box, is clearly discernible.

Fig. 6.30 shows plots of two subsets of SuperWASP data. In the top plot, a similar dip in magnitude occurs while in the bottom plot, the minimum V mag of the system increases from 10.4 to 10.35. There is evidence that the light curves of the system are not constant. Examples are shown in Fig. 6.31. The variations in the heights of the maxima show that while both vary in height, they do not vary simultaneously. The minimum at phase zero varies in depth. These changes may be due to magnetic activity. This system was selected for analysis to determine if the orbital period of the system changed and, if so, whether the changes occurred at the same time as the observed flux changes. The O−C diagram for the first subset of data obtained using the ASAS period of 0.41469 d is shown in Fig. 6.32. The diagram suggests that the period of the system increased, remained constant with a period similar to the ASAS period, and then increased again.

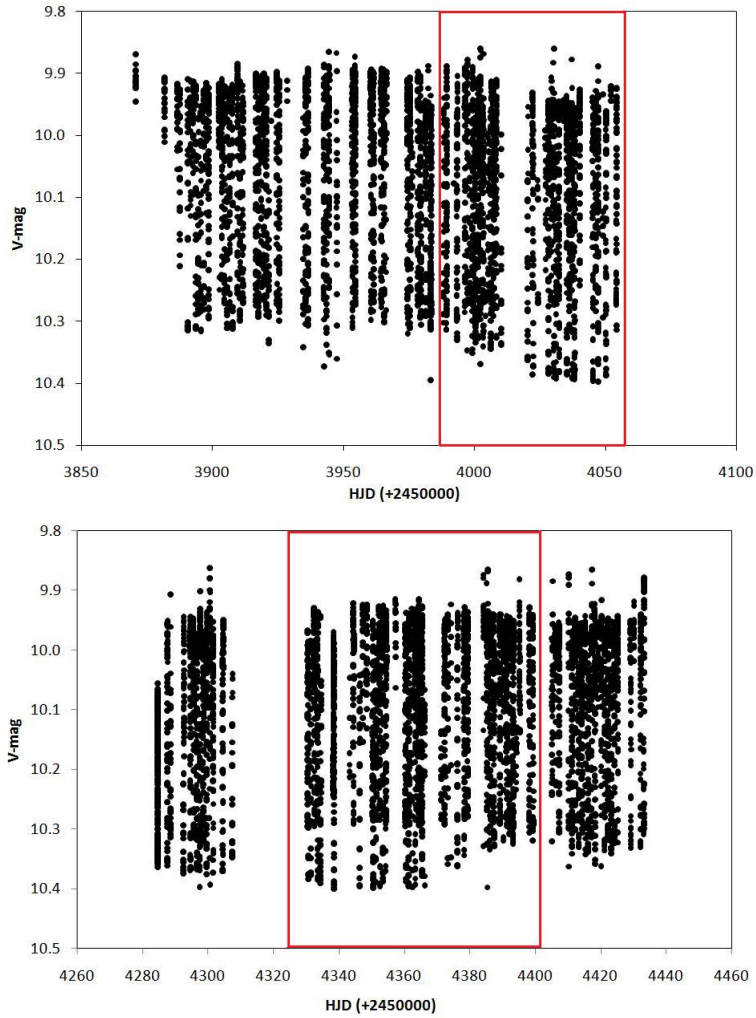

Figure 6.30: Plots of the SuperWASP data (top and bottom). A dip in magnitude similar to that observed in the ASAS data, highlighted by the red box, is seen in the first subset of data. The second subset does not appear to show the same dip in magnitude but what is noticeable is the change in the minimum brightness of the system (data in red box).

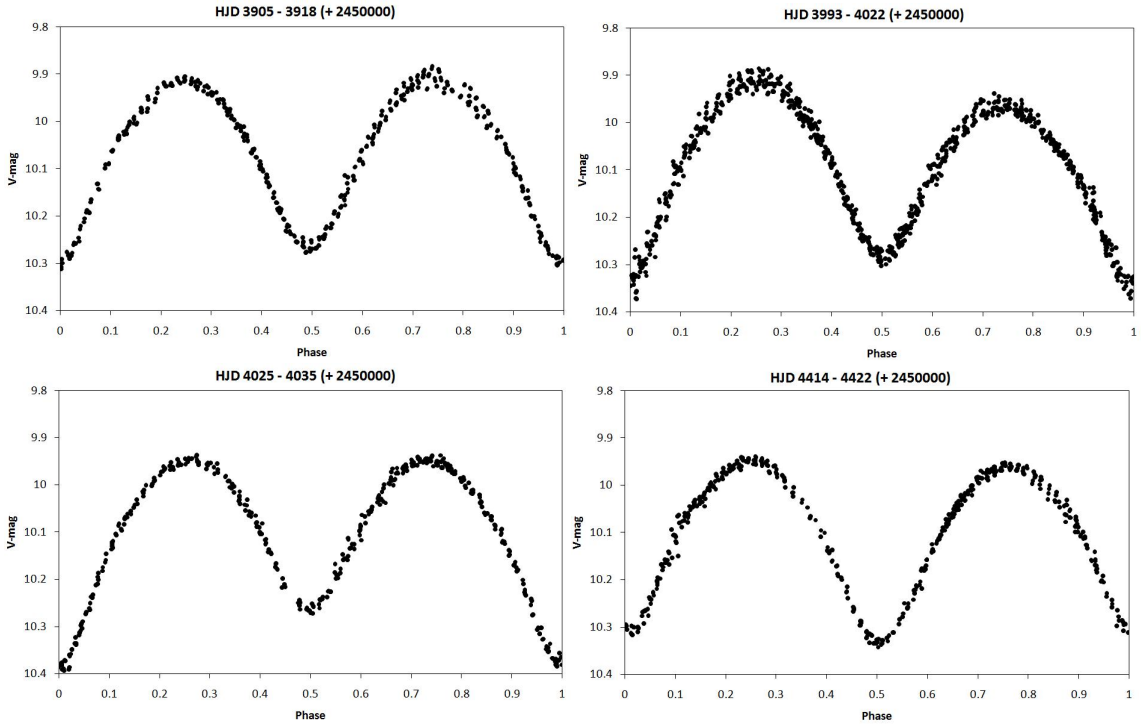

Figure 6.31: WASP light curves of ASAS 002328−2041.8. The maxima vary in height and the minimum at phase zero varies in depth. These changes cause the observed flux changes.

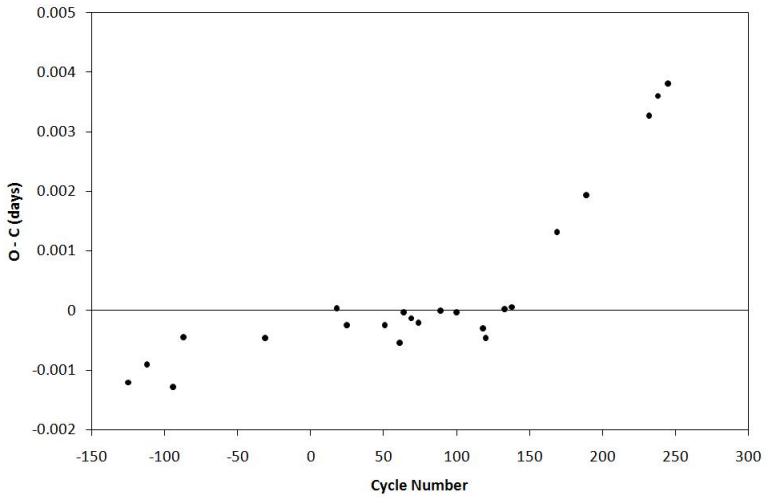

Figure 6.32: O−C diagram for the first subset of data for ASAS 002328−2041.8. The system appears to have undergone a change in period, followed by a constant period and then a change in period.

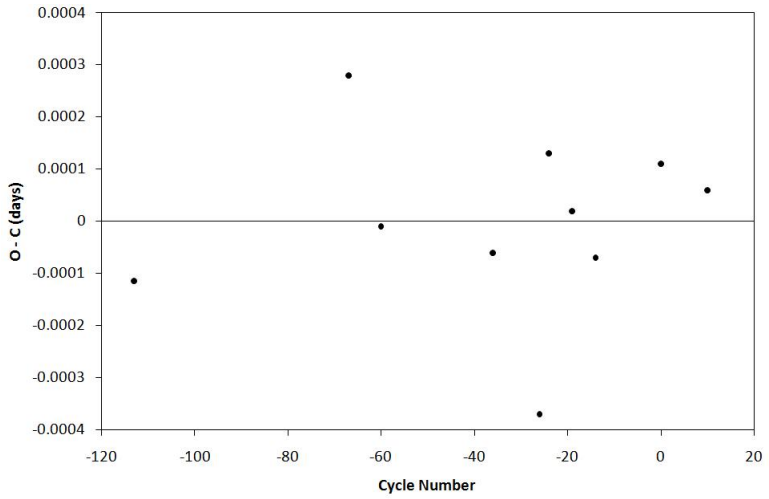

Figure 6.33: Plot of the O−C residuals for the second interval of data of ASAS 002328−2041.8.

Due to the shape of the O−C diagram, the data were split into intervals. These were based on the sections in the data where the flux changed and are as follows:

- Interval 1: HJD 2453905 - HJD 2453942
- Interval 2: HJD 2453942 - HJD 2453993
- Interval 3: HJD 2453993 - HJD 2454050

For the first interval, the magnitude of the system appears to increase. Because only four usable minima were extracted from the data, an analysis was not performed. For the second interval, the magnitude of the system remains unchanged. From the analysis of the data, the following ephemeris was determined:

$$\text{Min. I} = \text{HJD } 2453989.37334(08) + 0.414692(02)\epsilon \tag{6.23}$$

The plot of the O−C residuals obtained using this ephemeris is shown in Fig. 6.33 and the observed times of minimum are listed in Table 6.15.

For the third interval, the following ephemeris was determined:

$$\text{Min. I} = \text{HJD } 2454047.43364(06) + 0.414726(01)\epsilon \tag{6.24}$$

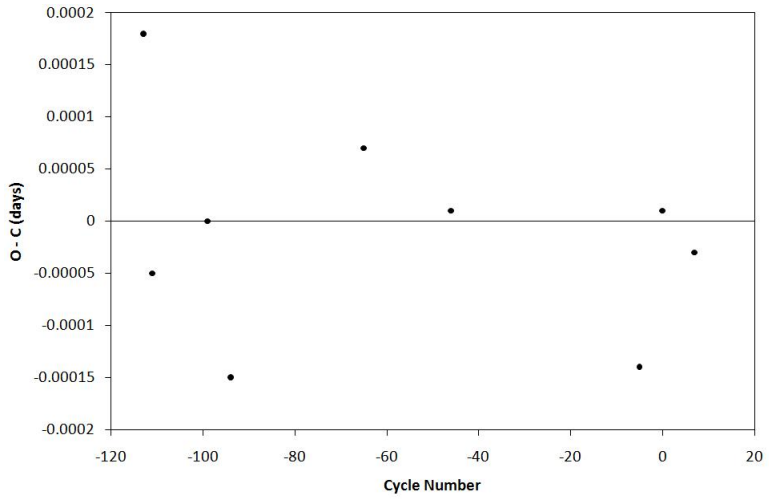

Figure 6.34: Plot of the O−C residuals for the third interval of data of ASAS 002328−2041.8.

The plot of the O−C residuals obtained from this ephemeris is shown in Fig. 6.34. Table 6.16 lists the observed times of minimum.

Interval 3 coincides with the decrease in magnitude. During the decrease in magnitude, the period increased from 0.414692 d to 0.414726 d. Using the values of the periods determined for the second and third intervals, $\frac{\Delta P}{\Delta t} = 2.2 \times 10^{-4}$ d yr^{-1}.

The O−C diagram for the second subset of data obtained using the ASAS period is shown in Fig. 6.35. The data were split into intervals based on the observed changes in flux. These are

- Interval 4: HJD 2454284 - HJD 2454366
- Interval 5: HJD 2454366 - HJD 2454411
- Interval 6: HJD 2454411 - HJD 2454433

For the fourth interval, the following ephemeris was determined:

$$\text{Min. I} = \text{HJD } 2454353.48202(16) + 0.414697(01)\epsilon \tag{6.25}$$

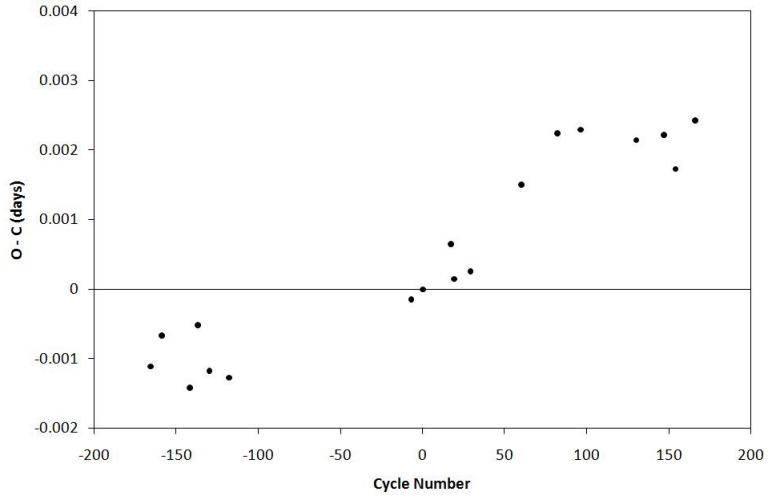

Figure 6.35: O−C diagram for the second subset of data for ASAS 002328−2041.8.

The plot of the O−C residuals is shown in Fig. 6.36. The observed times of minimum for the fourth interval are listed in Table 6.17.

For the fifth and sixth intervals, three and four minima respectively were extracted from the data therefore an analysis was not performed. If the two intervals are combined, the following ephemeris is returned by the analysis:

$$\text{Min. I} = \text{HJD } 2454393.29420(16) + 0.414693(03)\epsilon \tag{6.26}$$

The plot of the O−C residuals obtained using the above ephemeris is shown in Fig. 6.37. The observed times of minimum brightness for both intervals are listed in Table 6.18. Between the fourth interval and the combined fifth and sixth intervals, the period decreased with $\frac{\Delta P}{\Delta t} = -1.9 \times 10^{-5}$ d yr^{-1}.

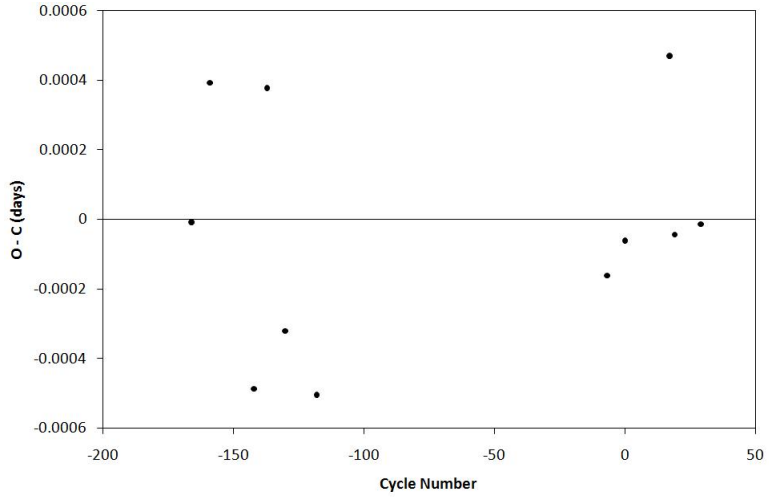

Figure 6.36: O−C residuals for the fourth interval of data of ASAS 002328−2041.8.

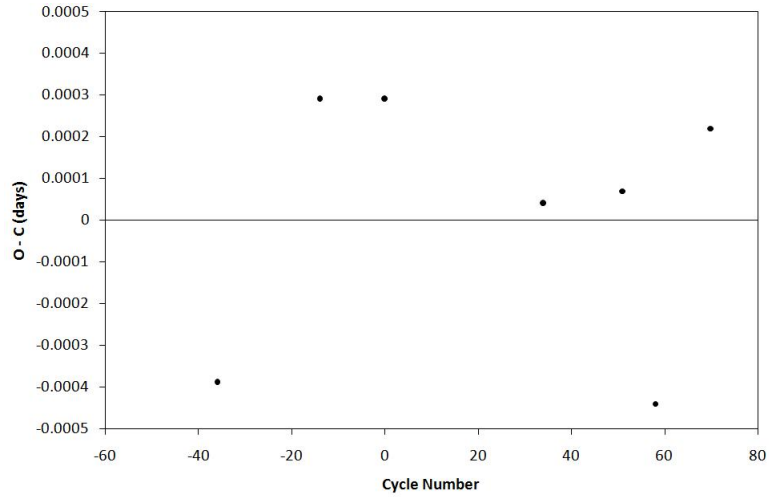

Figure 6.37: Plot of the O−C residuals for the combined intervals (five and six) of data of ASAS 002328−2041.8.

Cycle Number ϵ	Observed +2450000 (HJD)	Calculated +2450000 (HJD)	O − C (d)
−113	3942.51303(05)	3942.51314	−0.00011
−67	3961.58926(14)	3961.58898	0.00028
−60	3964.49181(08)	3964.49182	−0.00001
−36	3974.44437(24)	3974.44443	−0.00006
−26	3978.59098(16)	3978.59135	−0.00037
−24	3979.42086(23)	3979.42073	0.00013
−19	3981.49421(28)	3981.49419	0.00002
−14	3983.56758(26)	3983.56765	−0.00007
0	3989.37345(17)	3989.37334	0.00011
10	3993.52032(15)	3993.52026	0.00006

Table 6.15: Observed times of minimum for the second interval of data of ASAS 002328−2041.8.

Cycle Number ϵ	Observed +2450000 (HJD)	Calculated +2450000 (HJD)	O − C (d)
−113	4000.56978(08)	4000.56960	0.00018
−111	4001.39900(09)	4001.39905	−0.00005
−99	4006.37577(16)	4006.37577	0.00000
−94	4008.44925(37)	4008.44940	−0.00015
−65	4020.47652(66)	4020.47645	0.00007
−46	4028.35625(08)	4028.35624	0.00001
−5	4045.35987(11)	4045.36001	−0.00014
0	4047.43365(17)	4047.43364	0.00001
7	4050.33669(06)	4050.33672	−0.00003

Table 6.16: Observed times of minimum for the third interval of data of ASAS 002328−2041.8.

Cycle Number ϵ	Observed +2450000 (HJD)	Calculated +2450000 (HJD)	O − C (d)
−166	4284.64231(02)	4284.64232	−0.00001
−159	4287.54559(11)	4287.54520	0.00039
−142	4294.59456(15)	4294.59505	−0.00049
−137	4296.66891(30)	4296.66853	0.00038
−130	4299.57109(16)	4299.57141	−0.00032
−118	4304.54727(08)	4304.54777	−0.00050
−7	4350.57898(09)	4350.57914	−0.00016
0	4353.48196(09)	4353.48202	−0.00006
17	4360.53234(07)	4360.53187	0.00047
19	4361.36122(12)	4361.36126	−0.00004
29	4365.50822(13)	4365.50823	−0.00001

Table 6.17: List of observed times of minimum for the fourth interval of data of ASAS 002328−2041.8.

Cycle Number ϵ	Observed +2450000 (HJD)	Calculated +2450000 (HJD)	O − C (d)
−36	4378.36486(14)	4378.36480	0.00006
−14	4387.48879(24)	4387.48831	0.00048
0	4393.29449(04)	4393.29418	0.00031
34	4407.39380(09)	4407.39415	−0.00035
51	4414.44361(20)	4414.44414	−0.00053
58	4417.34595(21)	4417.34707	−0.00112
70	4422.32293(22)	4422.32353	−0.00060

Table 6.18: List of observed times of minimum for the combined fifth and sixth intervals of ASAS 002328−2041.8.

6.4 Discussion

The O−C analyses of the selected binaries shows that the periods of the systems are changing. New periods are determined and where possible, values for $\frac{\Delta P}{\Delta t}$ are calculated. Based on the error analysis, minima determined from the SuperWASP data are much more accurate than many values in the literature.

For RW Com, the determined values of P are similar to values determined by other authors. For two systems studied by Pilecki et al. (2007), namely ASAS 002449 − 2744.3 and ASAS 002821 − 2904.1, linear and quadratic ephemerides were determined for both systems. The results of the analysis confirm that the periods of the systems have changed. For ASAS 002449 − 2744.3, both calculated values of $^{\Delta P}/_{\Delta t}$ are different to the value of dP/dt determined by Pilecki et al. (2007). For ASAS 002821 − 2904.1, when the period of the quadratic ephemeris is used, the calculated value of $^{\Delta P}/_{\Delta t}$ is similar to the value of dP/dt determined by Pilecki et al. (2007).

Pilecki et al. (2007) determined dP/dt $= -0.17(4)\times10^{-5}$ d yr^{-1} and $P = 0.302101$ d (equal to the listed ASAS period) for ASAS 052851−3010.2. The SuperWASP observations were not performed at the same time as the ASAS observations but the value of P determined from the analysis of the SuperWASP data suggests that the period of the system has remained constant. As there is only one set of usable data, a value for $^{\Delta P}/_{\Delta t}$ could not be determined. The results of the period analysis of ASAS 002328 − 2041.8 indicates that the period of the system is changing. The star displays concurrent period and flux changes. The available data indicate that when the magnitude decreases (increases), the period increases (decreases). The Applegate mechanism proposes that changes in flux and period occur at the same time and that increases(decreases) in flux are accompanied by decreases(increases) in orbital period. From the results presented here, this star appears to obey the Applegate mechanism, but further observations will be required to confirm this.

Compared to the dP/dt values presented by Pilecki et al. (2007) for the systems they consider to be high period change rate systems, the following systems have $^{\Delta P}/_{\Delta t}$ values that would make them high period change rate systems: RW Com, ASAS 120036−3915.6, ASAS 150452−3757.7 and ASAS 150934−3348.5.

The orbital period of the selected systems is found to be decreasing for four of the systems (RW Com, ASAS 002821 − 2904.1, ASAS 120036−3915.6 and ASAS 150452−3757.7), increasing for two of the systems (ASAS 002449 − 2744.3 and ASAS 150934−3348.5), unchanged for one system (ASAS 052851 − 3010.2) and increasing then decreasing for ASAS 002328−2041.8. If ASAS 002328−2041.8 is included with the systems whose period is decreasing (based on the period analysis of the second subset of data) then, of the eight systems studied, 63% have a decreasing period and 25% have an increasing period. Pilecki et al. (2007) present 31 interacting binaries with observed high period change rates. Of the 31 systems, 22 are contact binaries. The authors determined that the period of 17 (77%) of the contact binaries decreased, while the period of the other five (23%) systems increased. Comparing the percentages of Pilecki et al. (2007) and the percentages of the eight selected systems suggests that for most contact binaries, the orbital period is decreasing.

Chapter 7

Conclusion & Future Research

7.1 Unexpected Discoveries

In the paper by Pilecki et al. (2007), the authors noted that the flux of one of the ASAS EC systems they had studied had increased linearly over the time in which it was observed. For all the ASAS contact binaries that met the initial search criteria (listed in Chapter 5), their light curves were inspected to see if any changes in flux occurred. Interestingly, many systems display either an increase or a decrease in flux. Some plots are shown in Fig. 7.1. The light curve of ASAS $093818-6755.4$, Fig. 7.2, shows the system undergoing what appears to be a cyclic change in flux similar to the change observed in the light curves of ASAS $062426-2044.9$ and ASAS $002328-2041.8$. These changes in flux may be related to magnetic activity. It is also possible that the systems are undergoing changes in orbital period. The value of the WASP data is evident when the data of separate HJDs are inspected as opposed to looking at the combined, folded data. Changes in the depths of the minima and the O'Connell effect were observed in many of the selected binaries. Two stars of particular interest are ASAS $002328-2041.8$ and ASAS $150452-3757.7$. SuperWASP data for the two reveal some interesting features. The light curves of ASAS $002328-2041.8$ are constantly varying, as shown in Fig. 6.31 in Chapter 6. From the results of the period analysis, the period of the system changes at the same time that the flux changes. This star may be magnetically active and is a promising candidate for

future radio observations.

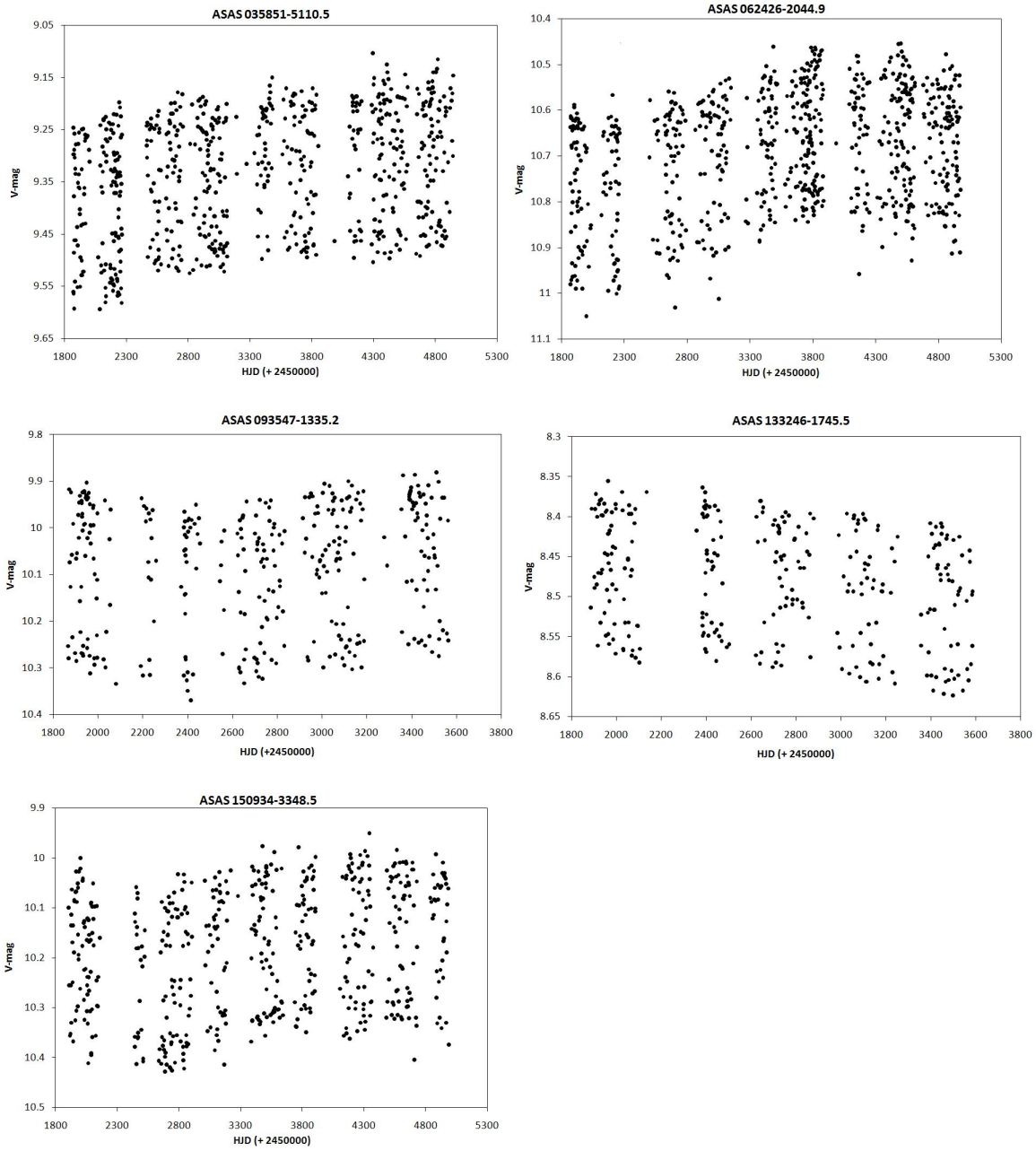

Figure 7.1: Magnitude plots of selected ASAS stars. The changes may be related to magnetic activity.

ASAS 150452 − 3757.7 displays unique features not seen in the light curves of the other

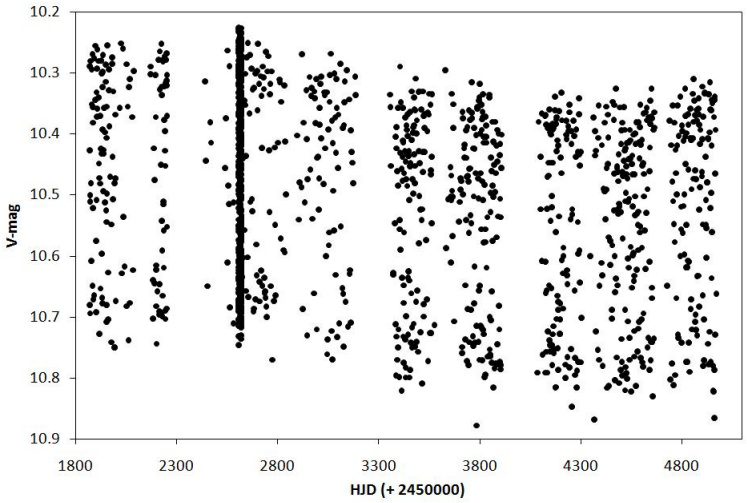

Figure 7.2: HJD-magnitude plot of ASAS 093818−6755.4. The change in flux appears to be oscillatory/cyclic.

systems. These features are shown in Fig. 7.3. On HJD 2454233, a slight dip in magnitude of one maximum of the system occurs. A similar dip in the magnitude of a maximum occurs on HJD 2454239. On HJD 2454254, a larger dip in magnitude occurs. The dip appears to have a flat bottom and a duration, measured from ingress to egress, of approximately 43 minutes. On HJD 2454272 another dip in magnitude occurs.

When the PMD of these events are plotted, as shown in Fig. 7.4, the events occur at around the same phase. The flux errors of the points are within the error range of the other WASP data. These dips are not observed in the rest of the WASP data of the system. The raw data display the same dips ruling out a data processing error. Data for stars in the same field of view, taken with the same camera, do not display these dips in magnitude. It is still unclear as to what caused the observed dips in magnitude. One other mystery is that the events occur at the same phase but, between the events, dips at that phase are not seen. As more SuperWASP data become available for the star, the light curves will be monitored to see if these dips occur again.

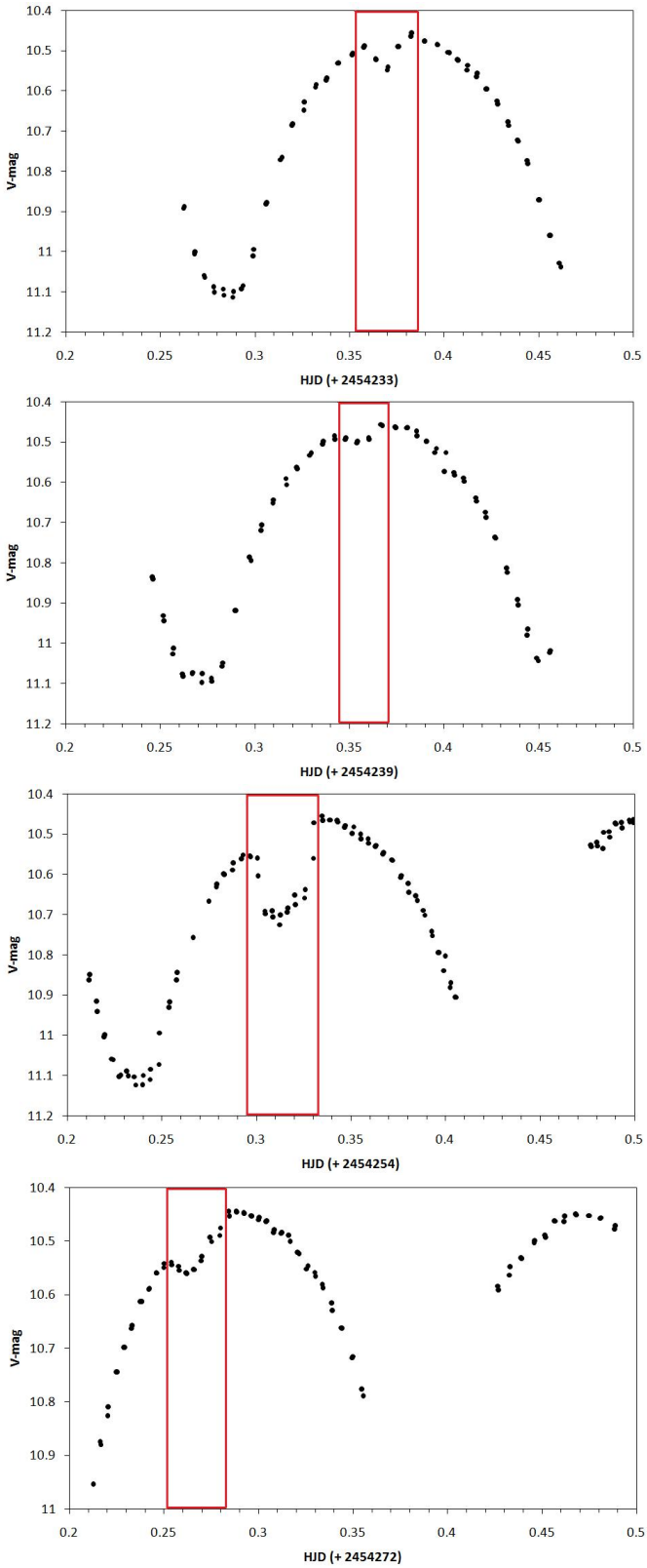

Figure 7.3: WASP light curves of ASAS 150452−3757.7 showing dips in magnitude. The event on HJD 2454254 displays a significant dip in magnitude.

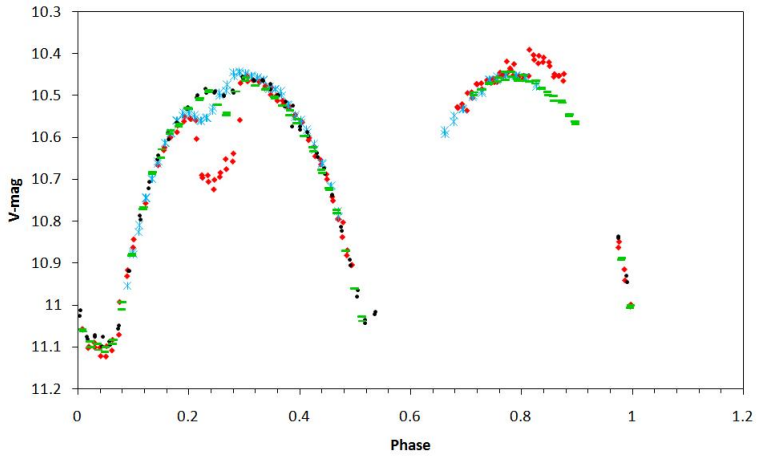

Figure 7.4: The combined PMD of the events observed in the light curve of ASAS 150452−3757.7 shows that they occur at the same phase.

7.2 Conclusion

Using data from the SuperWASP project, contact binaries from the ASAS database were selected for modelling and period analysis. Models for six total eclipsing systems are presented and the results of the period analyses of eight ASAS contact binaries are presented.

In Chapter 5, models (based on photometric data) of six contact binaries are presented. The results of the modelling have yielded two interesting candidates for future research namely ASAS 015937−0331.0 and ASAS 120036−3915.6. The former has a fillout value of 97% while the latter is at the opposite end with a fillout of only 3%. These two systems may represent two different stages in the evolution of contact binaries with one a shallow contact system and the other a low-mass ratio, deep contact system. Until radial velocity data are available, the parameters determined can not be confirmed.

The light curve residual values of the models for two systems, ASAS 015937−0331.0 and ASAS 150452−3757.7, were improved by using a spot model. Modelling contact binaries with spots should only be done if there is direct evidence of magnetic activity in the light curve of the system (O'Connell effect, shift in time of minimum). The reason is that different combinations of spots with different sizes, temperatures and positions can produce similar light curves. Yakut & Eggleton (2005) argue that spots are vital in understanding the light curves of contact binaries. They also suggest that systems

which do not display the O'Connell effect are not necessarily free of spots but are perhaps covered by a symmetric distribution of spots. When using the SuperWASP data and the light curves are observed to display either the O'Connell effect or asymmetric minima, the data may provide a unique way of determining the approximate position of a spot present on the surface of the star. Rovithis-Livaniou et al. (2003) showed that the minimum of a light curve can be affected by the presence of a spot on the larger component. The shape of the minimum determines which side of the larger component the spot is positioned. Therefore, an asymmetric minimum constrains the range of positions for a spot. Fig. 7.5 shows a WASP light curve of ASAS 150452 − 3757.7. The effect of a spot on the minimum of a light curve, as demonstrated by Rovithis-Livaniou et al. (2003), is clearly discernible. For this particular HJD, both minima are affected. Fig. 7.6 shows the WASP light curve of ASAS 150934 − 3348.5. The minimum is clearly asymmetric. Based on these observations, it may be possible to track spots by studying the effect they have on the light curve of a star when at different locations on the surface. By monitoring the light curves for these effects, it may be possible to determine if they occur cyclically.

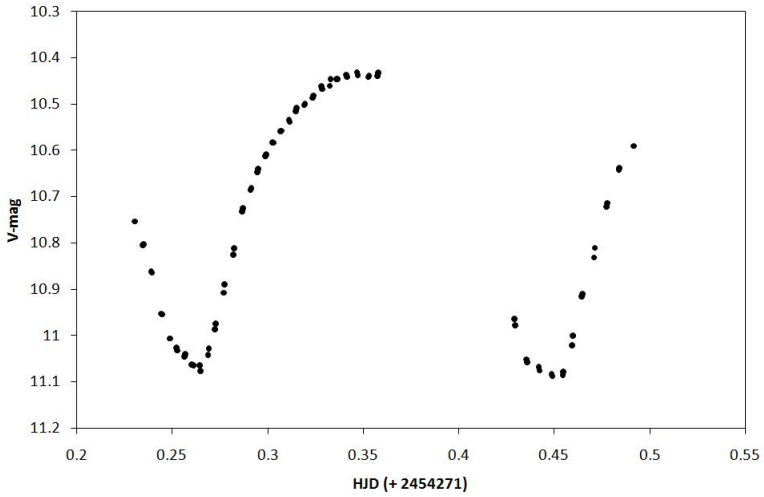

Figure 7.5: WASP light curve of ASAS 150452−3757.7. Both minima have been affected by the presence of a spot (or spots).

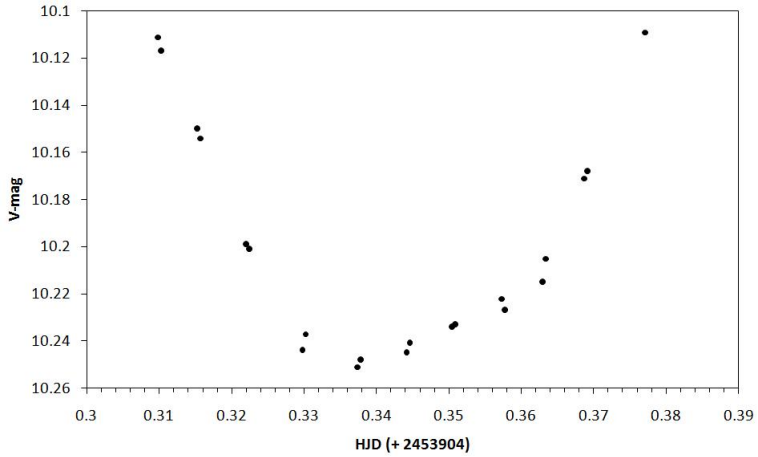

Figure 7.6: WASP light curve of ASAS 150934−3348.5. The direction of the shift, as demonstrate by Rovithis-Livaniou et al. (2003), gives an approximate location of the spot.

The models of the selected ASAS EC systems presented in this dissertation are based on photometric data and should be considered as being possible models of the stars.

The results of the period analyses indicate that the periods of some of the selected systems are changing. Of the eight systems selected, ASAS 002328−2041.8 appears to obey the Applegate mechanism, based on the results of the period analysis of the system presented in Chapter 6. Because the Applegate mechanism involves magnetic activity, this contact binary is a promising candidate for future radio observations. Pilecki et al. (2007) presented 31 binary systems, selected from the ASAS database, as high period change rate systems. Three of the contact binaries presented by Pilecki et al. (2007) were selected for period analysis. For two of the systems (ASAS 002449−2744.3 and ASAS 002821−2904.1) the change in period has been confirmed. The third system, ASAS 052851−3010.2, does not appear to have undergone a change in its orbital period. Three other systems, namely RW Com, ASAS 120036−3915.6, ASAS 150452−3757.7 and ASAS 150934−3348.5 could be considered to be high period change rate systems based on the calculated values of $^{\Delta P}/_{\Delta t}$ for each system.

The SuperWASP data have proven to be extremely useful for modelling of W UMa-type variable stars and have provided many minima for the variable stars which have been used

to determine if the periods of the systems are changing. The data have also shown that through continuous monitoring, many features such as the O'Connell effect and varying minima are observed.

7.3 Future Research

The ASAS team developed methods to detect variable stars and, while the SuperWASP project was designed to search for exoplanets, the SuperWASP data complement the ASAS data. Therefore, the SuperWASP data will continue to be used for research of W UMa-type stars. Paczynski et al. (2006) stated that their classification scheme of eclipsing binaries is preliminary. In particular, in the plot of the a_4 vs a_2 Fourier coefficients there are areas of overlap. For systems classified in the ASAS database as ESD/EC systems, the SuperWASP data could be used to determine the correct classification.

The SuperWASP data have shown that some of the selected ASAS EC systems are changing with time (in flux and/or period). Systems that are undergoing changes in flux are prime candidates for testing the Applegate mechanism. To confirm if the mechanism is responsible for the changes in flux requires monitoring the periods of the systems. The Automatic Photoelectric Telescope (APT) at the SAAO could be set up to monitor selected EW systems on a regular basis while mass ratios can be determined from radial velocity measurements obtained from the Southern African Large Telescope (SALT) or from the 1.9 m telescope fitted with GIRAFFE. Due to the short orbital periods of EW systems, complete light and radial velocity curves can be obtained in a single night's observing. By continuously monitoring the systems, any period changes can be detected. Combinations of radial velocity measurements and O−C analyses may reveal the presence of either a triple or mulitple body system confirming the suggestion that W UMa-type variables form from multiple star systems.

Hughes & McLean (1984) performed radio observations of 12 W UMa-type stars using the VLA. The stars that were observed were selected purely because they were within a distance of 150 pc. Of the stars observed, only two detections were made: V502 Oph was observed as a double source while a flare was detected from VW Cep. Similarly, in a

search for microwave emission from four southern contact binary stars by Beasley et al. (1993), the stars were selected as they were all within a distance of 62 pc. The ASAS has detected a large number of contact binary stars. The light curves of some of the stars display the O'Connell effect which is regarded as an indication of magnetic activity while for others, their WASP light curves show spot-induced shifts in the minima. Therefore, while previous radio surveys focussed on nearby W UMa-type stars, a database of ASAS EC systems known to be magnetically active can be created. By monitoring the systems, it will be possible to determine whether the O'Connell effect is a constant feature in the light curve (due to a permanent hot or cold spot) or if the systems display a stellar magnetic cycle. Stellar spots on the component stars may produce radio emission that could be detected with sensitive enough radio telescopes such as the VLA or the 100 m Green Bank and Effelsberg telescopes. As a future project, the sensitivity of the SKA will be ideal for performing radio observations of these systems. An initial goal of this dissertation was to identify EW systems that may be magnetically active (light curves display the O'Connell effect) and possible sources of radio emission. Of the six systems selected for modelling, the light curves of the two of the systems display the O'Connell effect: ASAS 015937−0331.0 and ASAS 150452−3757.7. From the period analyses, ASAS 002328−2041.8 appears to obey the Applegate mechanism. These three systems are potential sources of radio emission and are possible targets for future radio observations.

In light of the use of an exoplanet survey project to obtain photometric data for eclipsing binaries, there are other sources of data for binary star research. These include:

- Pi of the Sky - Main goal is to search for gamma ray burst opticals but Majczyna et al. (2008) have compiled a catalog of short period variable stars using data from the project.
- INTEGRAL/OMC - The data collected by the Optical Monitoring Camera (OMC) of the INTErnational Gamma-Ray Astrophysics Laboratory (INTEGRAL) has been used by Zasche (2008) for light curve analysis of eclipsing binaries.

These databases can be used as extra sources of data for the contact binary systems that will be studied.

The main focus of the future research will be to automate the processes of the O−C analysis used in this dissertation. The automated procedure that will be developed will include:

- Searching for ASAS EC and ESD/EC systems in the SuperWASP database and downloading the data.
- Using the SuperWASP light curves to determine the correct classifications of the EC/ESD systems.
- Obtaining observed times of minimum and constructing O−C diagrams. Periods can be calculated and compared to the periods listed by ASAS. Consequently, systems undergoing changes in orbital period can be identified.
- Plots of the data will show which systems are undergoing changes in flux. These changes may be related to magnetic activity.
- Systems undergoing simultaneous changes in flux and period will be used as tests of the Applegate mechanism.

The results of this dissertation show that continuous monitoring of W UMa-type variable stars reveal changes in flux and period that occur on short time-scales. Systems that are undergoing such changes may improve our understanding of the stability and evolution of W UMa-type variable stars.

References

Applegate, J. H. 1992, ApJ, 385, 621

Baran, A., Zola, S., Rucinski, S. M., et al. 2004, AcA, 54, 195

Beasley, A. J., Ball, L. T., Budding, E., Slee, O. B., & Stewart, R. T. 1993, AJ, 106, 1656

Binnendijk, L. 1970, VA, 12, 217

Bradstreet, D. H. 2005, SASS, 24, 23

Breinhorst, R. A. 1971, Ap&SS, 10, 411

Şenavcı, H. V., Nelson, R. H., Özavcı, I., Selam, S. O., & Albayrak, B. 2008, NewA, 13, 468

Chen, W. P., Sanchawala, K., & Chiu, M. C. 2006, AJ, 131, 990

Csizmadia, S. 2005, Ap&SS, 296, 185

Csizmadia, S. & Klagyivik, P. 2004, A&A, 426, 1001

Flannery, B. P. 1976, ApJ, 205, 217

Gazeas, K. & Stępień, K. 2008, MNRAS, 390, 1577

Gazeas, K. D., Baran, A., Niarchos, P., et al. 2005, AcA, 55, 123

Gazeas, K. D., Niarchos, P. G., Zola, S., Kreiner, J. M., & Rucinski, S. M. 2006, AcA, 56, 127

Hendry, P. D. & Mochnacki, S. W. 1998, ApJ, 504, 978

Hilditch, R. W. 2001, An Introduction to Close Binary Stars (Cambridge University Press)

Hilditch, R. W., King, D. J., & McFarlane, T. M. 1988, MNRAS, 231, 341

Huffer, C. M. 1934, ApJ, 79, 369

Hughes, V. A. & McLean, B. J. 1984, ApJ, 278, 716

Ibanoğlu, C., Soydugan, F., Soydugan, E., & Dervişoğlu, A. 2006, MNRAS, 373, 435

Kallrath, J. & Milone, E. F., eds. 1999, Eclipsing binary stars : modeling and analysis (New York : Springer)

Kopal, Z. 1955, AnAp, 18, 379

Kreiner, J. M., Rucinski, S. M., Zola, S., et al. 2003, A&A, 412, 465

Kuiper, G. P. 1948, ApJ, 108, 541

Kwee, K. K. 1956, BAN, 12, 330

Kwee, K. K. 1958, BAN, 14, 131

Kwee, K. K. & van Woerden, H. 1956, BAN, 12, 327

Lapasset, E. & Claria, J. J. 1986, A&A, 161, 264

Li, L., Han, Z., & Zhang, F. 2004, MNRAS, 351, 137

Li, L., Zhang, F., Han, Z., Jiang, D., & Jiang, T. 2008, MNRAS, 387, 97

Liu, Q.-Y. & Yang, Y.-L. 2003, ChJAA, 3, 142

Lucy, L. B. 1967, ZA, 65, 89

Lucy, L. B. 1968, ApJ

Lucy, L. B. 1973, Ap&SS, 22, 381

Lucy, L. B. 1976, ApJ, 205, 208

Lucy, L. B. & Wilson, R. E. 1979, ApJ, 231, 502

Maceroni, C. & van't Veer, F. 1993, A&A, 277, 515

Majczyna, A., Należyty, M., Biskup, M., et al. 2008, NewA, 13, 414

Meyer-Hofmeister, E. & Ritter, H. 1993, in , 143

Milone, E. F. & Kallrath, J. 2008, in , 191

Müller, G. & Kempf, P. 1903, ApJ, 17, 201

Mochnacki, S. W. 1981, ApJ, 245, 650

Mochnacki, S. W. & Doughty, N. A. 1972, MNRAS, 156, 51

Moss, D. L. & Whelan, J. A. J. 1970, MNRAS, 149, 147

Paczynski, B. 1997, in Variables Stars and the Astrophysical Returns of the Microlensing Surveys, ed. R. Ferlet, J.-P. Maillard, & B. Raban, 357

Paczyński, B., Szczygieł, D. M., Pilecki, B., & Pojmański, G. 2006, MNRAS, 368, 1311

Pilecki, B., Fabrycky, D., & Poleski, R. 2007, MNRAS, 378, 757

Pollacco, D. L., Skillen, I., Cameron, A. C., et al. 2006, PASP, 118, 1407

Popper, D. M. 1948, ApJ, 108, 490

Pribulla, T. & Rucinski, S. M. 2006, AJ, 131, 2986

Prša, A. & Zwitter, T. 2005, ApJ, 628, 426

Qian, S. 2002, A&A, 384, 908

Qian, S. 2003, MNRAS, 342, 1260

Rovithis-Livaniou, H., Kalimeris, A., & Rovithis, P. 2003, in Astronomical Society of the Pacific Conference Series, Vol. 292, Interplay of Periodic, Cyclic and Stochastic Variability in Selected Areas of the H-R Diagram, ed. C. Sterken, 163

Ruciński, S. M. 1969, AcA, 19, 245

Ruciński, S. M. 1973, AcA, 23, 79

Rucinski, S. M. 1997, IBVS, 4460, 1

Rucinski, S. M. & Seaquist, E. R. 1988, AJ, 95, 1837

Schilt, J. 1925, BAN, 3, 20

Shapley, H. & van der Bilt, J. 1917, ApJ, 46, 281

Shengbang, Q., Yuangui, Y., Liying, Z., Jiajia, H., & Jingzhao, Y. 2006, Ap&SS, 304, 25

Shore, S. N. 1994, in Saas-Fee Advanced Course 22: Interacting Binaries, ed. S. N. Shore, M. Livio, & E. P. J. van den Heuvel

Skelton, P. L. & Smits, D. P. 2009, SAJSc, 105, 120

Stebbins, J. 1910, ApJ, 32, 185

Stepien, K. 1995, MNRAS, 274, 1019

Sterken, C. 2005, in Astronomical Society of the Pacific Conference Series, Vol. 335, The Light-Time Effect in Astrophysics: Causes and cures of the O-C diagram, ed. C. Sterken, 3

Terrell, D. & Wilson, R. E. 2005, Ap&SS, 296, 221

van Gent, H. 1929, BAN, 5, 99

van Hamme, W. 1982, A&A, 105, 389

van Hamme, W. 1993, AJ, 106, 2096

van Hamme, W. & Cohen, R. E. 2008, in Astrophysics and Space Science Library, ed. E. F. Milone, D. A. Leahy, & D. W. Hobill, Vol. 352, 215

van Hamme, W., Wilson, R. E., & Guinan, E. F. 1995, AJ, 110, 1350

van't Veer, F. 1991, A&A, 250, 84

van't Veer, F. & Maceroni, C. 1989, A&A, 220, 128

Vilhu, O. 1982, A&A, 109, 17

Wadhwa, S. S. 2005, Ap&SS, 300, 289

Wadhwa, S. S. & Zealey, W. J. 2005, Ap&SS, 295, 463

Wang, J.-M. 1999, AJ, 118, 1845

Webbink, R. F. 2003, in Astronomical Society of the Pacific Conference Series, Vol. 293, 3D Stellar Evolution, ed. S. Turcotte, S. C. Keller, & R. M. Cavallo, 76

Willems, B., Kolb, U., & Justham, S. 2006, MNRAS, 367, 1103

Wilson, R. E. 1978, ApJ, 224, 885

Wilson, R. E. & Devinney, E. J. 1971, ApJ, 166, 605

Wolf, M., Molík, P., Hornoch, K., & Šarounová, L. 2000, A&AS, 147, 243

Yakut, K. & Eggleton, P. P. 2005, ApJ, 629, 1055

Zasche, P. 2008, NewA, 13, 481

Zavala, R. T. 2005, in Astronomical Society of the Pacific Conference Series, Vol. 335, The Light-Time Effect in Astrophysics: Causes and cures of the O-C diagram, ed. C. Sterken, 137

Zola, S., Kreiner, J. M., Zakrzewski, B., et al. 2005, AcA, 55, 389

Zola, S., Rucinski, S. M., Baran, A., et al. 2004, AcA, 54, 299